UNDERSTANDING THE INTEGRATED PATHOPHYSIOLOGICAL ROLE OF A MOONLIGHTING PROTEIN IN LUNG DEVELOPMENT

Dong Il Lee

Submitted to the faculty of the University Graduate School
in partial fulfillment of the requirements
for the degree
Doctor of Philosophy
in the Department of Cellular and Integrative Physiology,
Indiana University

August 2019

Accepted by the Graduate Faculty of Indiana University, in partial fulfillment of the requirements for the degree of Doctor of Philosophy.

Doctoral Committee

_____

Margaret Schwarz, MD, Co-Chair

_____

Johnathan Tune, Ph.D., Co-Chair

May 7, 2019

_____

Mark Kaplan, Ph.D.

_____

David Basile, Ph.D.

Dedication

To Jesus Christ, my Lord, who provides me with the strength and fortitude.

To Mom and Dad

Acknowledgment

The work presented in this thesis represents only one outcome of the mentorships, rapports, and fostering interactions with many people whom I met. It feels like it was not long ago when I moved yet again. At that time though, it was to work with Dr. Margaret Schwarz in her lab, however, and was the beginning of an enriching experience that I will fondly remember. I am very grateful and appreciative to Dr. Schwarz for mentoring me scientifically and helping me to help myself. Spelling her last name without a 't' as do so many wrongly assume, she stands out positively. She has nurtured such a positive and self-enabling atmosphere that has allowed me to work diligently and effectively while feeding my curiosities. Throughout my time here, the lab members have been supportive team; the many graduate students, medical students, undergraduates and even high schoolers that I have met, taught, and worked with, have in turn taught myself in various aspects. For them, I am thankful.

To Dr. Johnathan Tune, I give much gratitude for his openness and candor. He spelled his first name without an "h," so he had to stand out. He did so positively, in fact, from the beginning of this Ph.D. process at admission to the completion of this thesis, with his openness especially with regards to my working in both South Bend and Indianapolis. His approach too was positive and enriching, yet when needed, curt and frank. I thank the members of the Tune Lab. Dr. Adam Goodwill, with an emphasis on 'Dr. Goodwill' for posterity's sake, I would like to thank for his willingness to teach and share ideas both scientifically and personally.

One of the many things that my parents prepared me for life was how to handle the "no's." At times, deflection may be needed, or even facing it directly, but at other times, it may be prudent to change my perspective. During my time observing and learning from Drs. Schwarz and Tune, I have further equipped myself for how to handle the "no's" especially those that inevitably come in droves when working in science. There is no doubt that what I have observed and learned from their encouraging, complementing mentorships has molded my life and future career.

I would like to thank the Department of Cellular and Integrative Physiology for the opportunity, and the members of the office who have been supportive. I very much

thank Drs. Kaplan and Basile for their valuable time with me as part of my thesis committee even while their juggling multiple facets of life.

Finally, to my family, I am indebted. Thanks to my sister for teaching me invaluable life lessons. Final thanks and love are to my parents who have fostered, nurtured, steered both my curiosity and well-being in productive ways. Always having someone to count on and to provide sage wisdom from experience is a privilege not everyone gets to have. For that I do not take for granted. Not only did my parents give me life but also taught me such a wide-ranging range of lessons that I could not only teach myself but also to support and encourage others. Ultimately, to be able to have written more than a paragraph of gratitude, let alone a multitude of pages for my dissertation is something that I attribute to my parents for planting a seed of conviction and confidence within me. To let it sprout has been through not only my learned efforts but also all the wonderful mentors and people who have supported me during my thesis and the many things yet to come!

Dong Il Lee

UNDERSTANDING THE INTEGRATED PATHOPHYSIOLOGICAL ROLE OF A MOONLIGHTING PROTEIN IN LUNG DEVELOPMENT

Sensing, integrating, and relaying signals from the environment through proteins, metabolites, and lipids to the lung are critical for proper development. Moonlighting proteins, such as AIMP1, are a unique subset that serves at least two independent physiological functions. Encoded by gene AIMP1, AIMP1 has two known functions: (1) C-terminus EMAP II domain of full-length AIMP1 can be secreted out of the cell to chemoattract myeloid cells; (2) intracellular full-length protein interacts with tRNA synthetases in protein translation. However, despite the linkage of protein expression levels of with several lung pathologies such as bronchopulmonary dysplasia (BPD), effectively targeting the protein encoded by AIMP1 has been a challenge due to poorly understood mechanisms.

This thesis explores physiological, signaling, and immunological moonlighting mechanisms of first, the extracellular EMAP II then the intracellular AIMP1. Experiments utilize both in vitro and in vivo models, including a murine model of BPD and Cre-mediated exon-deletion knockout. Experimental results provide evidence that in the BPD model, EMAP II levels are elevated and sustained – first in bronchial epithelial cells then in macrophages. Mice exposed to sustained and elevated EMAP II protein levels resemble the BPD phenotype while neutralization partially rescued the phenotype, implying EMAP II as a potential therapeutic target against BPD. Results from studies exploring EMAP II's signaling mechanism identify transient stimulation of JAK-STAT3 phosphorylation, commonly found in inflammation-resolving macrophages. In contrast, it induces unique transcriptional changes that are reversible both by JAK-STAT inhibitor and siRNA-mediated knockdown of Stat3.

Studies using AIMP1 knockout mouse reveal a novel function for the intracellular AIMP1. AIMP1 knockout mice exhibited neonatal lethality with a respiratory distress phenotype, decreased type I alveolar cell expression, and disorganized bronchial epithelium, suggesting a role in lung maturation. In vitro experiments suggest that a

portion of AIMP1 residing in the cell's membrane interacts with various phosphatidylinositols and contributes toward F-actin deposition and assembly.

Data from these experimental studies provide insight into how the various functions of the promiscuous AIMP1 gene affect lung development. These studies exemplify not only characterize novel moonlighting mechanisms of AIMP1, but also highlight the importance of characterizing moonlighting proteins to promote therapeutic preventions.

Margaret Schwarz, M.D., Co-Chair

Johnathan Tune, Ph.D., Co-Chair

Table of Contents

List of Tables

List of Figures

Chapter 1

Chapter 2

Chapter 3

Chapter 4

Chapter 5

List of Abbreviations

BPD: Bronchopulmonary dysplasia

EMAP II: Endothelial Monocyte Activating Polypeptide II

AIMP1: Aminoacyl tRNA synthetase multisynthetase interaction protein 1

Anti-EMAP II: EMAP II neutralizing antibody

MLI: Mean Linear Intercept

PH: Pulmonary Hypertension

RAC: Radial Alveolar Count

qPCR: quantiative PCR

cDNA: complementary DNA

IDR: intrinsically disordered region

AJ: adherens junction

mRNA: messenger RNA

Chapter 1: Introduction

In mammals, lungs primarily serve to exchange oxygen from the external environment with metabolically generated carbon dioxide from the cardiovascular system. It accomplishes this function through a complex, paired structure of branched airways (i.e., the bronchiolar tree) and specialized spherical-like, air-blood gas exchanging units (i.e., alveoli). The conducting branched airways conduct, filter, and warm the air from the external environment into the alveoli where it facilitates the exchange of gas. A network of proteins, lipids, and metabolites spatiotemporally merge to differentiate the primordial anterior foregut endoderm into the highly specialized lung.

Activation and de-activation of the signaling networks regulates the progression of the five morphological stages of lung development: embryonic, pseudoglandular, canalicular, saccular and alveolar (**Figure 1.1**).

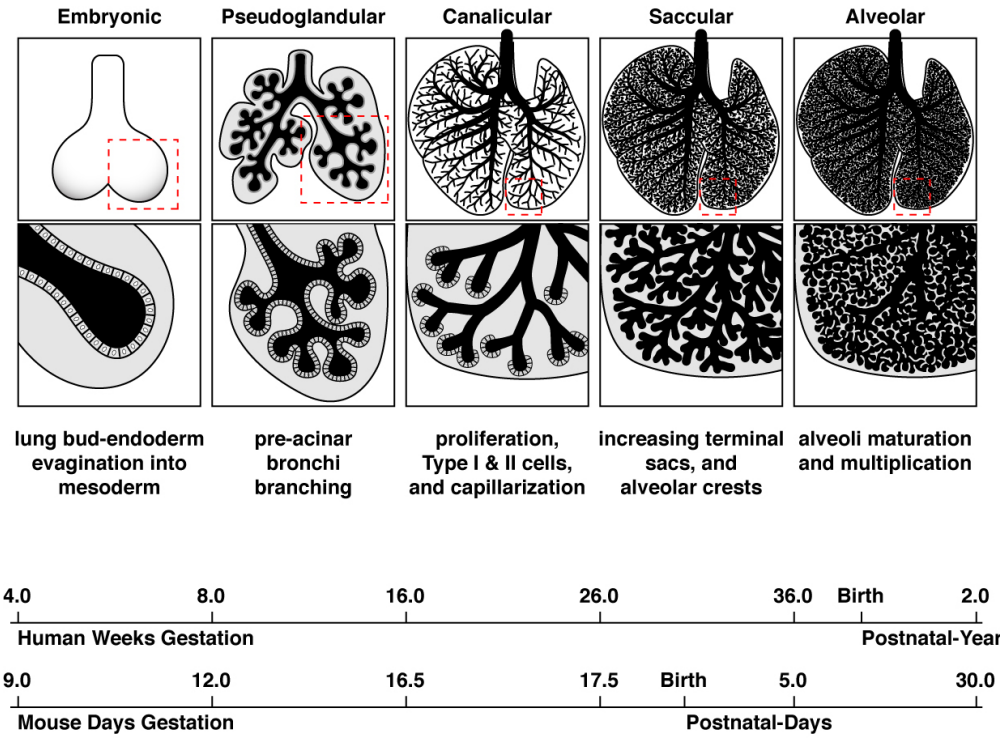

Figure 1.1. Schematic depicting the corollative timeline of lung development in both humans and mice (Adapted *from Schwarz and Cleaver,* 2009).

Throughout the stages, the networks elicit the heterogeneous cellular population of the lung to form coordinated complexes of transcription factors that specify lung-specifc

gene expression and development. Starting in the embryonic and pseudoglandular stages, a lung bud begins to form into the bronchial tree and the first few generations of alveolar sacs at which point marks the beginning of the canalicular stage. Terminal branches develop and narrow allowing for epithelial-mesenchymal sacs to mature into alveoli within the latter three stages. Branching morphogenesis and the formation of most of the distal airways occur during the canalicular stage. The formation of morphogenesis signifies the completion of the majority of the lung structure and the beginning of the saccular and alveolar stages. The saccular and alveolar stages are a vulnerable time period when perturbations can alter and limit the growth and maturation of functional gas-exchanging alveolar units. A prominent perturbation to proper lung development is preterm birth.

Preterm births are born during the vulnerable saccular and alveolar stages, even as early as 23 weeks of gestation in humans or 17.5 days in mice. The lungs of the preterm or prematurely born infant do not contain adequate number of mature alveoli to match their body's requirement of oxygen. This causes a requirement of both oxygen supplementation for the preterm infant with incompletely formed alveoli and surfactants as part of their standard of care. Although the supplementation is life preserving, it can lead to bronchopulmonary dysplasia (BPD), a chronic lung disease and major morbidity of the extremely preterm infants.

1.1 Research Motivation

The problem originally motivating this research lies in the need for a therapeutic target against bronchopulmonary dysplasia (BPD). The oxygen supplementation of preterm infants induces a strong pulmonary inflammatory response. Through a series of signaling events gone awry, chronic inflammation is central to the perinatal, multi-factorial pathogenesis of BPD by limiting the structural integrity and maturation of potential gas-exchanging alveoli including its vasculature. The therapeutic target thus would also need to be directed against the chronic inflammation.

Clinically, in addition to the standard of care, immunosuppressants such as antenatal steroids are administered to preterm infants in an attempt to curb the inflammation. Immunosuppressants are effective in brief intervals at low doses.

However, either long-term usage or high dosages associate with adverse effects such as neurological disorders. Inhibiting other prominent inflammatory mediators such as tumor necrosis alpha in sepsis-induced inflammation showed little improvement in survival rates of humans whereas in murine models, only a few features of BPD improved. This suggests a need for either an alternative strategy to target inflammation or a target that is upstream of the prominent inflammatory mediators to limit the pathogenesis of BPD.

An alternative strategy is to regulate the recruitment of myeloid cells that increase inflammation. Some of the protein factors that regulate the recruitment have at least two independent, physiological roles, which are called moonlighting proteins. Increased levels of the moonlighting protein Endothelial Monocyte Activating Polypeptide II (EMAP II) and its precursor protein Aminoacyl tRNA Multisynthetase Interacting Polypeptide 1 (AIMP1) has been linked to several lung pathologies. Encoded by the gene *AIMP1*, AIMP1 protein has two known functions: (1) chemoattracting of myeloid cells by its C-terminus EMAP II domain of full length AIMP1, which is cleaved and secreted out of the cell; (2) enhancing protein translation by interacting its full-length intracellular self with tRNA synthetases. Previously, the Schwarz laboratory, among others, linked increased protein levels of Endothelial Monocyte Activating Polypeptide II (EMAP II) with BPD. Additional evidence shows that EMAP II limits vessel formation as an anti-angiogenic factor during lung development. This presents EMAP II as a potential therapeutic target against BPD pathogenesis. However, effective targeting of the pathogenic roles of EMAP II requires a better understanding of its mechanisms in lung development, which are incomplete. The mechanisms of the protein encoded by gene *AIMP1* discussed in this thesis are needed as part of the evaluation for a potential therapeutic target against BPD.

1.2 Research Objectives and Aims

The overall objective of the research in this thesis is not only to present newly found moonlighting mechanisms of the *AIMP1*-encoded protein applied to lung development but also to demonstrate their effectiveness in the pathogenesis of BPD. The understanding of the mechanisms will enable effective targeting of the protein in future

clinical scenarios. The objective is achieved through a breakdown of smaller aims that are noted in the following.

Before the first main objective could be addressed, an offshoot, minor aim of the primary objective arose from the need to create a reproducible, quantitative tool for assessing messenger RNA (mRNA) expression in lung development. Guidelines to perform quantitative polymerase chain reaction (qPCR) were validated for each step of mRNA gene expression analysis, including, but not limited to, lung sample harvesting, isolation, integrity, and purity of RNA, amplicon size, and data normalization. The tool is important not only technically but also reconciled a conflicting result among individual laboratories; it is used throughout the entirety of the thesis when applicable.

The first aim is to study the molecular and physiological mechanisms of EMAP II during the pathogenesis of BPD. The hypothesis of this aim is that EMAP II would promote an inflammatory state through recruitment of macrophages during the pathological formation of BPD. Testing of this aim includes the usage of three neonatal murine models: (a) BPD (hyperoxia-induced), (b) delivery of recombinant EMAP II, and (c) BPD with neutralizing EMAP II antibody treatments. In the murine models, the following key questions are addressed in the pathogenesis of BPD: (1) What happens to protein expression of EMAP II during the pathogenesis? (2) When is EMAP II expressed? (3) What cell types express EMAP II? (3) What cellular impact does sustained EMAP II have on the pathogenesis? (4) What is the impact of the sustained EMAP II on the physiology of the lung? (5) Can the effects of sustained EMAP II be reversed i.e., neutralized?

The second aim is to determine the molecular and signaling mechanisms in the macrophages that were recruited in response to EMAP II. The hypothesis of the second aim is that EMAP II polarizes the recruited macrophages toward a pro-inflammatory state. Experiments for this aim utilize thioglycollate-elicited peritoneal macrophages, a partially activated population. In this aim, known pro-inflammatory M1 mRNA gene expression and activation of transcription factors are measured in macrophages exposed to EMAP II compared to those not exposed, i.e. control.

The third and final aim is to study the role of the intracellular AIMP1 in lung development. This aim is to completely characterize the other potential moonlighting

functions of the *AIMP1*-encoded protein, starting with the intracellular full-length form that is incompletely understood. This may be in part because there has not been a report of a complete knockout mouse of *AIMP1* until the generation of one in this thesis. Schwarz and others showed that at the cellular level, part of AIMP1 is expressed at the cell surface and at the tissue level, the epithelial-mesenchymal interface of the lung. The hypothesis of this aim is that cell-surface AIMP1 mediates the organization of the epithelium. The testing of the hypothesis is performed *in vivo* by comparing the lungs of knockout mice to characterize the physiological roles of AIMP1 while *in vitro* biochemical and molecular approaches to identify the localization and potential molecular interactions of AIMP1.

1.3 Thesis Background Along with Related Works

There are several important topics related to the moonlighting *AIMP1*-encoded protein and lung development discussed in this thesis: (1) animal models of lung development and BPD; (2) moonlighting properties; and (3) myeloid cells. The following subsections discuss the background and work done by other researchers that is particularly relevant to this research.

1.3.1 Strengths in Murine Models of Lung Development and Pathophysiology

The five stages of lung development have been well established through visual analysis of structural changes that occur in both human and non-human mammalian models over time. Without routinely accessible human lung samples, animal models have been invaluable to study not only lung development but also the etiology of BPD pathophysiology. In particular, non-diseased lungs to compare with the diseased lungs are difficult to acquire since samples are generally collected at the time of death. Thus molecular mechanisms and the refinement of key biological questions can be more easily addressed using animal models, and in this thesis, the mouse.

Murine, compared to other animal, models offer several advantages: a short life cycle combined with high fertility rates, increased sample size, readily available and validated biological tools such as antibodies and gene manipulation, and ease of husbandry. The lung development in the mouse parallels the development in the humans

with differences in duration of the stage and gestational age. In the mouse, the 5 stages are as follows: (1) embryonic (embryonic days 9.0 to about 12.5, denoted as E9.0 to E12.5); (2) pseudoglandular (about E12.5 to E16.5); (3) canalicular (E16.5 – E17.5); (4) saccular (E17.5 – Postnatal Day 5, PN5); (5) alveolar (PN5 – maturity)[3]. Of note, the saccular stage prepares the lung for extrauterine, perinatal life. In this stage, terminal airways deriving from bronchioles dilate and vascularize while the production of surfactant is initiated. Surfactant, a lipoprotein complex, reduces surface tension within the forming, maturing alveoli, and in effect, enhances their opening during inhalation; without sufficient amounts of surfactant, respiratory distress forms.

A notable difference between mice and human lung development occurs in the saccular stage. On the one hand, mice are born at term during the saccular stage, which in mice begins *in utero* and continues through birth at term until PN5. On the other hand, human infants born during the stage are premature. It is important to note that the mice born in the saccular stage have adequate surfactant and without either respiratory distress or morbidity issues. The human preterm infants born during the saccular stage are at high risk of developing respiratory distress due to their underdeveloped lungs. Since lungs of neonatal mice contain adequate surfactant but human preterm infants do not, this can be somewhat considered akin to antenatal steroids delivered to the human preterm neonate (reference). Thus mice are useful models of normal and pre-term birth. This will be important later in the discussion of BPD pathogenesis.

1.3.2 Signaling mechanisms and functional changes during BPD pathogenesis

Changes in the environment are conveyed through signaling networks of proteins, metabolites, and lipids. Broadly stated, extracellularly secreted proteins induce autocrinic, endocrinic, and paracrinic signaling to spatiotemporally regulate intracellular events. The extracellular secreted factors initiate various signaling processes through intracellular protein-protein interactions and the phospholipids. This enables progenitor cells to differentiate into the heterogeneous cell population that make up the lung. Mechanical forces during the pseudoglandular stage are one of the earliest changes in the environment of the lung, which activate BMP signaling. Then, several signaling pathways coordinate lung specification by gene expression changes controlled by

transcription factors. Among them, Wnt/Beta-catenin, BMP, and Shh signaling pathways are essential for lung development and fate specification[4]. Recently, JAK/STAT signaling, highly context specific has joined the signaling pathways that are necessary to initiate alveolar formation and to promote alveolar differentiation[5].

Within a single alveolar sac, there exists a multi-cellular population: Type I and II epithelial cells, endothelial cells, and macrophages. The epithelial cell organization is comprised of both Type I cells that cover roughly 95%-97% of the alveoli's surface area and responsible for gas exchange, and Type II cells that synthesize surfactants. It was long-standing dogma that in lung development, a single progenitor population yielded Type II cells, which in turn were precursors for Type I in a relatively linear fashion. However, a recent study proposed a revised model in which a bipotent progenitor cell population, emerging around murine E17.5, i.e. canalicular to saccular stage transition, differentiates independently into Type I and Type II cells, or pneumocytes, in both development and injury[6]. Cells whose fate is to become Type I cells begin to express podoplanin (*Pdpn* or T1alpha) during pre-sacculation but acquire aquaporin 5 (*Aqp5*) toward matured late-sacculation; cells whose fate is to become Type II cells express surfactant protein C (*Sftpc*) throughout the maturation process, but only the transcription factor Nkx2.1 in pre-sacculation. Whereas $Aqp5^+$ Type I cells largely mediate the direct gas-exchange of oxygen and carbon dioxide and contain relatively no organelles, $Sftpc^+$ Type II cells synthesize surfactants either *de novo* primarily from lipids, such as phosphatidylcholine or from an acylation/reacylation pathway generated from the airspace[7]. As found evident by knockout mouse models, insufficient timing or magnitude of differentiating cells result in a lethal phenotype. Similar deficiencies are present in the BPD preterm lung.

Proper regulation of the signaling pathways results in a fully differentiated lung that can expand and contract to enable breathing. Fetal respiratory movement has been observed as early as E14.5 in the mouse[8]. Upon extrauterine delivery, the lung undergoes physiological transition in preparation for its first contact with air and breath. The lung's airspace clears their fluids through active transport of chloride against a lower protein concentration gradient. Further endocrinic adaptions occur to activate Na^+/K^+ ATPase channels, and Type II cells primarily mediate these effects[9].

The pulmonary structure has been better described than pulmonary function throughout development. Technological tools are not yet advanced enough to directly test pulmonary function throughout neonatal development. Thus what is known about the function is generally inferred from morphological changes. By extension, how pulmonary function is affected by disrupting lung development is poorly understood. A useful determinant of pulmonary function to is to measure compliance. Compliance refers to change in lung volume for a given change in pressure and increases proportionally to the amount of matured alveoli, thereby can increase until alveologenesis has completed[10,11]. In light of this limitation, in this thesis, similar to clinical studies, we study how structural deformities impact later pulmonary function, as seen later in Chapter 3.

1.3.3 Inflammation disrupting alveolarization in the pathogenesis of BPD

Disruption in the differentiation of any one of the cell types that make up the alveoli is sufficient to disrupt the process of alveolarization as a whole. The disruption can be found in the BPD lung, where it also is defined by arrested alveolar development, inflammation although less so than the older counterpart, and airways being spared[1]. These clinical features are referred to as 'new BPD' in contrast to 'old BPD' that was defined by structural injuries to the alveoli (**Figure 1.2**). In this thesis, BPD refers to the 'new BPD.'

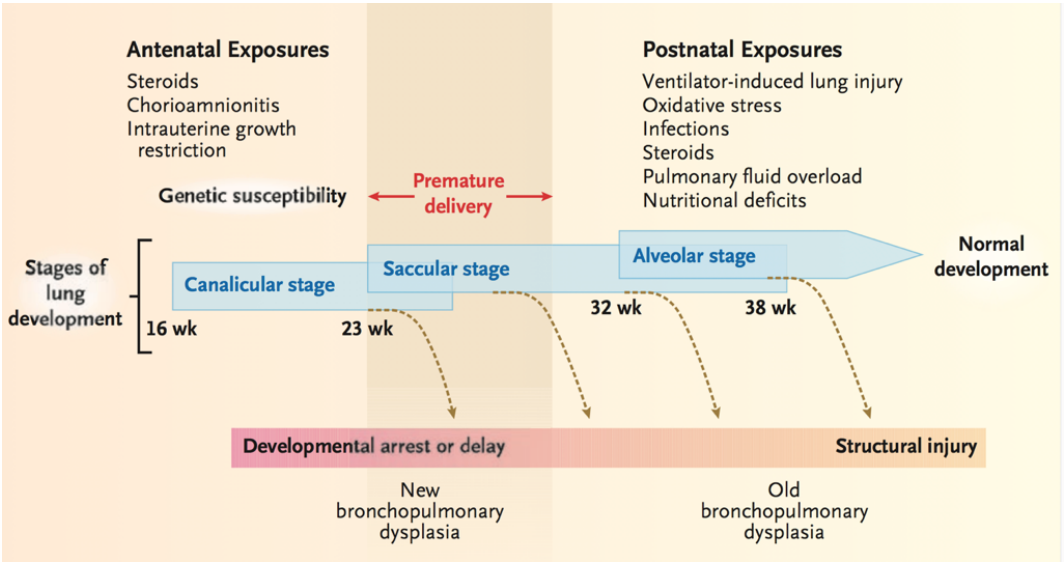

Figure 1.2. Diagram comparing 'old' to 'new' BPD over the 5 stages of lung development[1].

Although overall morbidity due to prematurity has decreased, premature birth remains a leading contributor toward neonatal mortality within the United States[12-14]. Primary prevention is thus still elusive while molecular and physiological mechanisms are lacking. Clinically, patients with BPD have a need for supplemental oxygen for at least 28 days that is determined at 36 weeks of postmenstrual age[15,16]. Of those patients, nearly 4 in 5 preterm BPD patients have secondary pulmonary hypertension (PH), which may also have higher odds of mortality (reference). Therapies for BPD neonates including those with PH are limited.

As previously stated, inflammation is central to the pathogenesis of BPD. Deregulated signaling pathways perpetuate the inflammation and recruitment of myeloid cells (e.g. neutrophils, monocytes/macrophages). The spatiotemporal signaling mechanisms that regulate lung development and pathogenesis also regulate macrophage activation. Macrophages maintain tissue homeostasis of the lung in waves of signaling networks, and disruption of this timing is frequently disrupted in pathogenesis. The regulation of macrophage activation, i.e., polarization, is crucial to maintain homeostasis yet is incompletely characterized, particularly in neonatal diseases.

Macrophage polarization refers to the degree of macrophage activation at any given time and space in a continuous, simplistic spectrum, inflammatory M1 at one end

and inflammatory-resolving or suppressing M2 at the other end[17]. Very polarized macrophages express specific genes that are minimally expressed or absent in their counterpart. On the one hand, in M1 macrophages, pro-inflammatory genes such as *Tnf*, *Il1b*, or *iNos/Nos2*, are highly expressed but almost absent in M2 macrophages. On the other hand, M2 macrophages express specific genes such as *Arg1* or *Il10* found minimally in M1. The JAK/STAT signaling pathway is important in not only lung development but also in macrophage polarization – it initiates the dampening pro-inflammatory transcription yet promotes anti-inflammatory transcription (**Figure 1.4**)[17].

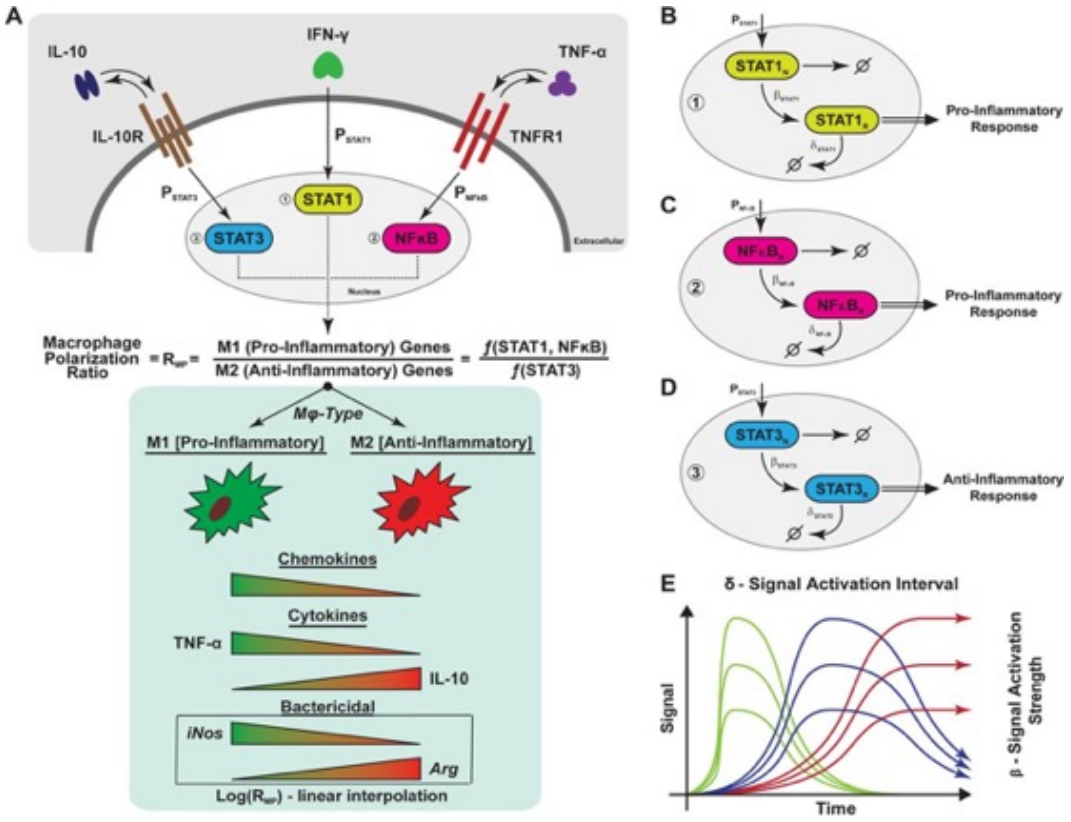

Figure 1.3. Model illustrating signaling factors that regulate the dichotomous extremes of macrophage polarization in bactericidal response. Simplified diagram depicting signaling pathways used by macrophages to cue pro-inflammatory (M1) or anti-inflammatory (M2) responses[2].

Generally speaking, STAT1 is commonly activated in macrophages soon after their encounter with a pathogenic insult, such as hyperoxia in BPD. Following STAT1 is NF-kB, and then a resolve by activation of STAT3. It is important to note that much of

what is known about macrophage activation comes from other contexts such as bacterial infection. What is known in context of lung development and BPD pathogenesis is very limited: anti-inflammatory monocytes, closely resembling M2 protect the lung from hyperoxia-induced BPD.

Many clinical studies utilizing various compounds to prevent BPD pathogenesis have been largely marginally effective[18]. Mechanisms of BPD pathogenesis remain yet unknown, especially due to an incomplete insight of how the transitions between stages of lung development are regulated. Many targets against BPD pathogenesis have been proposed but heavily have only been studied by relying on only either morphology or molecular biology. This presents a need to study the lung development comparatively to its pathogenic counterpart that encompasses an integrative approach through molecular, cellular, and physiological approaches. The evaluation of potential therapeutic targets used rescue approaches that resulted in the rescue of only certain BPD outcomes. This leaves a large scope for improvement in not only how the potential of BPD therapeutic targets are evaluated but also choosing a better target.

1.3.4 Moonlighting proteins including AIMP1

Several factors mediate the recruitment of macrophages in BPD, of which are moonlighting proteins. In 1999, Constance J. Jeffrey coined the term 'moonlighting protein' to describe a subset of proteins that have at least two independent, physiological functions which can occur simultaneously not due to either gene fusion, RNA splicing variation, or pleiotropic effects[19]. Recent technological advances in comprehensive proteomic and genetic studies have revealed hundreds of the proteins that moonlight in both homeostasis and pathogenesis[20]. For example, high-mobility group box-1 (HMGB1) can function as a DNA chaperones in the nucleus but also as both an intercellular-mediating cytokine and inflammatory mediator. Another example, and linked to HMGB1 is signal transducer and activator of transcription 3 (STAT3). It typically functions as a transcription factor of gene expression in the nucleus, but a portion of cellular STAT3 that is modified by serine phosphorylation at amino acid 727 functions as mediator of oxidative phosphorylation. This implicates the importance to comprehensively

investigate moonlighting mechanisms of a protein; in the context of lung development and pathology, moonlighting mechanisms have not been studied.

1.3.4.1 AIMP1-encoded protein, extracellular, secreted EMAP II

This thesis focuses on the moonlighting protein encoded by gene *AIMP1*. The ubiquitous gene *AIMP1* encodes for a 34 kilodalton (kDa) protein Aminoacyl tRNA Synthetase Complex Interacting Multifunctional Protein 1 (AIMP1). *AIMP1* in humans has two isoforms. One isoform generates a longer 336 amino acid form while the other a 312 amino acid protein that is conserved in mice has been linked to several cardiopulmonary pathologies[21-25]. In this thesis, AIMP1 refers to the intracellular 34-kDa protein. While many phenotypic effects of AIMP1 have been described, their mechanisms are not well understood. This underlies an importance of understanding the protein, particularly in context of recent discoveries that pose moonlighting properties. This thesis studies the undiscovered functions and mechanisms of the role of AIMP1 in lung development and pathogenesis.

From the full length AIMP1, the 23 kDa, C-terminal Endothelial Monocyte-Activating Polypeptide II (EMAP II) portion is cleaved and secreted, to which many functions have been attributed[24-31]. In this thesis, EMAP II refers to the secreted extracellular portion. EMAP II was originally described to recruit myeloid cells[32]. During normal lung development, its levels are transient, negatively correlating with pulmonary microvascularization; namely, it increases upon canalicular stage yet decreases during saccular and into alveolar stages[29,33]. It serves an anti-angiogenic function of endothelial cells by inhibiting VEGFR2 phosphorylation and integrin activation. Contrary to normal lung development, in premature lung disease, i.e. bronchopulmonary dysplasia (BPD), its levels are increased compared to age-matched controls[34]. How the increased amounts of EMAP II affect and the mechanisms that it plays during BPD is unclear. BPD will be discussed in further detail in 1.4.

1.3.4.2 Unknown role of intracellular AIMP1

AIMP1 is one of the three proteins that collectively scaffold nine tRNA synthetases and altogether make up the multi-synthetase complex (MSC). It is the only

one of the protein scaffolds that is expressed in all organisms although in varying levels[35]. Various *in silico* and structural analysis and crystal structure analysis show that AIMP1 comprises 3 domains: (1) N-terminal leucine zipper; (2) intrinsically disordered region; (3) the aforementioned EMAP II (**Figure 1.3**). Although its structure has been partly characterized, the knowledge of the function of the intracellular AIMP1 is quite limited.

Within the MSC, AIMP1 interacts pairwise with arginyl-tRNA synthetase (RARS) and glutamyl-tRNA synthetase (QARS) by way of its leucine-zipper N-terminal domain[36]. However, conflicting studies report that AIMP1 neither influences the aminoacylation activity of RARS nor alters global protein translation[36,37]. With its ubiquitous and highly conserved nature, therefore, an intracellular function is plausible to be independent of its involvement in protein translation, i.e., another moonlighting function. A recent report from Sabatini's laboratory further substantiated the plausibility: cells with deletion of QARS and RARS but not AIMP1 did not survive[38].

A previous report from Schwarz's laboratory showed that part of AIMP1 was at the cell surface membrane. The function of surface AIMP1 is not known. Its localization suggests that may interact with other components of the cell surface membrane, which include, but are not limited to, cytoskeletal proteins such as F-actin, and phosphoinositides. Phosphoinositides (PIs) represent only a small fraction of cellular membranes but are essential for a very diverse array of signaling pathways. Recent studies highlight varying subsets of PIs in physiology, playing a role in cell motility and F-actin assembly[39,40].

PIs affect cellular physiology through direct interaction with molecules on either side of the lipid membranes found throughout the cell or recruited to the membranes (**Figure 1.4**)[41]. Many interactions occur through inositide-binding protein modules, such as pleckstrin homology or FYVE domains. Recent studies have characterized lipid-interacting proteins without such inositide-binding protein modules but rather intrinsically disordered regions (IDR)[42,43]. IDRs are proteins sequences that do not conform to an ordered three-dimensional structure when expressed yet still functional. They generally lack hydrophobic amino acids as interaction with these are not favorable

and contain stretches of charged amino acids. However, its role in lung development is not known.

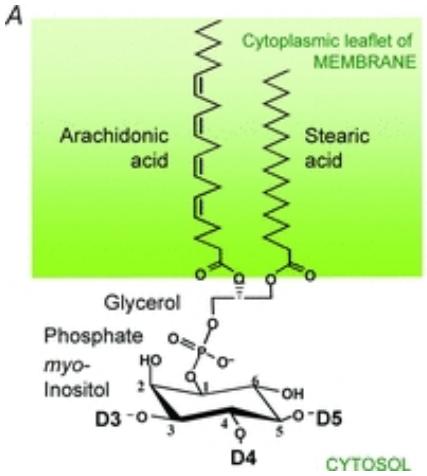

B

Lipid	Membrane	Protein domain
PI	ER & several	
PI(3)P	late endosome, MVB	FYVE(EEA1)
PI(4)P	trans Golgi	PH(OSBP)
	secretory granule	
PI(5)P	?	?
$PI(3,4)P_2$	early endosome	PH(Akt)
$PI(3,5)P_2$	late endosome	ENTH(ent3p)
$PI(4,5)P_2$	plasma membrane	PH(PLCδ1)
$PI(3,4,5)P_3$	plasma membrane	PH(Akt)

Figure 1.4. Phosphoinositides have fun. (A) Generalized structure of phosphoinositides, including 3 phosphorylated positions and a myo-inositol headgroup. (B) Location of phosphoinositides and their respective protein domains to which they interact.

1.4 Overview and Significance of the Thesis

The remainder of the thesis is divided into four chapters (**Figure 1.5**). In Chapter 2, the adapted methodology to quantify gene expression in the developing lung is discussed. The methodology found in Chapter 2 is in stark contrast with that found in many other studies: purity and integrity utilizing outdated technology, invariable amplicons lengths, and data normalization using the overabundant ribosomal subunit *Rn18s*. The adapted approach standardizes the quantification process of the developing lung using qPCR while being flexible for adjustments. Standardization of the workflow begins with the rapid freezing of the lung tissue that contains high RNase activity and then with the verification of the not only purity but also integrity of RNA. Having the highest RNA integrity is optimal, but in cases of non-ideal integrity, designing primers for short amplicon length and normalizing of the data using multiple, yet biologically independent reference genes allowed for flexibility to a certain degree. Data normalization using multiple reference genes from independent biological pathways minimizes biological and technical error. Application of this approach is to analyze angiogenic *Vegf* mRNA in the hyperoxia-induced BPD murine model.

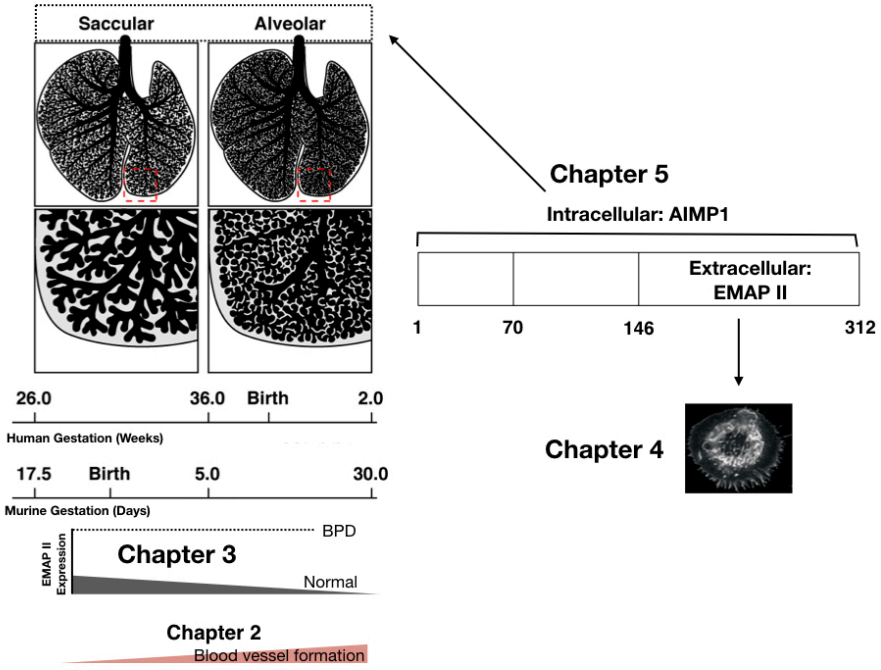

Figure 1.5. A schematic presentation depicting the aims addressed in this thesis by Chapter (see Section 1.1 Research Outlines and Aims for details). Chapter 2 addresses a minor aim of developing a tool used to quantify gene expression in lung development with an application on assess Vegf mRNA expression. Chapter 3 addresses the first aim of studying the molecular moonlighting mechanisms of elevated EMAP II in the pathogenesis of BPD using a comprehensive, integrated approach. Chapter 4 addresses the second aim of characterizing the gene expression and signaling mechanisms in macrophages exposed to EMAP II (black and white photo of macrophage, adapted from EMBO). Chapter 5 addresses the third aim of understanding the moonlighting mechanisms of AIMP1 in lung development. Adapted from Schwarz and Cleaver.

In Chapter 3, after establishing the quantitative method, the *AIMP1*-encoded protein is introduced as a therapeutic target in BPD pathogenesis. The study found in Chapter 3 address the first aim that is to study the molecular and physiological mechanisms of EMAP II during the pathogenesis of BPD. Elevated EMAP II levels in a murine model of BPD corroborate the previously identified baboon and human BPD. A series of experiments assesses the molecular, structural, and physiological mechanisms of EMAP II and its impact on BPD outcomes. In BPD, EMAP II is initially a bronchial

club-cell-specific protein-derived factor that later is expressed in galectin-3^+ macrophages as BPD progresses. EMAP II protein levels is not only increased but also sustained. The elevated and sustained EMAP II recruits galectin-3^+ macrophages, which is followed by an inflammatory state that resembles a severe BPD phenotype characterized by decreased pulmonary compliance, arrested alveolar development, and signs of pulmonary hypertension as measured by Fulton's index of right ventricular hypertrophy and elastin deposition. Neutralization of EMAP II could reverse the BPD phenotype: inflammation, recruitment of myeloid cells, alveolar simplification, and secondary pulmonary hypertension. These results are important because of its effectiveness against all BPD phenotypes, which appears to be the only study to date that does so while utilizing a comprehensive approach to assess molecular, structural, and functional outcomes. Neutralization of EMAP II protects against most outcomes of BPD more than other previously proposed targets that improve only structure or functional outcomes such as pulmonary compliance and usually without regard for secondary pulmonary hypertension.

In Chapter 4, experiments address the second aim that is to determine the molecular mechanisms in the macrophages recruited by EMAP II. The experiments arose from the results in Chapter 3 that indicate EMAP II is elevated in macrophages, including day 20 when the hyperoxic stimulus had been removed. It is unclear how EMAP II affects gene expression in the recruited macrophage and what signaling pathways are activated. The experiments utilize thioglycollate-elicited peritoneal macrophages as a generalizable model of partially activated, recruited macrophages. The study uses the elicited macrophages to measure mRNA of key functional genes in macrophages exposed to EMAP II. The transient transcription profile induced by EMAP II does not conform to the profiles that are known to be stimulated by the polarizing factors of the macrophage polarization spectrum: inflammatory, M1-inducing interferon gamma or the anti-inflammatory M2-inducing interleukin 4. A luminescence-based screen identified the activation of STAT3 by EMAP II. EMAP II activates JAK2 upstream of STAT3. Inhibition of the JAK-STAT3 signaling pathway mediates some of the EMAP II-induced gene expression profile.

In Chapter 5, the study addresses the third and final aim that is to study the role of the intracellular AIMP1 in lung development. This is addressed by using a newly generated complete knockout mouse (Aimp1 -/-). The progeny of timed heterozygous matings are at Mendelian ratios throughout embryogenesis and lung development until the day of birth. On the day of birth, the Aimp1 -/- mice exhibit neonatal lethality with mild cyanosis yet do not have significantly different wet:dry lung ratios, suggesting a lack of pulmonary edema. The morphology of Aimp1 -/- lungs remains normal until the saccular stage, when bronchial epithelial cells appear disorganized and Type I cell differentiation is significantly decreased. Immunofluorescence analysis confirmed the disruption of E-cadherin deposition and focal adhesion dependent F-actin cytoskeletal deposition when Aimp1 was ablated compared to its littermate controls.

In the final chapter, the results of the research and future directions based on the results are summarized. The successive outcomes of novel moonlighting mechnisms and applications with the aforementioned aims and extensive studies presented in this thesis sum up an important contribution to the understanding of lung development and BPD etiology in four distinctive, functional significances. *First*, it reconciles conflicting reports of *Vegf* mRNA expression while delineating a robust workflow to examine gene expression in lung development. *Second*, it identifies new molecular and physiological mechanisms of EMAP II in the pathogenesis of BPD using an integrated approach. *Third*, it uncovers new moonlighting functions of intracellular and precursor AIMP1 protein, which may aid in effective targeting of EMAP II for BPD. *Fourth*, it serves as an example of a comprehensive characterization of a moonlighting mechanism in lung development.

Chapter 2: Adapted approach of mRNA quantification in lung development

2.1 Introduction

Gene expression alters mammalian lungs during development, injury, and then recovery from either genetic or environmental defect. The genes encode products such as messenger RNA (mRNA), which can be translated into proteins that subsequently modulate the above processes. Understanding changes in gene expression is important in order to design new therapies or drugs that can alleviate developmental defects. Since it is not feasible to take lung biopsies from normal human infants, animals such as mice or cells are used to examine development and therapeutic strategies.

There are five stages of normal mammalian lung development: embryonic, pseudoglandular, canalicular, saccular, and alveolar. Gene expression differs not only across the stages but also between the cell types of the evolving lung that govern distal and alveolar regional development and functionality[6]. As lung cell type-specific mRNA fluctuates during maturation, mRNA transcript number also decreases over time[44]. Injury during development alters gene expression. Furthermore, disruption in any of the five stages generally alters distal lung development results in abnormal formation of air-exchanging alveoli growth, which usually occurs during the alveolar stage[45-49]. The gene expressions we quantify in this paper are mRNA levels. To measure these mRNA level changes, we utilize the widely used and highly sensitive quantitative PCR (qPCR) technique[50].

Proper assessment and validation of a technique is essential to obtaining robust results that minimize variation from developmental changes that occur during lung formation and sample processing. This requires validation of each of the following steps: (A) tissue handling including dissection and storage, (B) total RNA extraction, (C) total RNA purity and integrity check, and (D) data collection including primer design, and (E) data analysis.

Challenges toward optimal practice are present in lung RNA preparation. These include the time from when a sample is harvested to its storage impacting total RNA degradation. Importantly, RNase A, H, and other RNases activity in the lung make it the third highest tissue with endogenous RNase activity, only behind the pancreas and spleen. During the extraction process, lung tissue remains extremely fragile due to both the high

endogenous RNase activity and instable, single-stranded RNA structure, which tends to undergo hydrolysis reactions[51,52]. Due to these challenges, RNA integrity should be determined. Traditionally, RNA integrity was assessed from the examination of 28S and 18S bands agarose gel electrophoresis. This method has been shown to be inconsistent and subjective while providing indirect information about messenger RNA integrity[53]. An RNA Integrity Number (RIN) calculated from the Agilent Bioanalyzer 2100 represents intactness of total RNA including gradient of mRNA degradation and most ribosomal sizes including 28S and 18S[53,54]. Minimum RINs of either 4.2 or 5 have been suggested in non-lung cell types[55].

In addition, variance in qPCR can occur as total RNA in these cells and RNA type degradation rates differ. Therefore qPCR data has to be normalized to minimize the variance. A single, stable gene has not been shown to exist[56]. Therefore, identifying and normalizing by more than a single gene would help yield accurate results[56,57]. Frequently these listed validation steps in lung development and injury are not widely performed.

To our knowledge, this is the first lung development and injury paper that utilizes these steps and demonstrates consistent expression following evaluation. Here we apply and assess the steps listed above as standard practice of qPCR on a lung developmental and injury model. Genetic deletion models of either one or both alleles encoding angiogenic cytokine *Vegf-a* exhibited vascular defects and are embryonic lethal[58]. Literature using similar variants of an injury model during lung development reports conflicting magnitude and direction of *Vegf-a* expression[59-63]. We determined that implementation of strict RNA parameters for RNA integrity, purity amplicon length, and the identification of stable candidate reference genes enhanced qPCR consistency and reproducibility. For normalization of data, reference genes that were independent of each other regarded biological function and chance of bias were identified; they were used in other lung development and injury studies[64,65]. Six candidate genes, *Rpl13a*, *Hprt*, *Ppia*, *Eef2*, *Gapdh*, and *Rn18s* were evaluated for their use as reference gene in normalization. In contrast to the contradictory *Vegf-a* expression when normalized to the least suitable housekeeping genes, application of this filter and normalization to most suitable three housekeeping genes, *Hprt, Eef2*, and *Rpl13a,* gave reproducible *Vegf-a* expression thus corroborating the sample filter. Finally, we show that applying these steps listed above in

the developing lung, we can circumvent the limitations of qPCR and decreased error amplification when comparing the uninjured to injured developing lung.

2.2 Materials and Methods

Developmental Oxygen Injury Mice Model

C57BL/6 mice were housed in twelve hour light-dark cycles according to the Institutional Animal Care and Use Committee approved protocol. Beginning on postnatal day 3, pups were exposed to either 21% oxygen (normoxia) or 85% oxygen (hyperoxia) until day 15, $n = 6$ and $n = 6$, respectively. Mice dams were kept with their brood until postnatal day 4, when they were subsequently exchanged between normoxia and hyperoxia every 24 hours to prevent oxygen toxicity.

Lung Organ Harvest

Pups were humanely euthanized, their lungs excised within three to five minutes directly into Eppendorf tubes, snap frozen immediately in liquid nitrogen, and stored at -80 degrees Celsius for up to one and a half years before analysis.

Primer Design and *In-silico* Validation

Primers were designed on IDT or Primer3. Primers were designed to span introns toward 3' end whenever possible, to amplify 65-160 base pair products of gene targets, and have little secondary structures. To check *in-silico* product specificity and secondary structure, primer sequences were entered in NCBI Primer-BLAST for product with no mismatches followed by mFold, respectively.

Experimental Primer Validation

The template to determine primer efficiencies was pooled single-stranded cDNA diluted by either ten-fold for reference gene candidates or four-fold for *Vegf-a*. All of the primers had single melt peak curve and single band when run on 2% agarose gel in TAE (data not shown).

RNA isolation

A coronal section through both the right and left lung was made to include lung tissue from the same plane. The lung cuts weighed about fifteen milligrams and were suspended in TRIzol (Invitrogen Cat. No. 15596-026). The tissue in TRIzol was then

homogenized in BBX24 Bullet Blender (Next Advance). The aqueous portion of tissue homogenate was transferred to a Qiagen RNeasy Mini Column (Qiagen Cat. No. 74104). Total RNA was isolated from the tissue homogenate according to manufacturer's protocol. RNA was eluted from the column in 40 microliters of nuclease-free water (Ambion Cat. No. AM9937).

RNA Purity then Quality Assessment

Nanodrop 2000 Spectrophotometer was used to measure UV absorbance ratios of both 260 nm/280 nm and 260 nm/230 nm, which are expected to be nearly 2 for pure RNA. One microliter of eluted RNA was diluted in four microliters of nuclease-free water. Two microliters of the diluted RNA was used for spectrophotometer reading.

Quality was assessed by running two microliters of the diluted RNA samples on RNA Nano Chip of Agilent Bioanalyzer 2100. The output of the Bioanalyzer is an RNA integrity number (RIN) from scale of 1-10, 1 predicting complete degradation of RNA and 10 predicting no degradation.

cDNA synthesis

500 total ng of each total RNA sample (150 ng/uL) was reverse transcribed by 200 U of SuperScript III (Cat. No. 18080-044) reverse transcriptase in 20 microliter reaction volume containing 5X First Strand Buffer, 50 ng of random hexamers (Cat. No. N808027), 40 U RNaseOUT (Cat. No. 10777-019), 0.1 M DTT, and water.

Quantitative Real-Time Polymerase Chain Reaction (qPCR)

Reverse transcribed cDNA template was diluted in nuclease-free water to a concentration within the 95-106% primer efficiency range determined. Two microliters of this diluted cDNA template was mixed with either 200 nM of each reference gene forward and reverse primer or 100 nM of each *Vegf-a* forward and reverse primer, 2X SYBR Master mix (ABI Cat. No. 4472908), and nuclease-free water to make a twenty microliter reaction volume. A no-template control was run along with these reactions. Reactions were run in technical triplicates on ABI StepOnePlus machine at 50°C for 2 minutes,

95°C for 2 minutes, and 40 cycles of 95°C for 15 seconds and 60°C for 1 minute. Following the run, melting curves were run at ramp rate of 0.2°C per second, obtaining single peaks for all products. Products were run on 2% agarose gel dissolved in TAE buffer to verify the expected amplicon size. These steps took into account the MIQE Guidelines[66].

geNormPlus algorithm

The algorithm premise is that for two genes to be an ideal reference, the expression ratio between them would be the same in all samples. Beginning from a gene pair, the V value is calculated by standard deviation of the ratio of two genes in all samples, followed by inclusion of a third gene, and so on. After including a certain number of genes, the V value would increase since the genes with more variance would be incorporated. The number needed for normalization would be the number of genes included before the V value significantly increased. For a final variability value of expression among samples, the M value is an arithmetic mean of all V. Since the lowest V value indicates lowest standard deviation of ratio, the genes with lowest M values are less deviating thereby more stable than the others[67].

Data Processing

Quantification cycles (Cq) are discrete logarithmic values obtained during exponential phase of time continuum when signal is above background threshold. There is a linear relationship between two logarithm scale Cq values. Residuals with Lowess smoothing were plotted to verify linear relationship. After assessing the relationship, Spearman rank correlation coefficient was determined to assess correlation between efficiency-corrected Cq values of all candidate reference genes. For *Vegf-a* expression analysis, calibrated relative quantity values (CNRQ) were calculated, which were normalized to one, two, or three reference genes' relative quantity.

A previous study indicated that mRNA transcripts generally approach normal distribution after log-transformation[68]. CNRQ values were transformed by factor of log base 2 in

order to approximate normal distribution. Base 2 was chosen to represent the doubling of PCR product.

Frequentist Statistical Analysis

All tests were chosen a priori having noted that the sample population was too small (i.e. less than 20) to accurately determine any sample distribution. In approximate log-normal distribution, geometric means of normoxia and hyperoxia *Vegf-a* CNRQ were calculated followed by parametric, unpaired t-test. Log-transformation generally minimizes differences in variance; Lowess smoothing lines of the residuals plotted were fairly flat (shown in results, Figure 2.4A). Together these can satisfy the assumption that there are relatively equal variance within each normoxia and hyperoxia distribution. The satisfied assumptions for the unpaired two-sample t-test of *Vegf-a* levels were that: (a) log transformed CNRQ values of both normoxia and hyperoxia sample distributions were approximately normal, (b) these sample populations were independent, and (c) log-transformed variance was relatively equal. Type I error, α level, was set at 5%, before the study. The null hypothesis for the unpaired t-test that there is no difference of means between normoxia and hyperoxia was rejected when p-values were less than the pre-set α level; these mean comparisons were then considered statistically significant. Bootstrapped 95% confidence intervals were calculated from geometric mean by sampling 10000 times with replacement from sample distribution.

qBase^{Plus} Software was used for analysis. Analysis verification followed by plotting was performed using Python 2.7.

2.3 Results

Characteristics of Selected Genes Studied

Six genes with known biological functions in lung development and injury literature were selected as candidates for the normalization step of qPCR data analysis (Table 2.1). Qualifications as a normalization gene included each gene to have independent biological function to reduce the possibility of co-regulation of each other

thereby minimizing variation in normalization step. A literature search did not result in any papers suggesting co-regulation among these six genes.

Validating Similar Primer Efficiencies and Specificity

After gene selection, primers were designed to target these genes efficiently and specifically as possible during qPCR (Table 2.2). To check primer efficiency, known quantities of cDNA were serially diluted and plotted against the quantification cycle (Cq) that was measured by qPCR (not shown). Cqs, the qPCR output, are the number of cycles needed for the signal measured from theoretical, ideal doubling of transcript amplification to cross a set threshold over set time, making Cqs a discrete value. They indirectly represent transcripts per input, and as a result, lower Cqs can be interpreted as higher abundance of transcripts. Thus the Cq magnitude is limited by the signal measured from transcripts. Primer efficiencies are measured to check not only how specific and well primers bind to a template, but also the limits of signal. Efficiencies calculated from the slope of these plots were close to 100%, with the range being 95 – 106%, well within the generally suggested 90 – 110% range. After qPCR, melting curves of the products were run. There was one peak, suggesting specificity (data not shown). In addition to melting curves, the products were run on agarose gel and visualized to check for one expected-size product (data not shown). Amplicons were predicted by using Primer-Blast and UCSC in-silico PCR. Together these results show specific products.

Highly Pure RNA Did Not Suggest High Integrity of RNA

Having evaluated primers to be used for qPCR, RNA was extracted from the lung tissues. Both 260/280 and 260/230 absorbance ratios of the extracted RNA were assessed by Nanodrop 2000 Spectrophotometer (Table 2.3). Only 260/280s ratios are generally reported in literature for qPCR since obtaining 260/230 ratios near 2.0 can be dependent on tissue type. But for this study, both ratios are greater than or equal to 2.0, indicative of pure RNA. Although the RNA was pure, the ratios do not reflect integrity[53]. Table 2.3 shows RIN of all samples with the integrity of normoxia RNA samples being 5.0 ± 0.3 and hyperoxia RNA samples 8.3 ± 0.1 (arithmetic mean ± standard error of mean).

Expression Distributions of Candidate Reference Genes

Following total RNA extraction, total RNA purity and integrity check, we performed qPCR to compare mRNA levels in uninjured and injured lungs of newborn mice. Including multiple lung samples per group minimized biological variability. Three technical replicates per lung RNA sample minimize variability of the Cq reading by qPCR. The arithmetic average of the three technical triplicate Cqs of each sample represent a single lung sample. A single Cq representing a single sample were then plotted to assess the overall distribution (Figure 2.1A**)**. The width of the violin plot indicates the number of Cq values at a certain magnitude while the length reflects the Cq range. The width increases around 24 Cqs for *Rpl13a* representing multiple lung samples having similar transcript abundance. The Cq magnitude of one gene, *Rn18s*, is about 10-15 lower then the other 5 genes. PCR theoretically doubles input, so this indicates that Rn18s, a ribosomal RNA, is about 2^{10} - 2^{15} fold more abundant than the other transcripts; this holds true because ribosomal RNA, the most stable of all the RNA's, comprises most of the total RNA that was reverse transcribed.

The RIN of three samples were less than the suggested RIN cutoff of 5, which indicated degraded RNA (Table 2.3). When RNA samples with an integrity RIN of less than 5 were then excluded, (Figure 2.1B shows the average Cq values following the exclusion), the Cq distribution of *Eef2*, *Hprt*, *Ppia*, and *Rpl13a* all look similar while *Gapdh* does not. There was little change in distribution of Cq values of *Rn18s*. Not only was *Rn18s* overabundant relative to mRNA, but also was not reflective of RIN, meaning any genes normalized to *Rn18s* would be overestimated. Plots of Cqs grouped by oxygen levels show that the lower RIN, degraded RNA samples were in the normoxia group (Figure 2.1C, D).

Two Genes Sufficient, But Three Best for Normalization Across Oxygen Injury in Newborn Mice

Acquiring any lung tissue and then RNA extraction from tissue takes precious time, money, and effort, requiring cost-effective accuracy in analysis. So the least number of genes sufficient for accurate normalization is important, which was determined by *geNormPlus* algorithm's V value. This V value, further defined in Methods, represents

the standard deviation of ratio between a minimum of two genes and three genes. The suggested V value cutoff is 0.15[57]; but this value should be empirically determined. If the V value increases as one gene is included in the comparison, then the included gene adds deviation. Thus, it is better not to include the gene. V values are plotted in Figure 2.2A and 2.2B. Both before and after RIN-based exclusion, the V values of 2/3 and 3/4 reference genes were relatively similar (shaded bars). Before and after RIN-based exclusion, the V value gradually increased as additional genes were included. From this analysis, a minimum of two reference genes are needed since inclusion of the third candidate gene did not greatly alter V value. The two reference genes were determined by the *geNormPlus* M values, with a low M value correlating with the least deviation while the highest value has both the greatest variation and the least reliability.

Eef2, Hprt, and Rpl13a Expression Exhibit the Most Stable M Values After Oxygen Exposure

In contrast to the marked variability of *Rn18s* and *Gapdh* M values, *Hprt*, *Eef2*, and *Rpl13a* had the lowest three M values among the tested reference genes across normoxia and hyperoxia (Figure 2.2C and 2.2D). Even after excluding samples with RIN less than 5, *Hprt*, *Eef2*, and *Rpl13a* remained the most stable gene set. Note that before and after exclusion, M values of the three genes are close. This suggests that a gene of interest normalized to any of the three would be very close, and collectively, all three would provide the most accurate normalization. If the two genes are the best reference genes for normalization, strong correlation between Cq values can be observed. Cq values are on logarithmic scale; when two logarithmic scale values are plotted against each other, there usually is a linear relationship. To verify that there was a linear relationship between Cq values, residuals of one reference gene mean was plotted against another reference gene's Cq values were plotted along with Lowess smoothing (Figure 2.3A and 2.3B). Most of the Lowess smoothing of the residuals was generally flat, suggesting that there is linear relationship; however, as seen in residual plot of *Rn18s* against *Rpl13a*, Lowess smoothing was not flat. Since not all relationships were linear, correlation between all pairs of reference genes was determined by rank-ordered Spearman correlation coefficient (Figure 2.4A and 2.4B). Of all Cq correlation pairs

between reference genes in all samples, the largest correlation coefficient was between the two most stable reference genes, *Rpl13a* and *Eef2* ($\rho = 0.99$, $p < 0.001$). The smallest correlation coefficient was between the two lowest ranked reference genes, *Rn18s* and *Gapdh* ($\rho = 0.17$). Based on these results, *Rpl13a* and *Eef2* were the two genes used for normalization for further qPCR studies.

Vegf-a Expression Decreases in Hyperoxia-Exposed Newborn Lungs When Normalized to Eef2, Hprt, Rpl13a

Previous studies do not show consensus of *Vegf-a* expression in the newborn model of hyperoxia with these studies relying on a single reference gene for normalization (2, 18, 25, 28, 29). For our study, *Vegf-a* expression was normalized to three, two, or one reference genes. *Vegf-a* expression was normalized to *Hprt*, *Rpl13a*, and *Eef2* in order to calculate relative quantities. The relative quantities of individual samples in both normoxia and hyperoxia groups were similar (data not shown). Comparing the relative quantities in normoxia against hyperoxia resulted in 3 fold down-regulation ($p < 0.001$). In agreement with normalizing to three reference genes, when normalized to two genes, *Eef2* and *Rpl13a*, there was still a 2.98 fold down-regulation in hyperoxia compared to normoxia ($p = 0.001$). Even after filtering samples with RIN less than 5, *Vegf-a* expression decreased.

Vegf-a Expression in Opposite Direction When Normalized to Rn18s

When *Vegf-a* was normalized to single, lowest ranked *Rn18s*, there was 2.2 fold up-regulation in hyperoxia relative to normoxia (Figure 2.5, $p = 0.099$). Although this up-regulation was not statistically significant at our *a priori* set alpha level, this shows a trend that is completely opposite to the direction when normalized to highest ranked *Hprt*, *Rpl13a*, and *Eef2*. Importantly, when samples with a RIN of less than 5 were excluded and normalized to Rn18s, there was reversal in *Vegf-a* expression where a 0.07 fold down-regulation ($p = 0.5563$) was determined. In contrast to normalizing expression by *Rn18s*, after samples with RIN less than 5 were excluded, *Vegf-a* expression normalized to *Hprt*, *Rpl13a*, and *Eef2* was still statistically significantly down-regulated

by 2.2 fold (p = 0.006). When normalized to *Rpl13a* and *Eef2*, there was 2.1 fold down-regulation (p value = 0.01).

2.4 Discussion

qPCR remains widely used as an economical technique to determine and verify selected mRNA expression for its high sensitivity[69,70]. Due to the high sensitivity of this technique, we adapted and assessed the steps involved in qPCR to compare transcript levels in uninjured and injured developing lungs. Based on high RNase activity, RIN of the lung RNA was measured.

We then sought a way to minimize the impact of inferior RIN. Previous studies showed that on one hand, amplicons greater than 400 base pairs were affected by loss of RNA integrity and suggested using samples with RIN greater than 5. On the other hand, less than 400 base pair amplicons were minimally affected by RIN[71,72]. Not only would primer efficiency be minimally affected, but also amplicon length would be helpful to obtain consistent primer efficiency followed by accurate evaluation of gene expression[54,72]. Based on the RIN of our samples, primers were designed to generate amplicon lengths of 65-160 base pairs long, which is much less than the 400 base pairs suggested. This primer validation step is one of many that are known to influence cDNA transcription. Other examples include, but are not limited to, the reverse transcription of RNA to cDNA and priming strategy[73,74]. No reverse transcriptase or priming strategy is perfect. This study used random hexamers; oligo dT's are an alternative that could be used for isolated poly-A^+ mRNA. On one hand, poly-A^+ mRNA enrichment followed by reverse transcription that includes oligo dT's can increase signal to noise ratio in qPCR. On the other hand, during the enrichment process, there is possible loss of poly-A^- tail RNA such as deadenylated mRNAs and nuclear mRNAs or 3' bias of mature mRNAs that may of interest. Either case adds additional steps of technical variability.

This study used these validated primers to determine *Vegf-a* expression in hyperoxia relative to normoxia. Intra-group relative quantities of *Vegf-a* were similar suggesting precision despite three samples with RIN below 5. In addition to comparing relative quantities, inter-sample variability was assessed. Bootstrapping the 95% confidence interval of *Vegf-a* expressions implies a lower and upper bound into which the mean will fall in 95% of the time. By applying this bootstrap, when normalized to the

three reference genes, all normoxia samples overlapped with the confidence interval of RIN-based excluded samples ($p = 0.999$). No statistically significant difference between the mean expression of all hyperoxia samples and the RIN-based excluded samples ($p = 0.09$) was identified. Similar to expression normalized to the three genes, when normoxia samples were normalized to a single gene- *Rn18s*, there was no difference in *Vegf-a* geometric mean expression ($p = 0.999$). However, in hyperoxia samples, there was statistically significant decrease in the *Vegf-a* geometric mean expression ($p < 0.00001$) when normalized only to *Rn18s*. This is in direct contrast to the findings when normalized to the three idyllic reference genes. This suggests that normalizing to experimentally evaluated, idyllic reference genes reduces the inter-sample variation of *Vegf-a in* the hyperoxia samples even with RIN variation. Furthermore, without adequate and reliable genes for normalization, obtaining a robust and accurate interpretation of the impact of hyperoxia on *Vegf-a* expression would be difficult. Not only is there a difference in the mean expression in hyperoxia between RIN filtered samples, but also *Vegf-a* expression was contradictory when normalized to a single gene (*Rn18s*) compared to the three stable reference genes. These findings suggest that variable RNA integrity, amplicon size, and lack of adequate genes for normalization have given rise to reports conflicting in magnitude and direction of *Vegf-a* expression using similar variants of an injury model during lung development. Based on these results, although a strict RIN cutoff of 5 was set, both generating 65-160 base pair amplicons and finding the best reference genes to normalize to minimized the effect of RNA integrity on means of *Vegf-a* expression.

Proper normalization was possible by evaluating genes with independent biological functions. A dependent function between two candidate reference genes could mean co-regulation, producing a multiplicative error if normalized by these genes. Applying the geNorm algorithm requires an assumption of genes having independent biological function for valid results.

The six candidate genes were chosen since their biological functions in cells are known and used in other fields. Tools such as *RefGenes* were used to scour public access microarray data to propose genes that are similar in expression signal to a gene of interest[75]. However, there was limited knowledge of function for many of the genes,

making it difficult to assess independence of biological function. Verifying independence of biological function of any candidate reference gene is difficult when RNA amounts obtained are small. For example, one of the six candidate reference genes *Eef2*, translational function is predominantly based on phosphorylation. Hyperoxia has been speculated to stimulate phosphorylation of Eef2 protein[56]. However, in Ross et al.'s cell culture model, neither mRNA transcript levels were examined nor total Eef2 protein levels change[56]. No other literature suggests hyperoxia affects *Eef2*. Based on the known biological function of *Eef2* and our data suggesting that *Eef2* transcript levels were not affected by hyperoxia, it was used as a reference gene.

While *Eef2* was used as reference, *Gapdh* and *Rn18s* were not because they were the two least stable genes. This finding corroborates with lung-based literature that suggest *Gapdh* is affected by oxygen level, and this has not shown in any lung development models. For example, hyperoxia has been shown to disrupt glycolysis, including *Gapdh* levels, while hypoxia can stimulate HIF-1, which in turn activates *Gapdh*[76-78]. In contrast to *Gapdh*, *Rn18s* levels have not been shown to be regulated by oxygen levels. However, *Rn18s* was still unstable across all samples. Two possible reasons that *Rn18s* was most unstable despite smallest Cq range are (a) overabundant *Rn18s* ribosomal RNA transcript levels would not correlate with mRNA levels in a given lung sample since there are different number and types of cells. Within each cell, about 80% in a total RNA population is ribosomal RNA, of which 18s ribosomal RNA comprises about 20%; there is about 1-3% of mRNA in total RNA population. The exact same area of lung cannot be sampled, especially in clinical tissue, meaning that there will be variable number of cells being sampled. Less confidence can be made about normalizing to such an abundant transcript that correlates with neither mRNA levels nor RNA integrity. (b) By using same input cDNA amount for qPCR to quantify gene expression, Cq values of *Rn18s* was invariably much lower than the other mRNA genes. Describing changes in lower transcript mRNA levels would be less sensitive if *Rn18s* is used for normalization, which is especially true for samples with non-ideal RNA integrity. *Rn18s* represented ribosomal RNA component and would be the last of the RNA types to undergo degradation. Furthermore, RNA Polymerase I reverse transcribes *Rn18s* whereas RNA Polymerase II reverse transcribes messenger RNA. The listed

reasons above are in contrast to the ideal characteristics of reference genes, which include, but are not limited to, most closely reflecting the mRNA transcript stability fo the gene of interests, levels, and reverse transcription enzyme; this is to further minimize any variance during the qPCR steps.

Rigorous measures must be employed for validation of RNA integrity. Quantification must include multiple reference genes: using a single gene is highly likely to yield inaccurate results. Failure to include multiple genes yields conflicting results, as we have shown in the case of *Vegf-a*. In our study, normalizing with both *Rn18s* and *Gapdh* resulted in means that were outside bootstrapped 95% confidence intervals of means generated from normalizing with any of the other stable genes i.e. *Hprt*, *Rpl13a*, *Eef2*. These findings further suggest that normalizing with more than one but up to three genes i.e. *Hprt*, *Rpl13a*, *Eef2* result in accurate fold change.

Our study suggests meaningful PCR results can be obtained despite non-ideal RNA in lung development. The criteria for meaningful and reproducible qPCR results in lung tissue should include optimization of RNA integrity, both amplicon size and primer location, and analysis including idyllic, appropriate rigorously assessed reference genes. By following these criteria, this rigor minimized the effect of non-ideal RNA integrity typically found in lung-derived RNA.

2.5 Figures and Tables

Candidate reference gene name	Gene Symbol	Accession Number	Function
Ribosomal 18S	*Rn18s*	NR_003278.3	Structural component of 40S ribosomal subunit
Glyceraldehyde-3-phosphate dehydrogenase	*Gapdh*	NM_002046	Catalyzes reduction in sixth step of glycolysis
Hypoxanthine guanine phosphoribosyl transferase	*Hprt*	NM_013556	Catalyzes purine salvage pathway
Eukaryotic elongation factor 2	*Eef2*	NM_007907.2	Promotes translocation of growing protein peptide during translation
Cyclophilin A	*Ppia*	NM_021130	Promotes protein folding
60S ribosomal protein L13a	*Rpl13a*	NM_009438.5	Structural component of 60S ribosomal subunit

Target Gene	Gene Symbol	Accession Number	Function
Vascular endothelial growth factor-A	*Vegf-a*	NM_001025250.3 NM_009505.4 NM_001025257.3 NM_001110266.1 NM_001110267.1 NM_001110268.1	Structural component of 40S ribosomal subunit

Table 2.1. Candidate genes for the normalization step of qPCR data analysis

Gene Symbol	Sense Primer Sequence	Antisense Primer Sequence	Length (bps)	Efficiency	Slope	L.O.D. (Cq)	T_a (°C)	T_m (°C)
Eef2	ACATTCTCACCGACATCACC	GAACATCAAACCGCACACC	135	1.992	-3.34	39.4	60	83.8
Gapdh	CAGAGGCCCTATCCCAACTC	GGTCTGGGATGGAAATTGTG	65	2.000	-3.27	36.5	60	80.6
Hprt	CCCCAAAATGGTTAAGGTTGC	AACAAAGTCTGGCCTGTATCC	76	1.952	-3.44	37.9	60	78.6
Ppia	GCAGACAAAGTTCCAAAGACAG	CATTATGGCGTGTAAAGTCACC	139	2.060	-3.28	36.9	60	79.9
Rpl13a	TCCCTCCACCCTATGACAAG	GTCACTGCCTGGTACTTCC	136	1.999	-3.44	37.9	60	84.7
Rn18s	AAACGGCTACCACATCCAAG	CCTCCAATGGATCCTCGTTA	155	1.995	-3.33	21.2	60	83.2
Vegf-a	TCTCCCAGATCGGTGACAGT	GGCAGAGCTGAGTGTTAGCA	71	1.961	-3.42	36.4	60	76.2
Length	Amplicon Length							
bps	Base Pairs							
L.O.D	Limit of Detection							
T_a	Primer Annealing Temperature							
T_m	Amplicon Melting Temperature							

Table 2.2. Primers designed to target selected genes

	RIN	260/280	260/230
Normoxia	3.2	2.0	2.2
	5.3	2.0	2.4
	7.4	2.0	2.3
	3.5	2.0	2.2
	4.6	2.0	2.3
	5.9	2.0	2.1
Mean ± S.E.M.	5.0 ± 0.3	2.0	2.2
Hyperoxia	7.5	2.0	2.0
	8.8	2.0	2.4
	9	2.0	2.0
	8.1	2.0	2.1
	8.4	2.0	2.3
	8.2	2.0	2.4
Mean ± S.E.M.	8.3 ± 0.1	2.0	2.2

Table 2.3. RINs and absorbance ratios of lung samples. S.E.M: Standard error of mean.

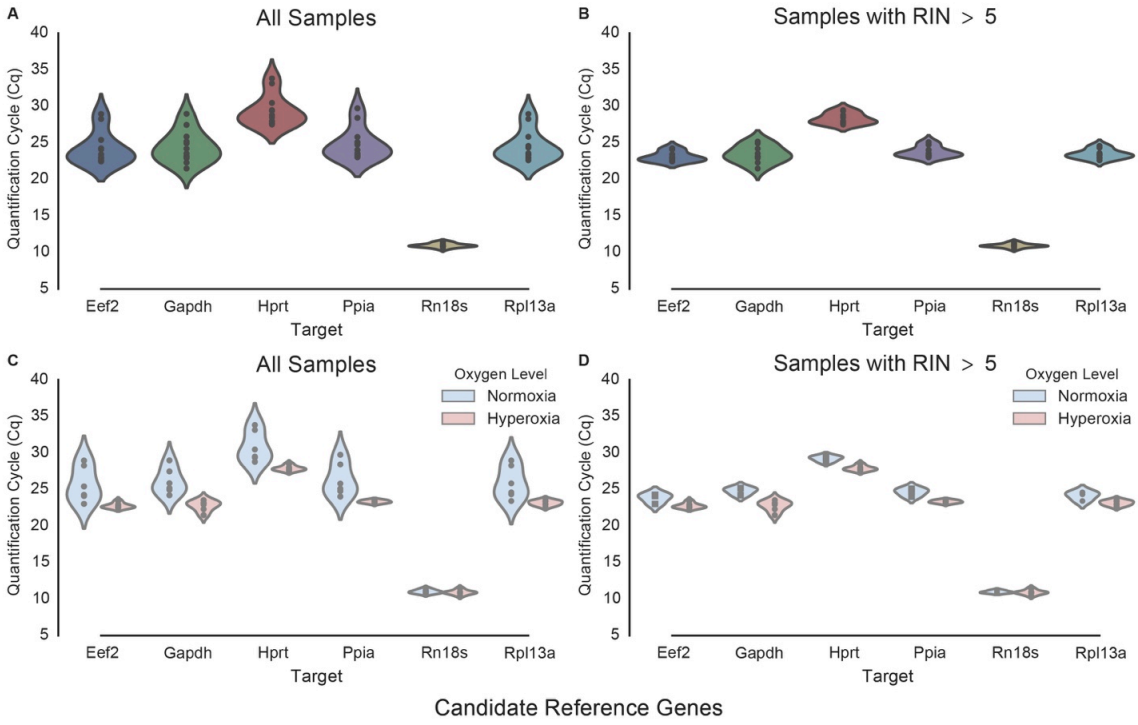

Figure 2.1. Quantification cycle (Cq) distribution reflecting differences in mRNA integrity, tissue heterogeneity and reverse transcription efficiency, which are reflected in *Eef2*, *Hprt*, *Ppia*, and *Rpl13a* but reflected in neither *Rn18s* nor *Gapdh*. The violin plots above show Cq data points of the six candidate genes in alphabetical order while representing both the density and spread of Cqs. The width of the plot for each gene changes based on Cq density while the height indicates the spread of the Cqs. (A) Cqs of all samples show are generally clustered together, except for the two or three apical points representing individual samples that are distant from the cluster, which can be reflected by its integrity (n = 12). Due to ribosomal transcript overabundance relative to mRNA population, Cqs of *Rn18s* are much lower while showing minimal difference after removing samples with RIN greater than 5. Gapdh has a longer spread and less clustering of Cqs compared to *Eef2*, *Hprt*, *Ppia*, and *Rpl13a*, and can be attributed to reasons including the differences in integrity, heterogeneity of lung tissue sampling, or reverse transcription efficiencies. (B) Three samples with RIN less than 5 were excluded, *Eef2*, *Hprt*, *Ppia*, *Rpl13a* all exhibit similar distributions whereas Gapdh maintains the largest spread while Rn18s does not appear to change at all (n = 9) suggesting that *Rn18s* does not reflect the change in mRNA. In (C), Cqs are grouped by oxygen levels, normoxia and hyperoxia. As mentioned before in (A), the apical points are samples in normoxia and are much more clustered once removed as seen in (D).

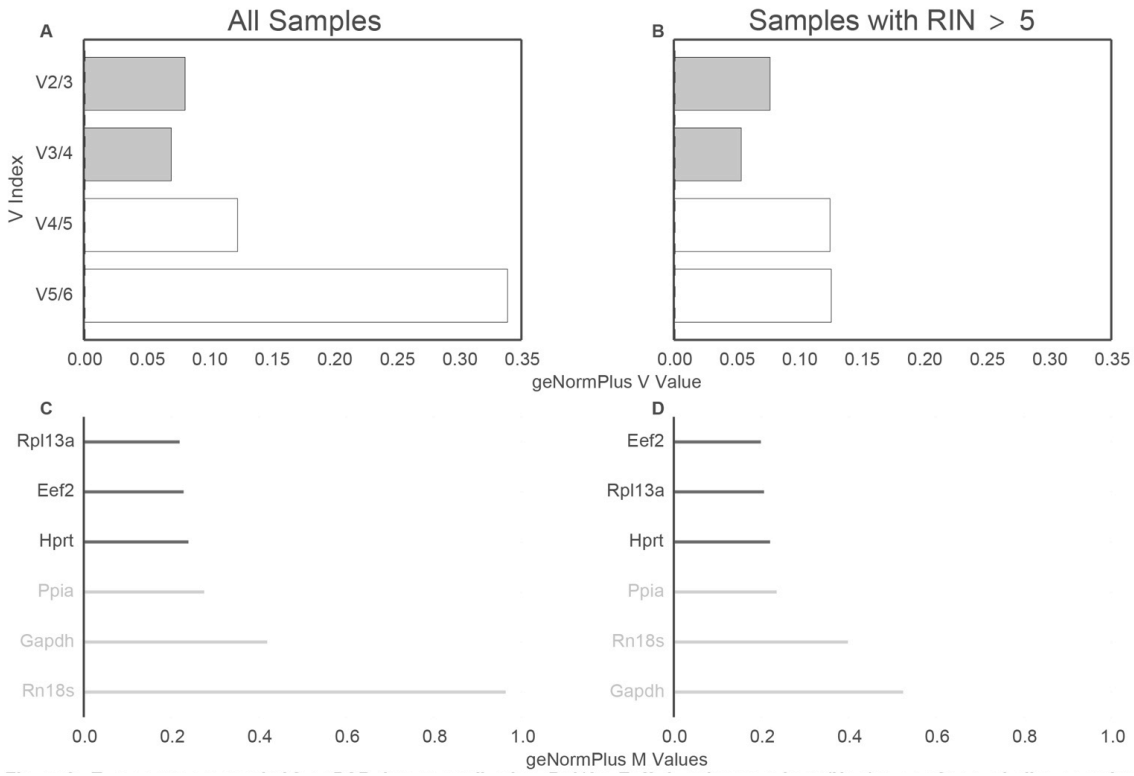

Figure 2.2. Determination of the required number of reference genes for quantitative PCR (qPCR) data normalization related to RIN. Two genes are needed for qPCR data normalization, *Rpl13a*, *Eef2*, but three are best (*Hprt*) even after excluding samples with RIN less than 5. The required gene numbers are based on V value, which is the standard deviation of ratio between expression of two and three reference genes, three and four, and so on, in all samples. This increases as less stable genes are incorporated. After determining the gene number required for normalization, genes ranked by geNormPlus M Value. A similar value indicates less variation among the compared genes. (A) Two or three genes are needed since V increases once a fourth gene is incorporated, which are shaded above. There is clearly a fifth gene that greatly increases this value with respect to the others. (B) By excluding samples with RIN greater than 5, the discrepancy between including and not including a fifth diminishes. (C and D) The two or three genes that can be used for normalization are the three highest ranks, namely *Rpl13a*, *Eef2*, and *Hprt*. The two genes that remain as lowest ranks are *Gapdh* and *Rn 18s*.

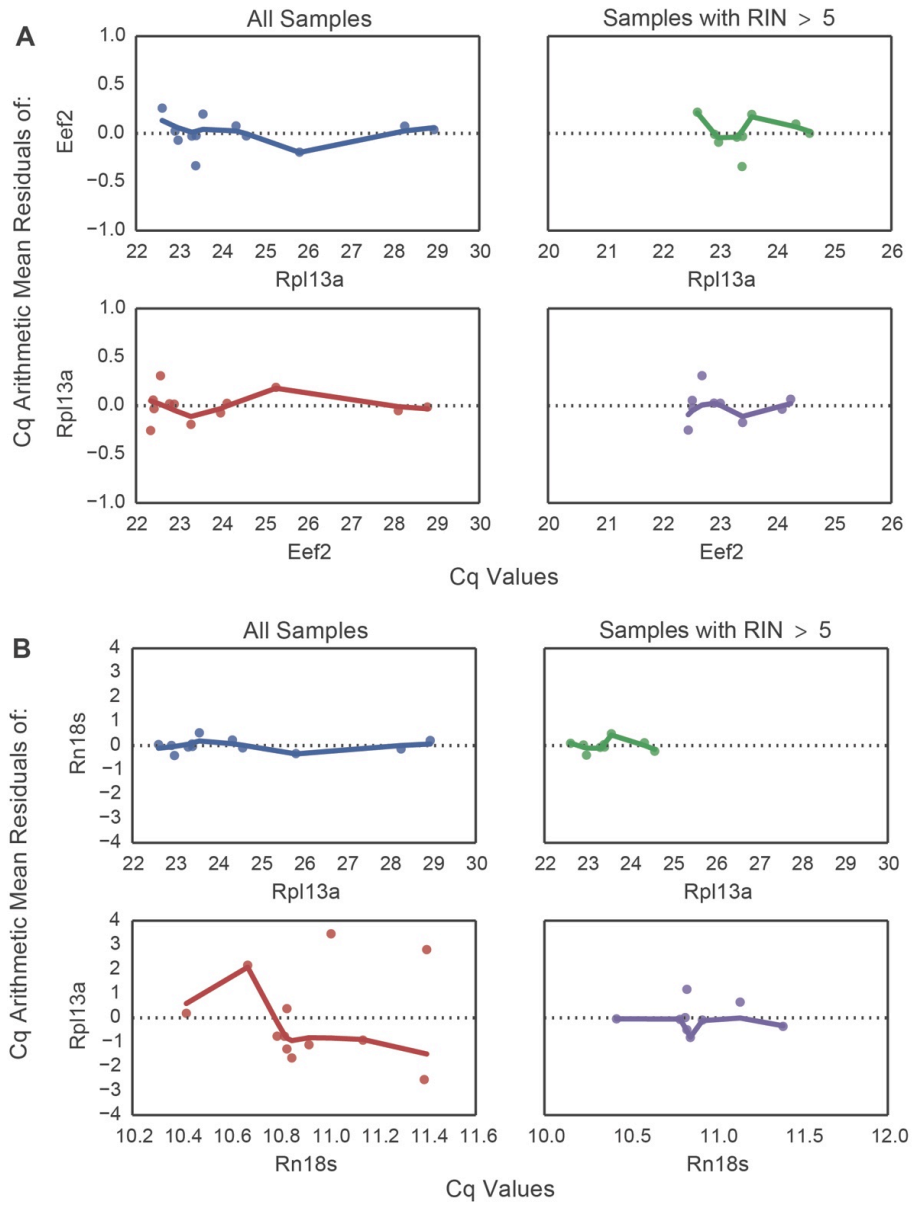

Figure 2.3. Lowess smoothing of residuals depicting variance between reference genes. *Eef2* and *Rpl13a* demonstrate a strong linear relationship supporting their efficacy as reference genes. Lowess smoothing of residuals between two stable genes will be mostly a flat, straight line, which means that there is a strong linear relationship. Cqs are logarithmic and the relationship between two logarithmic values can be linear. To test this, examples of the residuals are shown. (A) Residuals between the two highest ranked genes *Eef2* and *Rpl13a*, vice versa form a nearly flat line. In contrast, (B) there are sharp peaks, exhibiting a non-linear pattern between lowest-ranked *Rn18s* and *Rpl13a*. Since there was still a general trend of liner relationship, this suggested preference for a rank-based test, i.e., Spearman correlation test, over a non-ranked based Pearson correlation test.

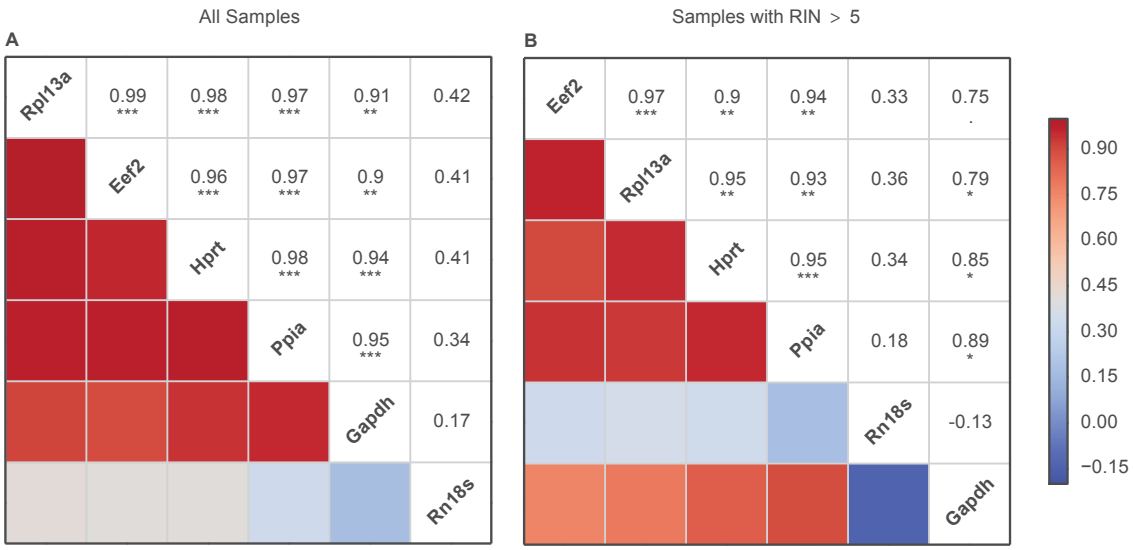

Figure 2.4. Correlation coefficients and M values. *Rpl13a* and *Eef2* demonstrate the highest correlation coefficient and the lowest M value and are the most stable reference genes for normalization in qPCR of newborn lungs exposed to hyperoxia. A permutation test that samples Cq values from each gene was performed to test statistical significance against the null hypothesis that there is zero correlation. Shown above are correlation plots of efficiency-corrected Cq between every candidate gene pair. Genes are listed in ascending order of the M value rank found in Figure 2.2, *C* and *D*. In all samples, the highest Spearman correlation coefficient was between *Rpl13a* and *Eef2* ($\rho = 0.99$, $^{***}P < 0.001$) whereas the lowest was between *Rn18s* and *Gapdh* [$\rho = 0.17$, not significant (n.s.)]. The highest correlation coefficients suggest the stability of the 2 genes for normalization; thereby the 2 genes are most appropriate for normalization. *A*: in Cqs of all samples, correlations between the 2 highest ranked gene pairs are *Rpl13a* and *Eef2*. *B*: the highest correlation coefficient was still obtained between *Rpl13a* and *Eef2* after exclusion of samples with RIN greater than 5. Because of sample exclusion, the sample size decreased, so the number of possible ranks decreased. Hence, Spearman correlation fluctuates. However, permutation test shows highest statistical significance between *Rpl13a*, *Hprt*, and *Ppia*. Both lowest coefficients and statistical significance was between any pairing using either *Gapdh* or *Rn18s* ($^{**}P < 0.01$, $^{*}P < 0.05$)

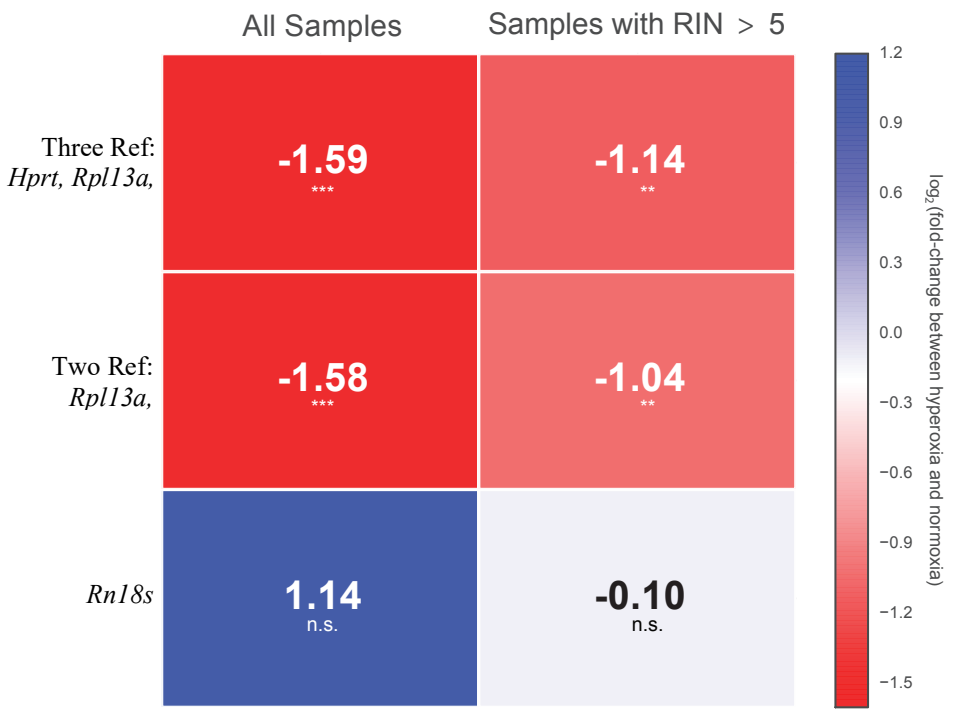

Figure 2.5. Application of the workflow to assess *Vegf-a* in lung tissue. *Vegf-a* tissue expression is accurately and consistently represented across oxygen levels normalized to *Hprt*, *Rpl13a*, and *Eef2*. When normalized to either the 2 or 3 appropriate reference genes (Ref.) or *Rn18s*, there are conflicting *Vegf-a* mRNA $\log_2$-fold changes between lungs exposed to hyperoxia and normoxia. *Vegf-a* expression in all samples appears to increase when normalized to *Rn18s* ($P = 0.09$, n.s.), but decreases in samples with RIN greater than 5 ($P = 0.56$, n.s.). This is in contrast to the expression that statistically significant decreased when it was normalized to either the 2 (***$P < 0.001$) or 3 genes, *Hprt*, *Rpl13a*, and *Eef2* (***$P \leq 0.001$) both in all samples and after excluding samples (**$P < 0.01$).

Chapter 3: EMAP II mediating macrophage migration in BPD pathogenesis

3.1 Introduction

Lung disease of prematurity is among the disease states driven by inflammation. Placed on supportive care, prematurely born children with underdeveloped lungs commonly progress toward development of chronic lung disease, specifically bronchopulmonary dysplasia (BPD). Currently, premature birth is the leading cause of death in children under the age of five affecting 1 in 10 births and representing approximately 15 million births per year worldwide[12,16,43,44]. In its most severe form, BPD can result in secondary cardiovascular sequelae such as pulmonary hypertension (PH) that persist into adulthood and abnormal ventilatory response[45-50]. Despite advances in clinical ventilator management, the introduction of surfactant, and antenatal glucocorticoids, there is a marked lack of adjunctive therapies.

Pulmonary inflammation significantly contributes to the multifactorial pathogenesis of BPD[15,51-54]. Like other lung injuries that are driven by inflammation such as asthma, in BPD, bronchial epithelial cells and myeloid cells, including, but not limited to macrophages are key effectors driving the secretion of both cytokines and chemokines such as IL-1β and MCP-1, respectively.

Clinically, current therapies administered to the premature infants from birth include either surfactants to aid alveolar plasticity or glucocorticoids to limit inflammation and thereby to prevent BPD progression in premature infants. As expected, tracheal aspirates of infants exposed to hyperoxia had elevated inflammatory mediators primarily secreted by macrophages, notably IL-1β and TNF-α[53,54]. In infants with sepsis-induced inflammation, inhibitors against the two cytokines showed little improvement in survival rates; in mouse models treated with inhibitors against these cytokines, only some BPD features improved[55-59]. This suggests that alternative, more broadly functioning or upstream targets are needed to prevent BPD.

In BPD, studies have identified candidate cytokines to be predictive of BPD onset. However, the source, function, and physiological mechanisms that drive the inflammatory state are poorly understood. In this study, we propose Endothelial Monocyte-Activating Polypeptide (EMAP II) as a potential target in the prevention of BPD in infants undergoing supportive care with hyperoxia. EMAP II (*Aimp1*) encodes

one component of the Multi-Aminoacyl tRNA Synthetase Complex, is ubiquitously expressed, and conserved across species. EMAP II is defined by its secreted, cleaved extracellular moonlighting functions with recent studies focusing on its anti-angiogenic properties[21,24,28,33,60]. EMAP II has also been indirectly shown to recruit macrophages in various injury models[30,61,62]. EMAP II expression localizes between the epithelial/ mesenchymal interface in early stages of normal murine lung development, while later saccular and alveolar developmental stages coincide with low levels of EMAP II expression confined to the perivasculature[27,29].

We previously identified an association between elevated EMAP II levels and BPD in premature baboon and human infants[34]. As a result, we hypothesized that EMAP II drives macrophage recruitment in BPD, which intensifies the inflammatory state. Using three mouse models, we identified sources of EMAP II throughout BPD progression and showed functional roles for EMAP II in the disease progression of severe BPD. We determined not only that its chemotactic role on macrophages leads to an inflammatory state exacerbating the development of BPD, but also represents a specific upstream, novel target for preventing BPD development.

3.2 Methods

Mice Studies

C57BL/6 mice were obtained from Jackson Laboratories. Studies complied with the animal protocols approved by the Indiana University Institutional Animal Care and Use Committee. Newborn pups were randomly selected for treatment groups while mice dams were exchanged every 24 hours to prevent oxygen toxicity. For details on normoxia and hyperoxia treatments, see Figure 3.1A. Regarding recombinant EMAP II injection studies, see Figure 3.2A. Antibodies neutralizing EMAP II were delivered according to Figure 3.4B.

Mouse model of bronchopulmonary dysplasia and therapy

Newborn pups were randomly selected to receive either rabbit non-specific immunoglobulin G or rabbit anti-EMAP II neutralizing antibody (2 mg/kg) as illustrated in Figure 3.4C above. Bronchopulmonary dysplasia during alveologenesis was then

modeled and illustrated in the above figure[63]. To collect tracheal aspirates from mice, a small incision was made along with the anterior portion of the trachea. An angiocatheter was then inserted within the tracheal incision. Two hundred microliters of fluid was inserted and aspirated. Fluid was then centrifuged at 5,000 g for 5 minutes at 4°C.

EMAP II treatment of mice

Mice were subcutaneously injected with recombinant EMAP II (80 μg/kg in 100 μL) daily beginning from day 3 to day 14 as shown in Figure 3.2. This dosage had been previously established as having an anti-angiogenic effect[64].

Immunoblotting

Sections of the right lung were placed in tubes containing modified lysis buffer. The tubes were then placed and homogenized in Bullet Blender Storm (BBY24M, Next Advance Inc.). Protein concentrations were determined by Bradford reagent (Bio-Rad). Twenty micrograms of lung tissue homogenates were loaded into NuPage Novex 4-12% Bis-Tris Protein gels (Invitrogen), incubated in 20% ethanol for 5 minutes, and transferred onto nitrocellulose membranes using iBlot v2 (Invitrogen). The membranes were placed in 5% blocking buffer (BioRad) in Tris-buffered saline with 0.05% Tween-20 for 1 hour at room temperature. Membranes were incubated overnight at 4 °C in primary antibodies listed in Supplementary Table.

Lung Microscopy

Lung tissues were inflation fixed by dripping 4% paraformaldehyde (w/v in PBS) at a height of 25 cm mm·H_2O above the lung for 10-15 minutes. Lungs were excised from the mouse *en bloc* and placed in 4% paraformaldehyde overnight before embedding in paraffin. Embedded tissues were sectioned 5.0 μm thick (Zeiss). Antigen retrieval and antibody staining was performed according to Table 3.1. Hematoxylin and eosin staining and Masson's Trichrome staining was performed according to manufacturer's instructions (Thermo Fisher). Co-localization staining was performed using Enzymatic double-staining IHC kit (Abcam). Images were captured on Hammamatsu Orca-ER or

DP70 camera at magnifications indicated in the appropriate figure legends using CellSens software.

Lung Morphometry Analysis

Mean linear intercepts and radial alveolar counts were calculated from H&E stained lung sections counted blind, decoded[65].

Pulmonary Function Testing

Only male mice were tested for pulmonary functions to minimize possible confounders related to estrogen. Mice were anesthetized with ketamine (100 mg/kg) and xylazine (6 mg/kg) followed by pancuronium (1 mg/kg) to induce paralysis. A metal cannulus was inserted through a small incision in the trachea followed by single-model and complex model measurements of lung function using FlexiVent Software (SCIREQ Inc.).

Macrophage Count

Light microscopy images were taken on Olympus using MicroBiological Suites with a 40X objective lens. The images were then randomized and the number of Galectin-3^{+} positive cells were counted in a blinded manner. The images were then decoded and analyzed using Python.

Quantitative PCR

Lung harvest, RNA extraction, RNA quality determination, quantitative PCR, and analysis were performed according to the methods in a previous study[66]. Primers are listed in Table 3.1.

Transmigration Assay

RAW264.7 cells were cultured in phenol-red free DMEM media containing 10% FBS, antimicrobial and antifungal supplement, 5 mM HEPES, and 5 mM L-Glutamine until approximately 70 – 80% confluency. The media was then exchanged for transmigration media which contained phenol-red free DMEM containing 1% FBS for 2 hours before being scraped, incubated in CD16/32 to block non-specific F'ab interactions on ice for

approximately 15 minutes; the media containing the antibody was centrifuged at 400 x g for 5 minutes at 4 ºC and aspirated. 5 x 10^4 cells were resuspended in transmigration media and loaded into a single 5.0-micron pore transwell insert. Regarding treatments in Figure 4, EMAP II protein was either boiled for 30 minutes at 100°C or pre-incubated with EMAP II neutralizing antibody at room temperature for 30 minutes at respective dosages. LPS (Serotype *E. Coli* 055:B4, Sigma) was also pre-incubated with EMAP II neutralizing antibody. The bottom inserts were filled with 500 microliters containing the listed treatments. Transmigration occurred for 4 hours at 37ºC, fixed in 4% paraformaldehyde (w/v in PBS) overnight, and stained in crystal violet solution. Images were captured at 20X magnification on DP70 using MicroSuite Biological Software. n = 4-6 for each treatment.

Outliers

Data that were statistically significant by Grubb's Outlier test were removed from analysis.

3.3 Results

EMAP II levels in lung disease of prematurity. We exposed neonatal mice to 85% O_2 saturation level (i.e. hyperoxia) compared to room air (normoxia) during lung alveologenesis to induce BPD formation (Figure 3.1A). EMAP II protein levels were quantified by immunoblotting (Figure 3.1B). Confirming previous studies, EMAP II expression was perivascular in normoxic day 5 (Figure 3.7). Compared to mice at normoxia, EMAP II levels were significantly elevated in lungs of mice exposed to hyperoxia over time, peaking at postnatal day 15 (Figure 3.1C) (from hereon, mice exposed to hyperoxia and analyzed between 5 to 15 days are termed "early BPD mice," mice analyzed at later time points are termed-15 days, "BPD mice," and for 20 days and beyond, "late BPD"). However, analysis of EMAP II protein levels in tracheal aspirates of BPD mice revealed an early increase at day 10 but a decline toward that of normoxia control mice by day 15 (Figure 3.1F).

EMAP II expression differs in location during BPD formation.

A significant increase over time in whole lung but decreasing trend in tracheal aspirates suggested that EMAP II expression is localized and compartmentalized in response to hyperoxia. EMAP II has been shown to augment inflammatory cell counts[67]. We proposed that the localization of EMAP II would be distributed in cells near the tracheal aspirate collection site and thus histological analysis by co-staining EMAP II with Galectin-3 (known as GAL-3), an activation and differentiation marker of macrophages was performed. In contrast to normal perivascular localization of EMAP II expression, by day 5, EMAP II expression was found in both proximal bronchiolar epithelial-rich regions, indicated by club-cell-specific-protein expression, and perivasculature (Figure 3.1D). By day 10, EMAP II expression was limited to GAL-3$^+$ macrophages that were located in both bronchiole and distal airways (Figure 3.1E); subsequently by day 15, EMAP II was localized only within macrophages of the distal airways. In agreement with the localization moving distally away from bronchiolar airways, analysis of tracheal aspirates showed a significant decrease in EMAP II expression (Figure 3.1F).

***In vivo* effect of EMAP II on macrophages.** As there was a recruitment of macrophages over time found in BPD mice (Figure 3.1E), we postulated that excess EMAP II in early BPD directly recruited macrophages. We administered recombinant EMAP II to mice until the time point when there was maximal EMAP II expression on day 15 (Figure 3.2A). The dosage followed previous studies that determined the alternate moonlighting anti-angiogenic role of EMAP II[64]; as previously observed, there were decreased angiogenic genes without a compensatory effect on transcription (Figure 3.8A,B). We found a significant increase in the number of macrophages in lungs of mice administered EMAP II as compared to controls (Figure 3.2B,C). This suggested that there was direct macrophage chemoattraction by EMAP II.

The pro-inflammatory cytokine interleukin-1 beta (IL-1β) has been a target of interest in the pathogenesis of BPD. As it is primarily secreted by macrophages, and having seen a significant increase in macrophage recruitment, we evaluated IL-1β expression in whole lung (Figure 3.2D). There was significantly elevated IL-1β expression in lungs

administered EMAP II (Figure 3.2D,E) suggesting contribution to macrophage pulmonary sequestration.

Effect of EMAP II on lung structure and BPD pulmonary outcomes. In addition to increased macrophage counts in mice administered EMAP II, we observed loss of lung structural integrity similar to that of BPD. As EMAP II has other reported functions, we sought out to define effects of sustained, elevated EMAP II on the lungs. Compared to control mice, the body weight of mice administered EMAP II was significantly lower, suggesting impaired overall growth (Figure 3.8B). Lungs of EMAP II-administered mice had severely dysplastic alveoli and increased elastin deposition (Figure 3.3A,F). There were larger distal airspaces as evidenced quantitatively by both significantly decreased radial alveolar count (RAC) and increased mean linear intercept (MLI) (Figure 3.3B,C). This suggested that excess amounts of EMAP II impaired development of the lung structure. However, structure does not always correlate with lung function or outcome measurements[68]. Compared to control, mice given EMAP II had significantly impaired pulmonary biophysical properties: the pressure volume loop was shifted downward, suggesting an inability of lungs to maximally inflate along with other biophysical properties (Figure 3.3D, Figure 3.8C). To test whether impaired lung biophysical properties were due to surfactant expression, we measured surfactant protein-C (SP-C), a common indicator of type II alveolar epithelial cells that secrete surfactants. Compared to controls, mice administered EMAP II had significantly elevated mRNA and protein levels of SP-C (Figure 3.7D,E). This suggested a compensatory mechanism in response to exogenous EMAP II thus the lung function change was independent of a lack of SP-C.

EMAP II-treated mice presented with signs of pulmonary hypertension. Macrophage counts were elevated following EMAP II injection, and previous studies link both the elevated counts and subsequent inflammatory cytokine release to pathogenesis of not only BPD but also its secondary sequel, pulmonary hypertension (PH)[69,70]. Lungs of mice injected with EMAP II had impaired alveolarization and blood vessel formation leading to decreased function, reflecting anti-angiogenic properties of EMAP II (Figure 3.3A); clinically, this implies cardiovascular sequelae, which are also prominent in poor

outcome of BPD patients[47,50]. We observed right ventricular hypertrophy in mice given EMAP II compared to controls (Figure 3.3E). Consistent with right-heart hypertrophy found in PH, we observed increased elastin deposition by Masson's Trichrome staining in distal vessels (Figure 3.3F).

We concluded that chronic, elevated EMAP II led to BPD-like disease, including the development of signs of secondary PH. As SP-C levels were not decreased by EMAP II yet elevated EMAP II levels and macrophage recruitment were found in BPD, an alternative mechanism of upregulating EMAP II in early BPD must exist that modulates macrophage recruitment, negatively influencing lung and heart outcomes.

Neutralizing excess EMAP II limits chemotactic effects upon macrophages. We tested if we could limit macrophage recruitment by neutralization of excess EMAP II. Using an EMAP II-neutralizing antibody (referred to as anti-EMAP II), we assessed macrophage transmigration *in vitro*. Consistent with the *in vivo* findings, we found that exogenous EMAP II significantly increased macrophage transmigration (Figure 3.4A,B). However, anti-EMAP II incubated with excess EMAP II significantly neutralized this chemoattraction in a dose-dependent manner (Figure 3.4A,B). As a control, heat-inactivating EMAP II did not increase the number of transmigrated cells. Macrophage chemotaxis was specific to EMAP II and further confirmed by treating cells with LPS, an inflammatory agent with a role in macrophage migration and activation, and anti-EMAP II (Figure 3.2A,B).

To assess whether we could prevent hyperoxia-induced BPD formation, mice were randomized and given the neutralizing anti-EMAP II antibody (Figure 3.4C). Delivery of antibody to lungs was confirmed (Figure 3.9A). Recruitment of macrophages in BPD mice was assessed by immunohistochemistry (Figure 3.4D). Following treatment with anti-EMAP II, however, there was a significant decrease in the number of macrophages and inhibition of a BPD-like phenotype (Figure 3.4E).

Neutralizing excess EMAP II improved lung structure and development of altered function. We considered that the inhibition of macrophages through neutralizing excess

EMAP II in BPD would mitigate murine pulmonary damage. The body weight of hyperoxia mice treated with anti-EMAP II was comparable to control groups kept in room air (Figure 3.9B). Following treatment (Figure 3.4C), there was an increase in the number of distal alveoli measured in blinded manner, and a visible lack of bronchiolar vessel distension (Figure 3.5A). As associated with parameters of the qualitative findings, there was a significant decrease in MLI counts, which reflects a decrease in empty air space (Figure 3.5B). RAC counts in lungs of mice treated with anti-EMAP II appeared to increase compared to control non-specific IgG (Figure 3.5C). By limiting macrophage recruitment, the hyperoxia mice treated with anti-EMAP II showed an improvement in pulmonary outcomes compared to mice treated with control IgG (Figure 3.5D, Figure 3.9E). There was a possibility that this improvement was not due to limiting macrophage recruitment but perhaps prevention of cellular apoptosis induced by either hyperoxia or EMAP II. We found increased apoptosis due to hyperoxia but an insignificant decrease following anti-EMAP II treatment (Figure 3.9C). Another alternative mechanism would be an increase in surfactant production. SP-C did not significantly change following anti-EMAP II treatment, suggesting that the treatment was independent of surfactant production (Figure 3.9D).

Anti-EMAP II treatment reduced signs of PH. To test whether anti-EMAP II treatment could impact development of PH, we assessed right ventricular hypertrophy. Significantly decreased right ventricular (RV) weight was seen in hearts of hyperoxia mice treated with anti-EMAP II over that of mice treated with control IgG, comparable to that of mice in room air (Figure 3.5E). Consistent with right ventricular hypertrophy, we observed that there was elastin deposition in distal alveolar vessels (Figure 3.5F).

Reducing macrophage numbers resolved inflammatory and chemotactic gene expression. We proposed that by limiting macrophage recruitment through anti-EMAP II, we would reduce the levels of pro-inflammatory and chemotactic gene expression. By immunoblotting, we detected IL-1β levels in lungs of hyperoxia mice (Figure 3.6A). Elevated IL-1β levels were significantly reduced in the hyperoxia mice treated with anti-EMAP II (Figure 3.6B). In addition, expression of pro-inflammatory genes, *Tnfa*, *Il6*,

Il1b and chemotactic genes, *Ccl2*, *Ccl9* were markedly decreased following anti-EMAP II treatment (Figure 3.6C).

3.4 Discussion

Premature birth, a major determinant of neonatal morbidity and mortality, is associated with long-term health consequences at an estimated expense of $26 billion per year in the United States alone. Lung disease of prematurity, BPD, is a preterm complication without a specific targeted treatment. After a call for more directed studies on pulmonary inflammation in BPD, clinical studies determined that inflammatory markers are not only elevated in BPD but associated with prognosis[15,54,71]. Some studies used untargeted anti-inflammatory therapies such as glucocorticoids, direct cytokines, or chemokines with minimal improvement in some attributes of BPD[58].

In contrast, our results provide an opportunity to consider targeting pulmonary immune response by addressing macrophage infiltration as a therapeutic component of BPD. Our experiments show that EMAP II is a specific target that directly contributes to the pathogenesis of premature lung disease in BPD. This is manifested when elevated EMAP II was sustained in lungs of BPD mice compared to controls, corroborating the temporospatial-dependent role of EMAP II in BPD development of baboons and humans – specifically, in the bronchial epithelium rather than in perivasculature, where it is normally expressed and declines over time[34]. In addition to sustained levels, the direct effect of EMAP II on BPD development was evident when mice treated with EMAP II developed a BPD-like phenotype: arrested alveolar development, right ventricular hypertrophy consistent with PH, macrophage recruitment, and heightened inflammatory state. Subsequently, anti-EMAP II treated mice in hyperoxia presented with a significant reduction in the inflammatory state and of the BPD-like phenotype.

The bronchial epithelium has recently been identified as the initial source of an immune response in various injury contexts[72,73]. Similarly, early marked elevated EMAP II expression in primary bronchial $CCSP^+$ cells following hyperoxia support the role of EMAP II as an inflammatory modulator in BPD development. Improvement in both macrophage counts and inflammation following anti-EMAP II treatment ascribes to its chemotactic function compared to its known anti-angiogenic function[24,25,27,28,33,34,60].

Neutralization of EMAP II limited chemotaxis of macrophages in cell culture and into the lung, ultimately limiting inflammation. Given the proximal $CCSP^+$ cell expression of EMAP II followed by macrophages expressing EMAP II in BPD mice, there exists a possible positive reinforcing cycle. Epithelial cells such as the $CCSP^+$ cells express EMAP II, which recruits macrophages; these cells, in turn, can produce more EMAP II, which further propagates and activates other immune cells. If this is the case, a novel mechanism can be substantiated in clinical BPD development as a potential therapeutic target through the continuous presence of EMAP II.

Moving away from a simple dichotomy in macrophage activation reveals the many varying functional subsets in not only other disease contexts but also BPD. Two recent studies indicate that rather than a simple dichotomy in macrophage activation, a threshold of varying functional subsets of unknown origins (e.g. blood-derived circulating, bone marrow egression) is at least sufficient for BPD progression[58,74]. The first showed that elevated macrophage numbers in conjunction with pro-inflammatory gene expression resulted in BPD despite decreased counts of immune response cells[58]. This suggests that a hyperactivated macrophage subset is crucial in hyperoxia-induced inflammation. The second study defined an alternative macrophage-like $CD11b^+$ monocyte origin that protected BPD mice independent of neutrophilia[74]. However, macrophage pro-inflammatory response is not only limited to lung disease of prematurity.

In agreement with the cited studies, our study implicates that the increased number of effectors cells due to EMAP II can significantly influence physiological function. Before any meaningful function is assigned to subsets recruited by EMAP II, further studies are awaited that determine the origin and functional consequence in normal lung development including that of the CD11b mononuclear subset.

A previous study showed that elevated macrophage numbers in conjunction with pro-inflammatory gene expression resulted in BPD despite decreased counts of immune response cells[58]. This suggests that hyperactivated macrophages may play a significant role in hyperoxia-induced inflammation. However, macrophage pro-inflammatory response is not only limited to lung disease of prematurity. Using this study of BPD as a working model the complex interactions of macrophages and their environment can be equally implicated as contributing or driving factors in other chronic inflammatory

disease such as Crohn's disease or rheumatoid arthritis[75-77]. Inhibition of excess macrophage numbers supports normal lung development, informing potential anti-inflammatory therapies.

In BPD, hyperoxia-induced inflammation has also been linked to impaired lung biophysical properties, but with conflicting results, as both increasing and decreasing compliance has been described[78,79]. Some studies suggest that hyperoxia increased compliance resembling emphysematous lungs, while other studies concluded hyperoxia decreased compliance due to the lungs being less pliable[78-80]. We tested murine pulmonary outcomes at 6 weeks in concordance with previous studies[68,78,80]. Sustained EMAP II was associated with decreased compliance (Figure 3.3D). For this reason, other biophysical properties, such as resistance, also need to be taken into account. Since impaired biophysical properties are collective, insufficient oxygen exchange, inflammation, and subsequent right ventricular hypertrophy contribute to pulmonary dysfunction. However, following anti-EMAP II treatment, vessels were not thickened, an indication of PH. Suppression of EMAP II inflammatory properties alleviated these pulmonary biophysical abnormalities associated with hyperoxia induced BPD including decreased resistance, decreased tissue damping, and decreased airway space.

Our results highlight an EMAP II-mediated inflammatory mechanism as a significant component of the multi-factorial pathogenesis of lung disease of prematurity, BPD. In contrast to other studies, the results of our experiments show not only robust protection from a BPD phenotype and signs of secondary PH but also reduction of macrophage recruitment and inflammatory status. Neutralization of EMAP II and curbing its ability to chemoattract macrophages is a possible future therapeutic goal in the prevention of BPD and secondary PH in the context of necessary chronic oxygen supplementation.

3.5 Figures and Tables

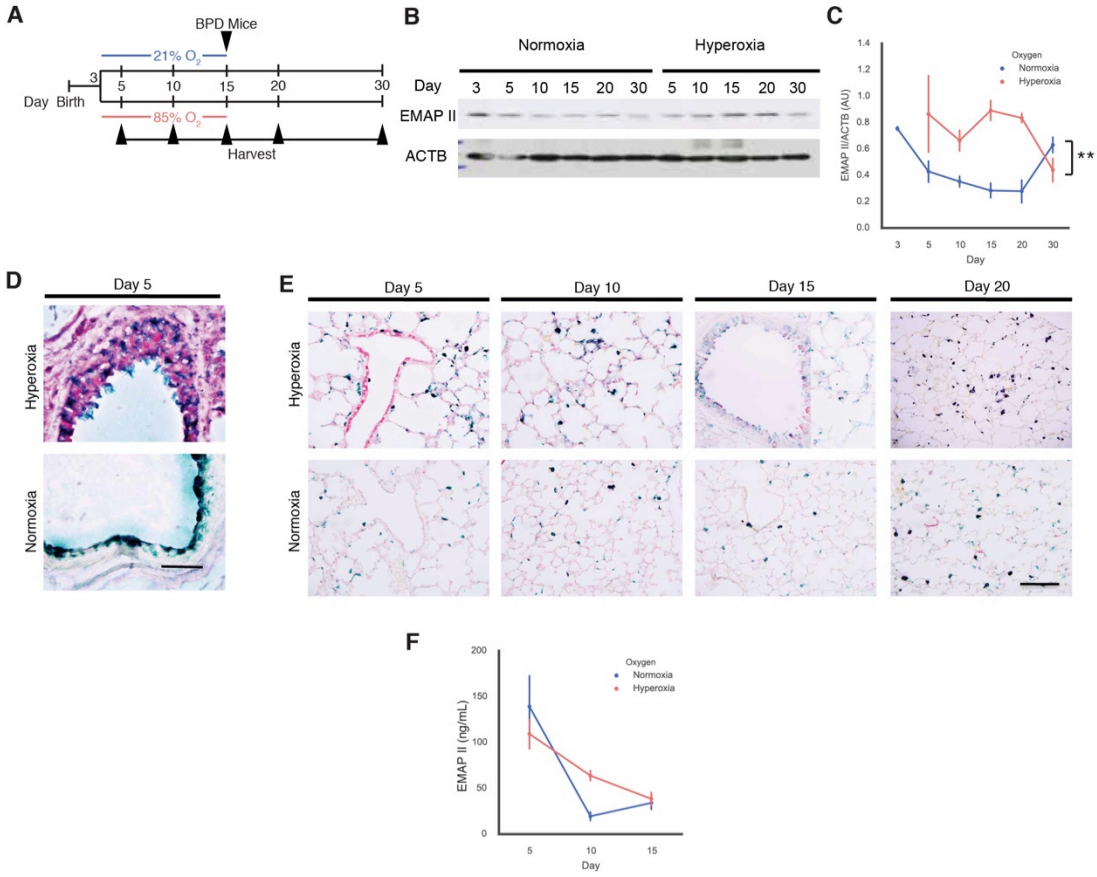

Figure 3.1. Expression of Endothelial monocyte-activating polypeptide II (EMAP II) in murine model of bronchopulmonary dysplasia (BPD). (*A*) Experimental schematic of neonatal mouse oxygen exposure to induce BPD. (*B*) EMAP II protein expression and (*C*) quantification in whole-lung lysates of normoxia and hyperoxia mice (normalized to β-actin, pooled samples of at least $n = 3$ for Day 3, $n = 2$ for Day 30, $n = 3$–4 for Day 10, $n = 6$–10 for other days; at least two independent experiments). Main effect of oxygen, $^{**}P = 0.0000322$, interaction of oxygen:age, $P = 0.788$. (*D*) Representative images of immunohistochemical co-staining for EMAP II expression (*red*) and Clara cell secretory protein (*green*). *Purple* indicates co-expression. *Scale bar*, 20 μm. (*E*) Representative images of immunohistochemical staining for EMAP II expression (*red*) and galectin-3 (*green*). *Purple* indicates co-expression. *Scale bar*, 100 μm. Note that compared with lungs exposed to normoxia, those exposed to hyperoxia and harvested on Day 15 were severely dysplastic so that both the bronchial epithelium and the alveoli could not be imaged in the same capture field, although the same magnification as that used in other images was used. (*F*) EMAP II concentration in tracheal aspirates by immunoblotting and quantification. Main effect of day, $P = 0.0187$; interaction of oxygen:day, $P = 0.711$; $n = 3$ per day. Data are presented as mean ± SEM. ACTB, protein name of β-actin.

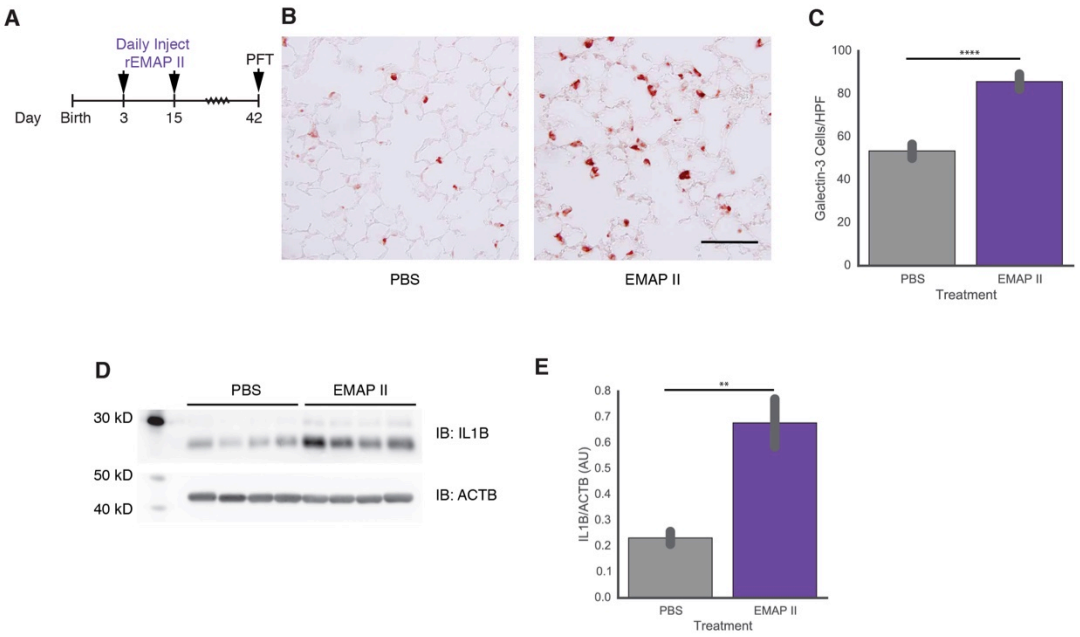

Figure 3.2. EMAP II protein mediates macrophage chemoattraction *in vivo*. (*A–E*) Mice treated with either EMAP II or vehicle (injection) from Days 3 to 15. (*A*) Schematic of EMAP II treatment in neonatal mice. (*B*) Representative immunohistochemical images of distal alveoli in lung sections of Day 15 mice showing macrophage (galectin-3, *red*) and (*C*) quantification by blinded analysis of galectin-3–positive cells per HPF ($n = 4$, $^{****}P = 0.00000235$). (*D* and *E*) Immunoblot probed for IL1β in whole lung lysate of Day 15 mice (normalized to β-actin, $^{**}P = 0.01$, $n = 4$). *Scale bar*, 100 μm. Results are representative of four (*B* and *C*) or two (*D* and *E*) independent experiments. Data are presented as mean ± SEM. HPF, high-powered field; PFT, pulmonary function tests; rEMAP II, recombinant EMAP II.

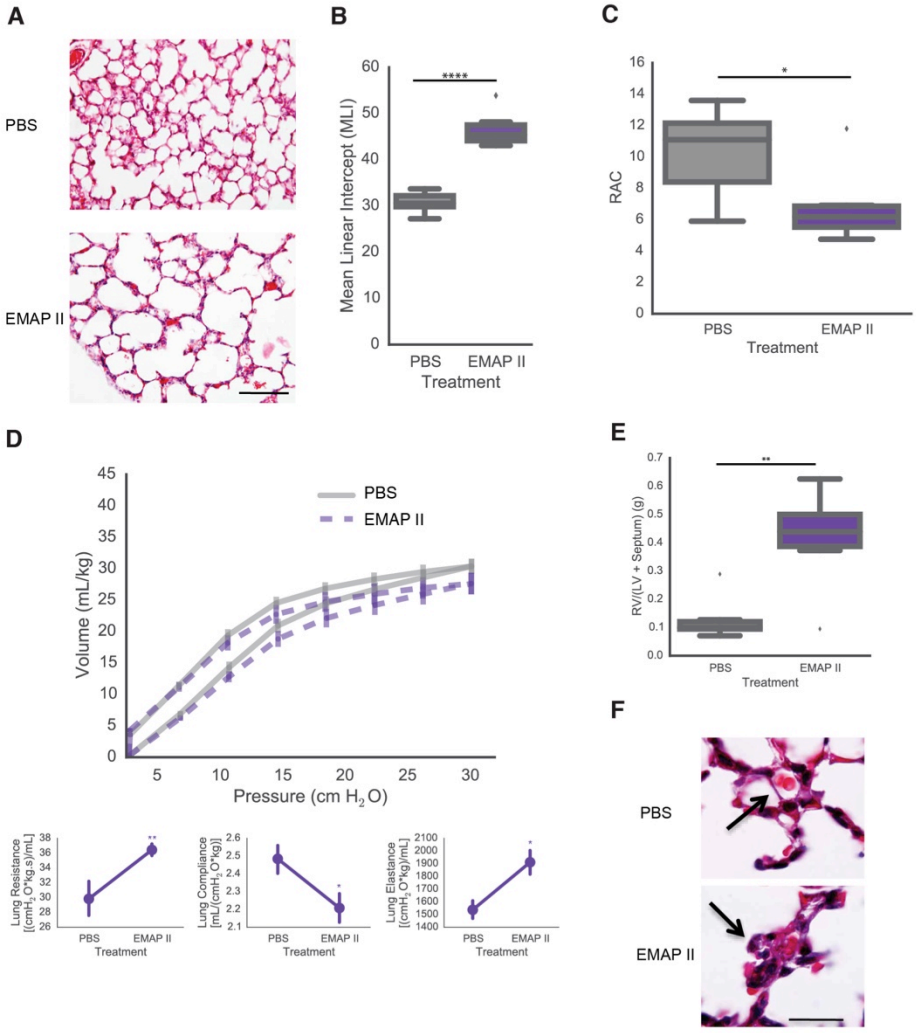

Figure 3.3. Lungs treated with EMAP II present BPD–like phenotype. The experimental design is the same as in Figure 3.2A. (*A*) Comparison of distal alveolar structure in inflation-fixed lungs (25 mm Hg) of mice killed on Day 15 by (*B*) mean linear intercept (*****P* = 0.00000719), and (*C*) RAC by blinded observer analysis (*n* = 8, **P* = 0.03337). (*D*) Biophysical parameters of lung function compliance, resistance, and elastance were assessed (*n* = 3–6; **P* = 0.011, ***P* = 0.023, **P* = 0.008, respectively) and representative pulmonary flow loops presented. (*E*) Right ventricular hypertrophy quantified by Fulton's index (*n* = 6 mice per group, ***P* = 0.00520) and (*F*) representative deposition of perivascular elastin (*arrows*) in distal lung tissue sections stained with Masson's trichrome. *Scale bars*, (*A*) 100 μm and (*F*) 10 μm. Results are representative of three (*A–C* and *F*) or two (*D* and *E*) independent experiments. *Diamonds* are data points past 75%. Data are presented as mean ± SEM. LV, left ventricular; RAC, radial alveolar count; RV, right ventricular.

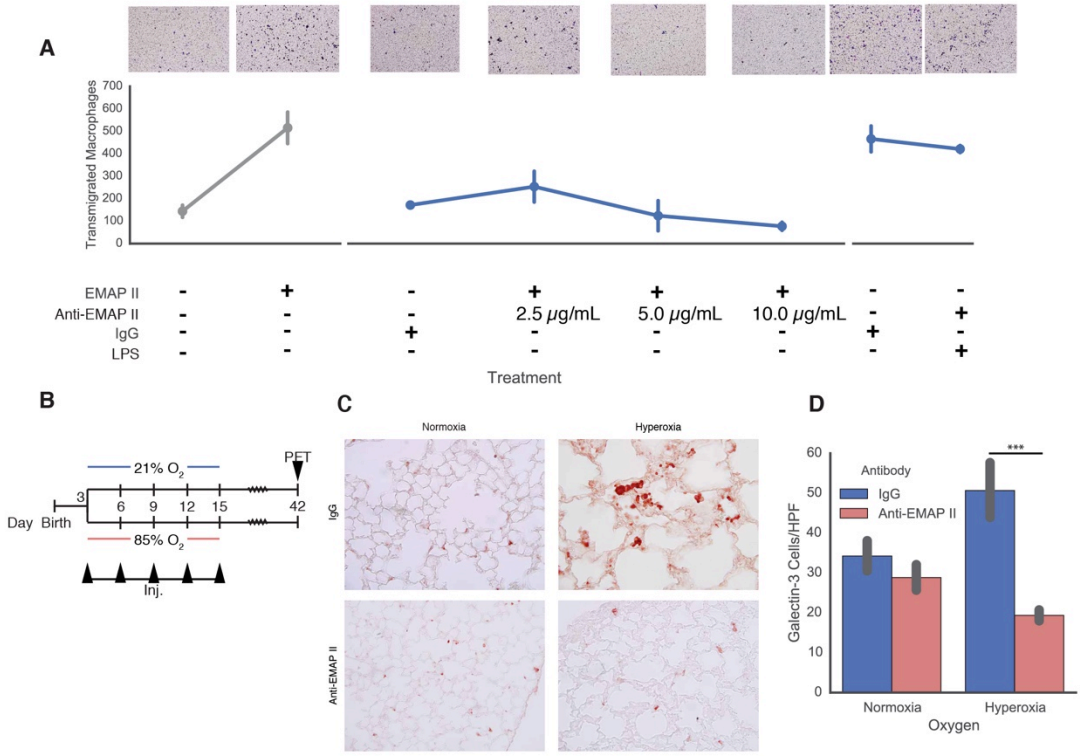

Figure 3.4. Neutralizing EMAP II limits macrophage recruitment both *in vitro* and *in vivo*. (*A*) Quantification of Transwell-migrated macrophages in response to EMAP II vehicle (phosphate-buffered saline), nonspecific IgG, and EMAP II preincubated with various concentrations of anti-EMAP II ($n = 2–4$ replicates, $P = 0.0044$, one-way analysis of variance across treatments). (*B*) Schematic of neonatal hyperoxia exposure protocol used to induce BPD, inj. of anti-EMAP II or IgG. (*C*) Representative immunohistochemical images of distal alveoli in lung sections showing macrophages (galectin-3, *red*) and (*D*) galectin-3–positive cells per HPF, quantified by blinded analysis ($n = 4$ mice, $***P = 0.000457$). Results are representative of samples collected from four (*D* and *E*) and two (*A*) independent experiments. Data are presented as mean ± SEM. Inj., injection.

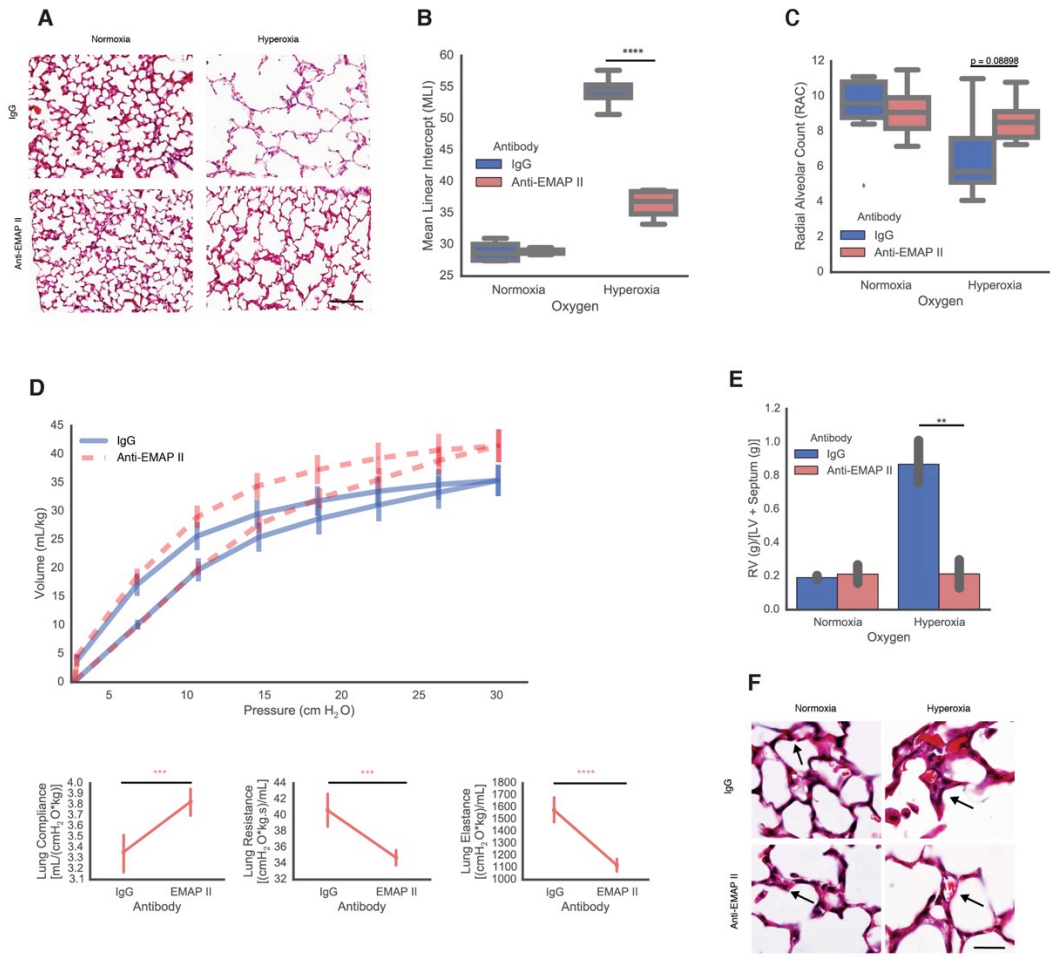

Figure 3.5. The rescued lung structure and function of BPD mice that are treated with anti-EMAP II. The experimental design is the same as in Figure 3.4B. (*A*) Comparison of distal alveolar structure in inflation-fixed lungs (25 mm Hg) of mice killed on Day 15 by (*B*) mean linear intercept and (*C*) radial alveolar count by blinded observer analysis ($n = 8$; ****$P = 0.0337$, $P = 0.08898$). (*D*) Biophysical parameters of lung function compliance, resistance, and elastance were assessed among hyperoxia groups ($n = 6$–8 mice; ***$P = 0.00642$, ***$P = 0.000209$, ***$P = 0.00183$) and representative pulmonary flow loops presented. (*E*) RV hypertrophy quantified by Fulton index (ratio of RV weight to LV plus septal weight, $n = 3$, **$P = 0.00537$) and (*F*) representative deposition of perivascular elastin (*arrows*) in distal lung tissue sections stained by Masson's trichrome. *Scale bars*, (*A*) 100 μm and (*F*) 10 μm. Results are representative of four (*A–F*) or two (*D–F*) independent experiments. *Diamonds* are data points past 75%. Data are presented as mean ± SEM.

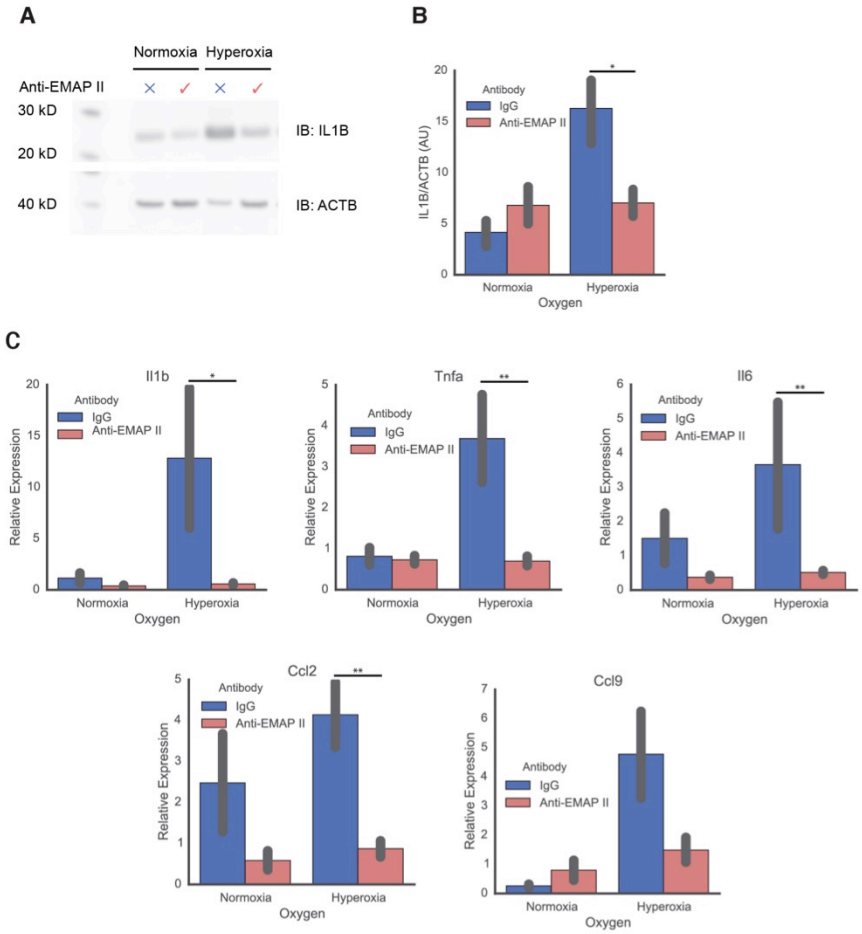

Figure 3.6. Neutralizing EMAP II limited macrophage recruitment and caused inflammation induced by high oxygen to subside. (*A* and *B*) Representative immunoblot probed for IL1β in whole lung lysate of Day 15 mice and quantified ($n = 3$, normalized to β-actin, $*P = 0.0498$). (*C*) mRNA expression of inflammatory *Il1b*, *Il6*, and *Tnf* and chemokine genes *Ccl2* and *Ccl9* in lungs determined by quantitative polymerase chain reaction calculated on the basis of *Hprt*, *Eef2*, and *Rpl13a* expression ($n = 6$–7; $*P = 0.0195$ [*Il1b*], $**P = 0.0489$ [*Tnfa*], $**P = 0.00594$ [*Il6*], $**P = 0.00227$ [*Ccl2*], $P = 0.0889$ [*Ccl9*]). Samples are from three independent experiments (*A*–*C*). Data are presented as mean ± SEM. IB, immunoblot.

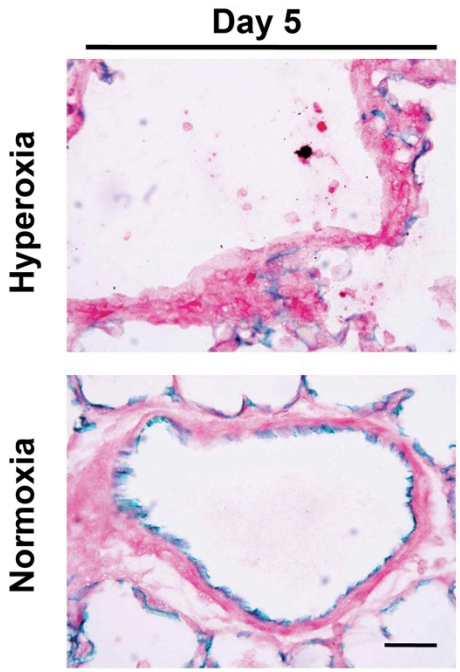

Figure 3.7. Perivascular EMAP II expression. Representative images of IHC co-staining for endomucin (green) and EMAP II (red) in Lungs of neonatal day 5 mice exposed to either normoxia or hyperoxia. Scale bar, 20 μm.

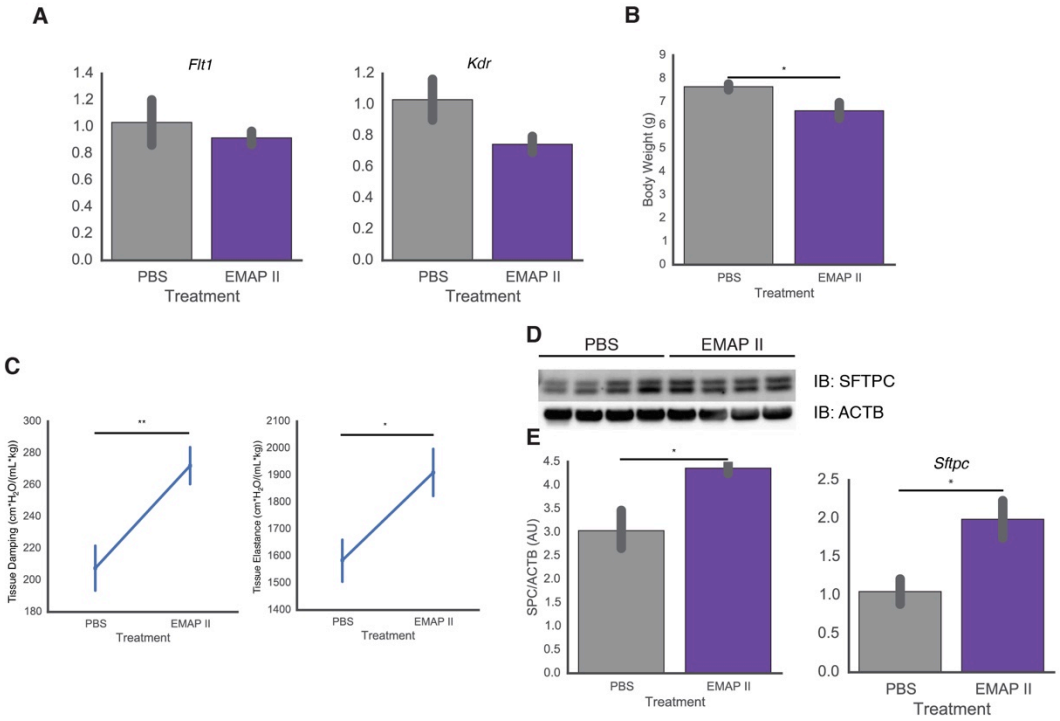

Figure 3.8. EMAP II protein induced compensatory mechanisms. The experimental design is the same as Figure 3.2A. (A) mRNA expression of *Kdr* and *Flt1* in lung tissue was determined by qPCR, calculated on the basis of *Eef2*, and *Rpl13a* expression (n = 4, p = 0.130, 0.582). Values are expressed as arithmetic mean ± 1 s.e.m. (B) Comparison of body weight on day 15 of life (n = 6, p = 0.0258). (C) Biophysical parameters of lung tissue damping and tissue elastance were assessed (n = 3-6 mice, p = 0.00466, 0.00928). (D, E) Immunoblot of SFTPC protein expression and mRNA expression of *Sftpc* determined by qPCR calculated on the basis of *Hprt*, and Rpl13a expression (n = 4, p = 0.03, 0.0315). Data are represented as mean ± 1 s.e.m.

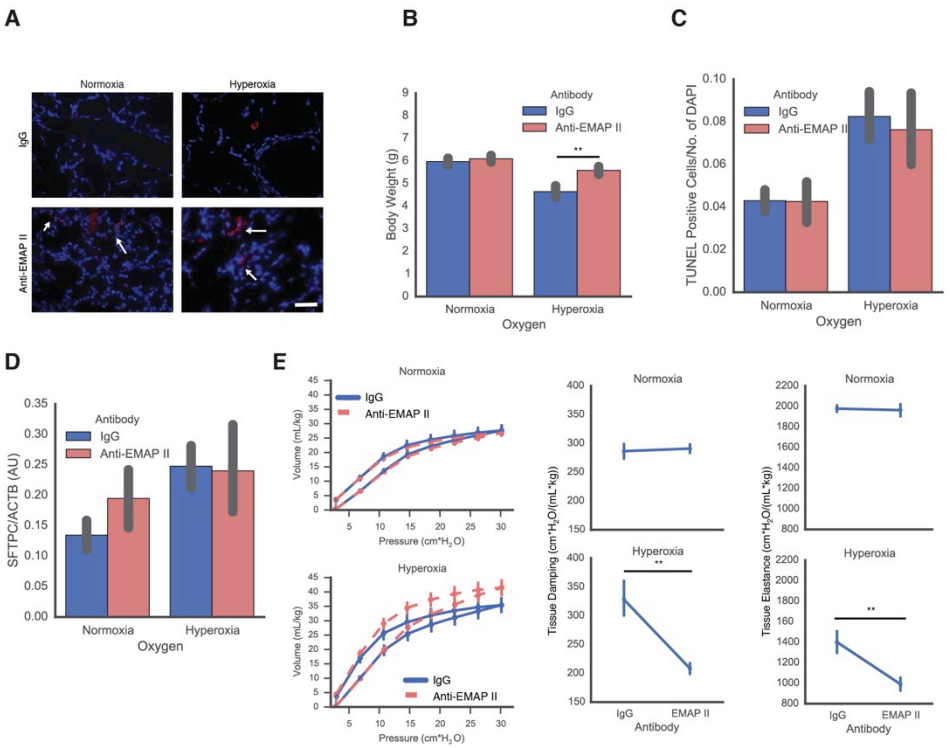

Figure 3.9. Neutralizing EMAP II compensatory mechanisms in BPD mice. The experimental design is the same as Figure 4C. (A) Representative images of antibody deposition (arrows) in day 15 lungs. Scale bars, 20 μm. (B) Comparison of body weight on day 15 of life (n = 17 per group, p = 0.00789). (C) Quantification of immunofluorescent TUNEL assessment of apoptosis in day 15 lungs by blinded observer analysis (n = 8, 3 fields per mouse, main effect of oxygen, p = 0.0000236, main effect of antibody, p = 0.728, interaction of antibody:oxygen, p = 0.732). (D) Quantification of Surfactant protein C expression by Western blotting densitometry (n = 6 per group, p = 0.732, two-way ANOVA). (E) Biophysical parameters of lung tissue dampening and tissue elastance were assessed (n = 3-6 mice, p = 0.00508, 0.0103). Data are represented as mean ± 1 s.e.m.

Target	Sense	Antisense	Length
Hprt	CCCCAAAATGGTTAAGGTTGC	AACAAAGTCTGGCCTGTATCC	76
Eef2	ACATTCTCACCGACATCACC	GAACATCAAACCGCACACC	135
Rpl13a	TCCCTCCACCCTATGACAAG	GTCACTGCCTGGTACTTCC	136
Kdr	GTACCGGGACGTCGACATAG	TCACTGACAGAGGCGATGAA	79
Flt1	ACTCTTGTCCTCAACTGCAC	GGTCAATCCGCTGCCTTATAG	112
Sftpc	ATGGACATGAGTAGCAAAGAGGT	CACGATGAGAAGGCGTTTGAG	

Target	Assay ID	Vendor
Il1b	qMmuCID0005641	BioRad
Tnf	qMmuCED0004141	BioRad
Il6	qMmuCID0005613	BioRad
Ccl2	qMmuCEP0056726	BioRad
Ccl9	qMmuCID0021820	BioRad

Antibody Used

Antigen	Clone	Company	Catalog No.	Usage	Antigen Retrieval	Dilution
IL1B	3A6	Cell Signaling	12242S	IB	--	1:1,000
ACTB	8H10D10	Cell Signaling	3700S	IB	--	1:10,000
SPC	--	EMD Millipore	AB3786	IB, IHC	None	1:1,000
GAL-3	M3-38	Antibodies-Online	ABIN1804652	IHC	Citrate	1:1,000
CCSP	--	Seven Hills	WRAB-3950	IHC	Citrate	1:1,000
CD16/32	93	eBioscience	130-0161-82	Transwell		
EMAP II	--	In-house	--	IB, IHC, Transwell	Trypsin	1:5000, 1:100

IB: Immunoblot

IHC: Immunohistochemistry

Table 3.1. The primers and antibodies used in the performed experiments of Chapter 3.

Chapter 4: The transient activation of JAK-STAT3 in macrophages by EMAP II

4.1 Introduction

Macrophages serve as key effector cells of innate immunity in tissue homeostasis, injury, and repair. During tissue injury and repair, critical functions include, but are not limited to, promoting recruitment of other inflammatory cells, phagocytizing of injured tissue, and mediating both the tissue remodeling process and more recently, the re-vascularization process[79,80]. Accordingly, macrophages remain adaptable to its environment by altering its highly plastic transcriptional profile, a process referred to as macrophage polarization.

Secreted factors in a milieu of injuries are the effectors that ultimately modulate macrophage transcriptional profiles. Previous studies highlight chemokine-like, yet pleiotropic ligands, secreted in the milieu of injuries that recruit monocytes and lymphocytes while impacting vasculature in injury processes. Endothelial monocyte activating polypeptide II (EMAP II) is an ancient and conserved among many species with pleiotropic effects: act upon endothelial cells of the vasculature through integrin-mediated mechanisms while recruiting hematopoietic derived cells[81].

Historically, EMAP II was identified in supernatant of fibrosarcoma-derived cells, a protein of approximately 23 kilodaltons (kDa), and discovered to induce tissue factor secretion, release of von Willebrand Factor, and expression of adhesion molecules in endothelial cells while promoting secretion of TNF-α[32]. Subsequent studies implicated transient, high amounts of EMAP II can disrupt vessel formation through inhibition of vascular endothelial growth factor-2 signaling and its downstream transcriptional effects[23,82].

We recently discovered a role for EMAP II in innate immunity as a recruiter of myeloid cells and as a ‘find-me’ signal, one that goes beyond vasculature. ‘Find-me’ signals such as EMAP II recruit phagocytes not only to maintain tissue homeostasis but also in injured states; if left unchecked, excessive amounts can actually promote further apoptosis and cellular damage. In line with this concept, we showed in a prior study of a murine model of bronchopulmonary dysplasia, not only was there a persistent expression of EMAP II in the macrophages that were recruited even after the injury stimulus, i.e.,

high oxygen levels, was removed, but also an increased number of macrophages in response to EMAP II[83].

However, the molecular mechanisms that occur in the recruited cells are unknown. Disrupted VEGFR2 signaling is a common signaling mechanism for the effects of EMAP II upon vasculature, however, only subsets of macrophages, primarily tumor macrophages, can express VEGFR2. This makes disrupted VEGFR2 signaling highly unlikely to contribute toward signaling in the recruited macrophages[84,85].

In this report, we set out to identify transcriptional effects and signaling events of EMAP II within the recruited macrophages. We characterized both the kinetics of transcriptional expression and determined the signaling mechanisms that were mediated by EMAP II in partially activated thioglycollate-elicited macrophages (TEPM). We hypothesized that recruited macrophages would shift toward an inflammatory polarized state by gene expression and signaling upon exposure EMAP II, but the results showed otherwise; rather, we found gene expression and signaling uncharacteristic of either macrophage polarization states. Our findings not only underscore the plasticity of macrophage transcription, but also extend mechanistic insight beyond of the vasculature and into the dynamics of EMAP II on recruited macrophages.

4.2 Methods

All studies complied with the animal protocols approved by the University of Notre Dame/Indiana University Institutional Animal Care and Use Committee.

Cell culture and primary macrophage preparation. Four percent (w/v) thioglycollate broth dissolved in sterile water was injected intraperitoneally into gender-matched, 6-12 weeks old C57BL/6 mice (Jackson Laboratories). Seventy-two hours following injection, peritoneal macrophages were collected by flushing the peritoneal cavity with 8 mL of PBS containing 5% (v/v) EDTA. Any red blood cells, if any, were lysed with red blood cell lysis buffer (Biolegend) for 5 minutes at room temperature. The cell suspension was then centrifuged, counted, and re-suspended to a concentration of 2 x 10^6 cells/mL in DMEM (Hyclone) containing 10% (v/v) heat-inactivated fetal bovine serum (FBS, Seradigm).

EMAP II Preparation 6x-His tagged EMAP II was prepared as mentioned previously[33]. The endotoxin levels in all preparations used for this study were below detectable limits, containing <0.1 ng/EU (GenScript). Also complementarily to this, as seen in the results, there was a minimal difference in NF-κB activation between EMAP II and its control, which is consistent with a previous report[88].

RNA Isolation and qPCR—Total RNA and qPCR was performed as previously described except with the following[66]: RNA isolation was performed with Direct-zol (R2050, Zymo Research).

TEPM Treatments, Cell Fractionation, Immunoblotting, and Cytokine Analysis. Cells were plated at 2 x 10^6 cells per well in 12-well plate containing 1 mL of media, were rested at 37^{o}C with 5% (v/v) CO_2 for 2-4 hours, washed at least 2 times with PBS, and then replaced with DMEM containing 1% (v/v) FBS overnight. The following morning, cells were treated with EMAP II (2 μg/mL) for the indicated time points. At the end time point, cell lysis followed by immunoblotting was performed as previously described[85]. Antibodies against total Histone H3, JAK2 (Y1007), STAT3 (Y705), and ACTB were all obtained from Cell Signaling Technology. Cellular fractionation to obtain cytoplasmic and nuclear isolates of TEPMs was performed using the Pierce NE-PER kit per manufacturer's instructions. At the end point, the supernatant was collected, centrifuged at 12,000 g at 4^{o}C for 5 minutes to clear debris, frozen in liquid nitrogen, and stored at -80^{o}C until further analysis by Eve Technologies (Canada).

Luminescence assay. Following the previously mentioned macrophage preparation and suspension, 10 x 10^6 TEPMs were seeded in a 10 cm petri dish. After overnight incubation with DMEM containing 1% (v/v) FBS, TEPMs were exposed to either vehicle or EMAP II (2 μg/mL). Once nuclei were isolated, the transcription factor activation assay was performed using 5 micrograms of nuclear isolate and as per manufacturer's protocol (Signosis). Once luminescence signals were obtained, fold changes were calculated and then log2 transformed.

Luciferase assays. HEK293-T cells were cultured in DMEM media containing 10% serum (Seradigm). 1 x 10^5 cells were reverse transfected with 200 ng of pGL3-STAT3 and 10 ng of pRL-null vectors (Promega Inc.) using Attractene (Qiagen) as per manufacturer's protocol. Cells were then incubated with either EMAP II, IL-6 (BioLegend) or both. Following overnight incubation with the listed ligands, the cells were lysed with Passive Lysis Buffer (Promega) and luciferase assay performed as per manufacturer (Dual-Glo Luciferase Assay, Promega). HEK293-T cells (ATCC) were tested for mycoplasma.

4.3 Results

Time-dependent, distinct transcriptional profile induced by EMAP II in partially activated thioglycollate-elicited macrophages (TEPM). Similar to other secreted cytokines, there is most likely a dynamic, transient transcriptional profile. Messenger RNA expression of genes notable in macrophage function was measured over a time course by quantitative PCR analysis (Figure 4.1). Expression levels of most genes in partially activated macrophages typically peaked between approximately 2 and 4 hours but all subsided by 21 hours. This indicates a transient response of macrophages exposed to EMAP II. It was expected that the expression levels of both inflammatory and chemokine effector genes would increase[24,85,89]. Accordingly, *Tnf*, *Il1b,* and *Il6* peaked nearly concurrently by 2 hours and subsiding by 4 hours while *Nos2* peaked later by 4 hours and subsided by 21 hours. Likewise, with EMAP II as an effector of myeloid cell recruitment, chemokinic genes were also expected to increase. The transient profiles of *Ccl2* and *Ccl9* were similar to that of the inflammatory effector genes – peaking by 2 hours and subsiding by 4 hours; meanwhile, *Ccl5* increased and remained elevated at the end of the time course by 21 hours (Figure 4.1A).

A part of the plastic transcriptional response of macrophages, levels of anti-inflammatory genes typically increase as a means of a brake to the inflammatory process. *Il10*, a key anti-inflammatory gene, significantly increases when exposed to pathogens or typically between 2 and 4 hours[17,90]. However, upon EMAP II exposure, *Il10* was actually decreased by 1 through 4 hours before returning nearly to baseline (Figure 4.1B). Although *Il10* did decrease, anti-inflammatory markers *Mrc1* and *Retnla* did not over the

time course (Figure 4.1C). Interestingly, a key gene in macrophage metabolism of arginine, *Arg1* levels increased by 0.25 hours (i.e. 15 minutes) and remained elevated until 3 hours; an inhibitor of JAK-STAT signaling, *Socs3* peaked at 2 hours (Figure 4.1C). Collectively, this transient transcriptional response in macrophages exposed to EMAP II is unlike that of other reported highly macrophage-polarizing secreted factors, suggestive of a unique, EMAP II-specific, distinct transcriptional profile.

Profiling for activated transcription factors in macrophages exposed to EMAP II. We noted the unique transcriptional profile in macrophages exposed to EMAP II. The transcription factors that are activated in response to EMAP II are unknown. According to classical transcription factor signaling principles, the activation of transcription factors typically includes phosphorylation followed by a translocation from cytoplasm to nucleus where it binds to DNA. We performed a luminescence-based screen that compared phosphorylated, translocated transcription factors contained in nuclear isolates fractionated from TEPMs treated with EMAP II for 2 hours to untreated nuclear isolates from TEPMs to experimentally identify EMAP II-activated transcription factors. STAT3 was the most highly activated transcription factor (Figure 4.2). Notable was a lack of difference in NF-κB p65 luminescence signal (Figure 4.2), an inflammatory transcription factor; similarly, there were minimal differences in both nuclear translocation and phospho-serine phosphorylation of the inflammatory transcriptional mediator, NF-κB p65 (Figure 4.3D).

EMAP II-induced tyrosine phosphorylation of STAT3 is time dependent. We focused on STAT3, as it was the highest ranked transcription factor associated with gene transcription programs that are anti-inflammatory. Interestingly, STAT3 activation was in direct contrast to our hypothesis of activation of a pro-inflammatory transcription factor[91]. Activation of STAT3 by Y705 is typically temporally dynamic. Time course dynamics revealed a biphasic pattern with peak activation of Y705 phosphorylation of STAT3 by approximately 0.25 and 4 hours (Figure 4.3A). These results show that there was a very rapid activation of STAT3 upon exposure to EMAP II in TEPMs.

Increased promoter STAT3 activity following exposure to EMAP II. The level of transcriptional expression of any gene can vary despite promoter activity. We measured the functional activity of STAT3 based on its binding to a consensus-binding element, c-fos sis-inducible element region by luciferase assay. Cells transfected with STAT3 transcriptional reporter plasmids were exposed overnight to either EMAP II or a positive well-established acute STAT3 activator, interleukin (IL-6). EMAP II alone increased transcriptional activity, although less than IL-6 (Figure 4.3B). These results show that EMAP II does modestly increase STAT3 transcriptional activity.

EMAP II induced STAT3 phosphorylation by JAK. There are many kinases that phosphorylate STAT proteins, including, but not limited to, Src, JAK1-3, or Protein Kinase C. A brief 2-hour pretreatment with JAK-STAT inhibitor, ruxolitnib, decreased nuclear translocation of STAT3 (Y705) comparable to control (Figure 4.3E). There was rapid JAK2 activation in macrophages exposed to EMAP II (Figure 4.3C). While EMAP II activated STAT3, pre-treatment of TEPMs with ruxolitinib, a specific inhibitor of JAK1/2, ablated EMAP II-mediated STAT3 (Y705) (Figure 4.3D). Complete ablation of phosphorylation made it unlikely that another kinase such as Src was involved in the activation of STAT3. As an additional control, we confirmed that STAT3 activation is EMAP II specific by pre-treating TEPMs with either functional neutralizing antibody of EMAP II or non-specific IgG; compared to control, pre-treatment with the neutralizing antibody of EMAP II did prevent STAT3 activation (Figure 4.3D). Together, these results suggested that EMAP II-mediated STAT3 phosphorylation occurred primarily through JAK.

EMAP II increased Y705 STAT3 into the nucleus. To validate the screen and increased STAT3 promoter activity downstream of JAK, we fractionated nuclei from macrophages that were pretreated with either ruxolitinib or its vehicle, DMSO, followed by the addition of EMAP II. Supporting previous results of the activation of JAK-STAT signaling, a 1.6-fold increase in phosphorylated STAT3 (Y705) translocation to the nucleus verified the screen, as well as a 2.0-fold increase in the cytoplasmic fraction (Figure 4.3E). These

results indicate phosphorylated STAT3 translocates to the nucleus in TEPMs exposed to EMAP II, downstream of JAK-STAT.

STAT3 transcriptional activity is distinct to EMAP II and not dependent on either autocrine IL-6 or IL-10. Both IL-6 and interleukin 10 (IL-10) are well-established activators of STAT3 (Y705). Based on transient mRNA expression changes in both *Il6* and *Il10* in TEPMs exposed to EMAP II, it is possible that the translated and secreted cytokines would cause an autocrine, indirect STAT3 activation. To rule out this possibility, we measured secreted IL-6 and IL-10 in supernatants of TEPMs exposed to EMAP II overnight. There was an insignificant difference in levels of both IL-6 and IL-10 (Figure 4.4A), suggesting that an indirect STAT3 activation by EMAP II through autocrinic activation due to these cytokines was highly unlikely. Levels of transcripts *Il6* and *Il10* were measured in TEPMs pretreated with either ruxolitinib or its vehicle followed by exposure EMAP II. Similar to the time course, *Il6* levels were significantly increased but were not rescued by ruxolitinib pretreatment (Figure 4.4B), suggesting that neither *Il6* nor *Il10* are regulated through JAK-STAT signaling.

EMAP II increases both JAK-STAT independent and dependent gene expression and cytokine secretion. We noted that there was a discrepancy between the mRNA increases and cytokine secretion while ruling out JAK-STAT3 activation by autocrine feedback. To measure acute transcriptional effects of JAK-STAT signaling, we pre-treated TEPMs with ruxolitinib or vehicle for 2 hours before the addition of EMAP II and then measured expression levels of *Il1a*, *Socs3, and Csf3*, which are downstream targets of JAK-STAT3 signaling. Whereas all three genes significantly increased after exposure to EMAP II, only *Il1a* was not significantly reduced by pre-treatment with Ruxolitnib (Figure 4.5A). To assess how JAK-STAT3 affects cytokine secretion, we exposed TEPMs to EMAP II with or without pre-treatment of Ruxolitinib and measured varying secreted cytokine levels in media. Both IP-10 and CCL2 (MCP-1) expression, important chemokines, did increase; however, its secretion was not reversed by JAK-inhibition suggesting other regulatory mechanisms are involved (Figure 4.5B). Consistent with other reports of other anti-angiogenic factors, exposure to EMAP II induced significant VEGF

secretion that was JAK-independent. Consistent with a JAK-STAT signature, both IL-1α and G-CSF secretion by EMAP II was elevated and could be prevented by JAK inhibition, suggesting a JAK-dependent cytokine secretion (Figure 4.5C).

4.4 Discussion

The results yield at least three new insights into the function of EMAP II on recruited matured macrophages: (1) it produces rapid changes in the transcriptional profile of macrophages that is not consistent with known pro- or anti-inflammatory programs; (2) it activates STAT3; (3) through JAK2. Local tissue mediator EMAP II recruits myeloid cells to sites of injury. However, molecular mechanisms of macrophages upon recruitment and its activation upon exposure to EMAP II is not well known in part due to its poorly understood leaderless-sequence-driven secretion, making difficult to genetically target it. Therefore, with an *ex-vivo* model, this study explores the response of matured, partially activated, and recruited macrophages to EMAP II.

Macrophages dynamically respond to their environment through polarization. In TEPMs exposed to EMAP II, the changes in inflammatory gene expression found in Figure 4.1 were suggestive of an activation of inflammation but unique comparatively to other known inflammatory mediators of macrophages. The unique response to EMAP II in macrophages is in line with what recent reports suggest in similar *ex vivo* systems – that the transcriptional profile is both not as dichotomous as once viewed in the past and is unique to an individual ligand[17]. For active pro-inflammatory shift, there is generally a consistent suppression of its counterpart, anti-inflammatory genes that was absent in our study. As examined by qPCR in Figure 4.1, although there was an early suppression of *Il10*, there was a lack of noticeable suppression of other anti-inflammatory genes *Mrc1, Retnla*; further, the *Il10* expression returned to baseline unlike other inflammatory mediators[92]. Notably, the rapid induction of *Arg1* seen as early as 15 minutes of exposure to EMAP II in this murine system is unlike other ligands that typically require at least 24 hours for maximal induction. The results here show that there is a unique, transient EMAP II-mediated, transcriptional reprogramming that can occur in recruited macrophages.

In searching for transcription factors activated by EMAP II, STAT3 was indeed activated as evidenced by the luminescence screen, functionally shown by measuring

promoter activity and key STAT3 target gene expression, downstream of its kinase JAK1/2. This is consistent with that of other 'find-me' signals such as sphingosine-1-phosphate and macrophage migration inhibitory factor that can also activate JAK-STAT3[93]. Whereas JAK-STAT target gene *Socs3* is an inhibitor of endothelial cell angiogenesis, its function in macrophages remain unclear as to as to whether it is important for the initiation or resolution of inflammation. There were clearly transient increases in its gene expression, partially mediated by the acute pre-treatment of JAK-STAT inhibitor. The transient increase suggested that there not only might be an EMAP II-mediated STAT3 role in macrophages but also other transcriptional complexes. Other activated STAT transcription factors can complex with STAT3 such as STAT1, but upon further examination, there were minimal, detectable changes in tyrosine phosphorylation. Many of the measured target genes can also be differentially regulated by NF-κB (p65), a transcription factor of many inflammatory genes especially in macrophages. There was a minimal difference in NF-κB activation, a transcription factor important for the activation of many of these genes[88].

Consistent with other "find-me signals" such as CX3CL1 or sphingosine-1-phosphate, the EMAP II-induced increase in tyrosine phosphorylation of STAT3 validated the transcription factor activation screen. Upon validation, there was a biphasic response STAT3 tyrosine phosphorylation similar to the response to IL-6, suggesting autocrinic mechanisms. In contrast to IL-6, EMAP II induces a longer window of STAT3 phosphorylation between each phase. Additionally, there may be an autocrinic mechanism to prolong the phosphorylation by known factors such as IL-6, IL-10, or EGF. However, in response to EMAP II, there was not a significant difference in both IL-6 and IL-10 in supernatants. Increased transcriptional activity suggest an autocrine feedback mechanism in favor of an IL-6 independent STAT3 activation by EMAP II. Future studies will identify the factors for the latter, prolonged STAT3 activation.

This is the first report of STAT3 activation in macrophages following exposure with EMAP II that has been regarded generally as a pro-inflammatory cytokine. Based on our previous study and results presented here, there may be different regulatory mechanisms of JAK-STAT3 activation that result in distinctive target genes. A reasonable expectation would be, similar to other pro-inflammatory ligands that signal through

JAK/STAT3, that only certain pools of STAT3 complexes are activated. Thus, the target genes of STAT3, such as IL-1A, G-CSF (encoded by *Csf3*), SOCS3 or MCP-1, that are activated by EMAP II should be reversed by inhibition[86,87]. Indeed, in our study, the elevation of STAT3 target cytokines such as IL-1A or G-CSF was prevented by JAK-STAT inhibition, but neither STAT3 target gene MCP-1 nor VEGF were inhibited. A possible explanation to be explored is that the transcription factor, nuclear factor 1 (NF-1) as seen in our screen, can also directly regulate MCP-1 expression[94]. Future studies will further explore the transcription factor complexes downstream of EMAP II-induced JAK-STAT signaling, including, but not limited to, NF-1 and those that may cooperate with STAT3.

The activation of STAT3 raises many possibilities into further mechanisms of EMAP II. For example, there may be early-phase and late-phase-specific STAT3 complex formations induced by EMAP II similar to TNF or other "find-me" signals. Initially, there might be an overall activation of inflammatory genes defined by competition of activated transcription factors on gene promoters; later, the complexes could rearrange to yield an anti-inflammatory profile. Our data presented in this dissertation highlight particularly early transcriptional changes in macrophages in response to EMAP II. Interestingly, some of these changes were reversed with the inhibition of JAK-STAT signaling suggesting that this competition might be controlled by upstream events. We show that the STAT3 activation was JAK1/2 dependent, similar to what is known about IL-6-dependent JAK-STAT activation. As seen in other modules of signaling by cytokines such as IL-6, typically the ligand binding to its receptor causes conformational change to activate the JAK family then recruit and phosphorylate STATs. Therefore, it is plausible that although not yet identified, EMAP II has multiple receptors, of which some of them function through JAK. Another laboratory suggested CXCR3 to be a receptor of EMAP II on endothelial cells but this has neither been shown in macrophages[95] nor has CXCR3 been shown to interact with JAK. Without receptor identification of EMAP II, it remains unclear if there are other factor(s) responsible for prolonging the observed biphasic JAK-STAT3 activation. For example, factors such as IL-6 or IL-10 can often prolong or promote STAT3 re-activation through autocrinic mechanisms. However, in our

experiments, we did not see a significant release of either factor, suggesting that neither factor is responsible for the observed STAT3 reactivation at 24 hours.

This study identifies a JAK-STAT molecular signaling pathway partially mediated by EMAP II in the recruited macrophage population following injury. We propose that after serving a role as a "find-me" signal in injury, EMAP II elicits a subset of STAT3 genes in recruited, activated macrophages. Its expression generally localized near the site of injury, suggesting it to be a local mediator of gene expression. This is supported by mixed and transient STAT3 signaling partially mediated through JAK in macrophages to activate them to a unique inflammatory profile. Overall, this presents an opportunity for future studies to explore the re-programming of macrophage gene expression induced by EMAP II and its pleiotropic functions in injury, remodeling, and repair.

4.5 Figures

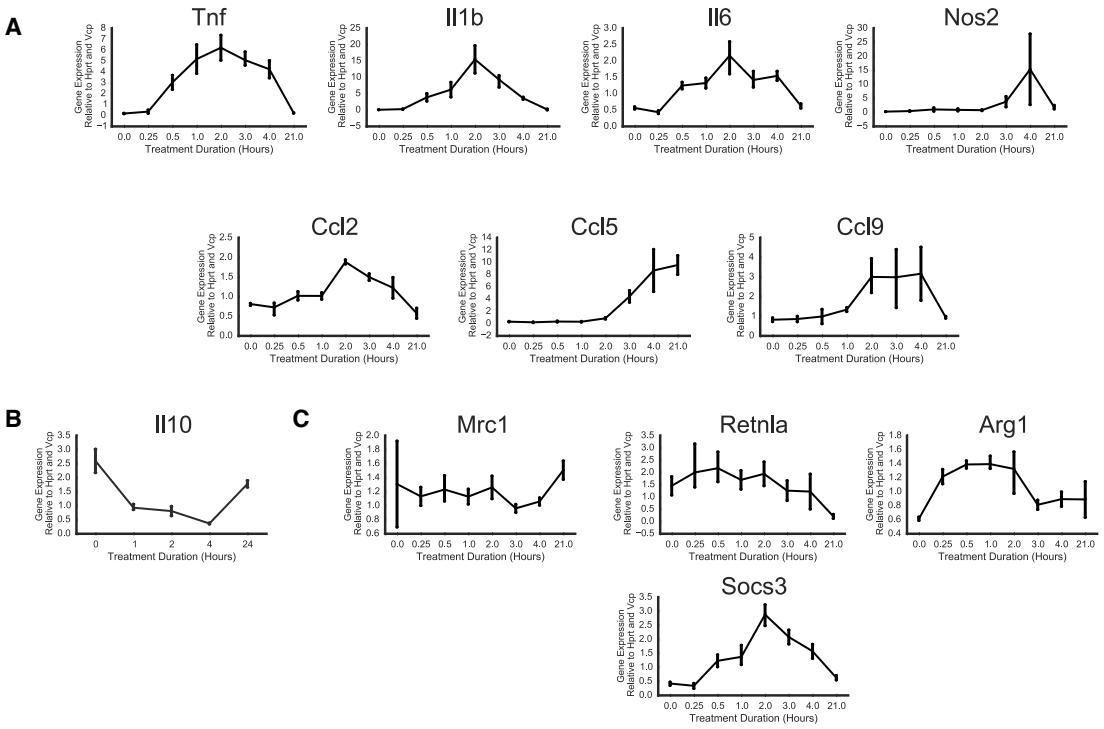

Figure 4.1. EMAP II activates a distinct, transient transcriptional profile in macrophages. Thioglycollate-elicited peritoneal macrophages were treated with EMAP II (2 μg/mL) for a time course of 21 hours as indicated. Quantitative PCR of (A) inflammatory, (B) anti-inflammatory *Il10*, and other genes associated with (C) an anti-inflammatory state in macrophages. Indicated on the line graphs is the arithmetic mean ± one standard error of mean (n = 3 independent TEPM isolations).

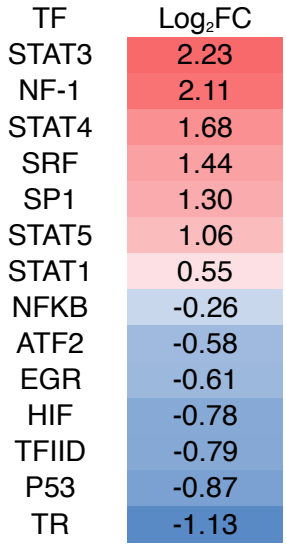

Figure 4.2. EMAP II mediated changes in transcription factor activation. Nuclei were isolated from TEPMs exposed to either vehicle (PBS) or EMAP II (2 μg/mL). Listed are the activated and de-activated nuclear transcription factors (TF), including STATs and NFkB, ranked by log2 transformed fold change (Log_2FC) between EMAP II and vehicle treatments.

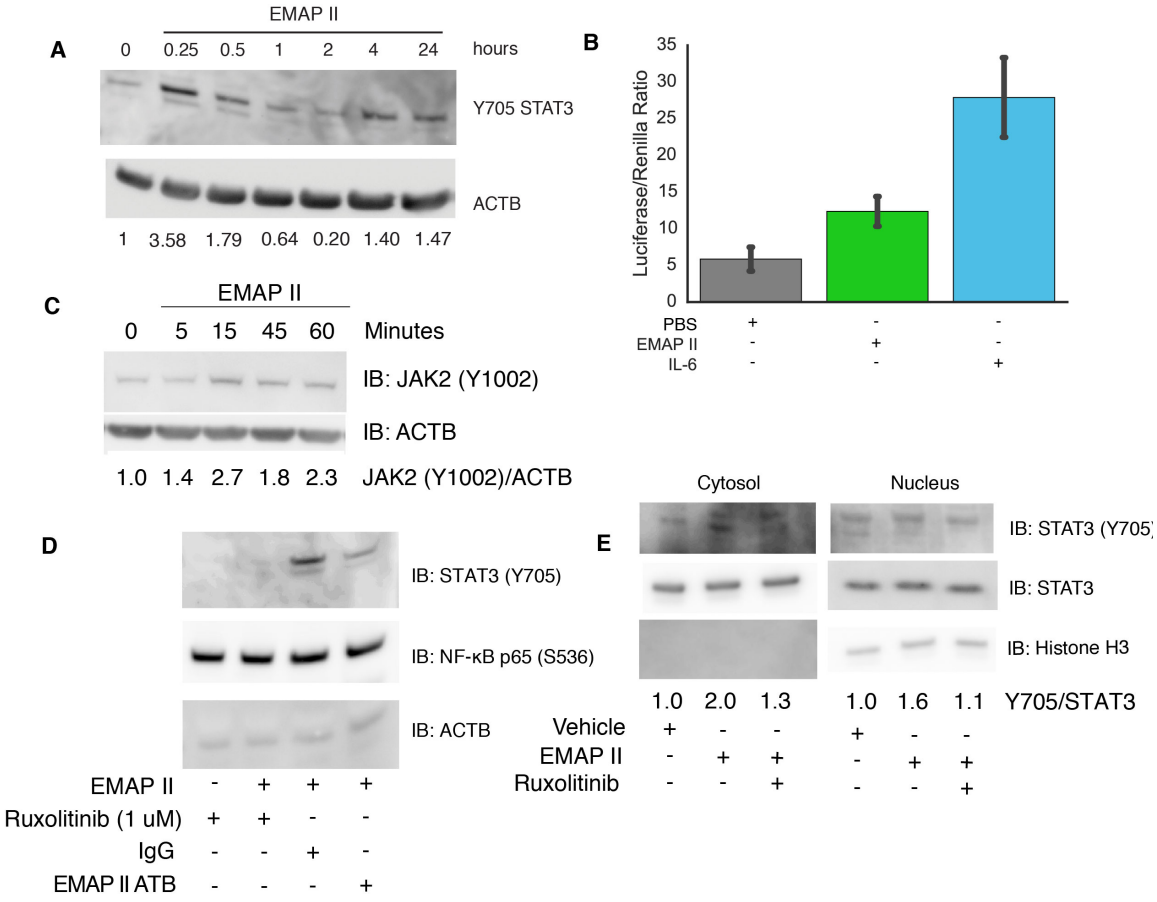

Figure 4.3. EMAP II-mediated activates JAK-STAT3 signaling. (A) STAT3 activation is time-dependent. TEPMs treated with EMAP II (2 µg/mL) for the indicated times and immunoblotted for Y705 STAT3. Results are representative of 3 independent, gender-matched experiments. (B) EMAP II induces STAT3 transcriptional activity. HEK293-T cells were reverse transfected with 200 ng of pGL3-STAT3 and 10 ng of pRL-null vectors then exposed overnight to vehicle, EMAP II, IL-6 (20 ng/mL) or a combination of both. Results are representative of 4 similar experiments each with at least 2 well replicates. (C) EMAP II induces STAT3 phosphorylation that is mediated by JAK2. TEPMs were treated with EMAP II and immunoblotted for phosphorylated JAK2, indicating activation. (D) TEPMs were pre-treated with control, non-specific rabbit IgG antibody (5 µg/mL) or EMAP II neutralizing antibody (5 µg/mL) for 1 hour and then treated with EMAP II (2 µg/mL) for 15 minutes. JAK1/2 dependency was assessed by pre-treating TEPMs with vehicle (DMSO) or Ruxolitinib (1 µM) followed by the addition of EMAP II for 15 minutes. Lysates were then immunoblotted for tyrosine phosphorylation of STAT3. Results are representative of (C) 3, (D) 2 independent experiments.(E) Nuclear translocation of phosphorylated STAT3. RAW264.7 cells were treated with vehicle or Ruxolitinib for 2 hours before the addition of EMAP II (2 µg/mL) for 15 minutes. Cells were then fractionated into nuclear and cytoplasmic fractions. Histone H3 was used to verify nuclear fractionation. Images are representative of 3 individual preparations.

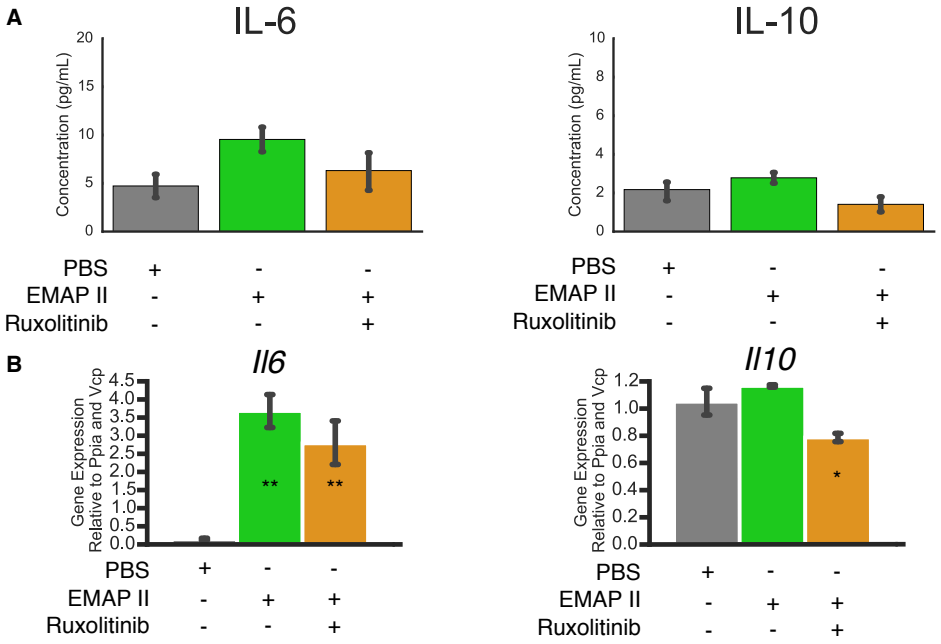

Figure 4.4. STAT3 activation does not depend on secreted IL-6 and IL-10. (A) Secreted IL-6 and IL-10 were measured in supernatants from TEPM exposed overnight to EMAP II (2 µg/mL) or control. Indicated is representative of one experiment containing three individual TEPM preparations. The experiment was performed twice with similar results. Indicated on the line graphs is the arithmetic mean ± one standard error of mean (n = 3 independent TEPM isolations). PBS was used as vehicle and a control. (B) Il6 and Il10 transcript levels measured in TEPM with the same experimental conditions as (A). Indicated are the arithmetic mean ± one standard error of mean (n = 3-4 independent TEPM isolations). ** p-value < 0.01, compared to PBS; * p-value < 0.05, compared to EMAP II).

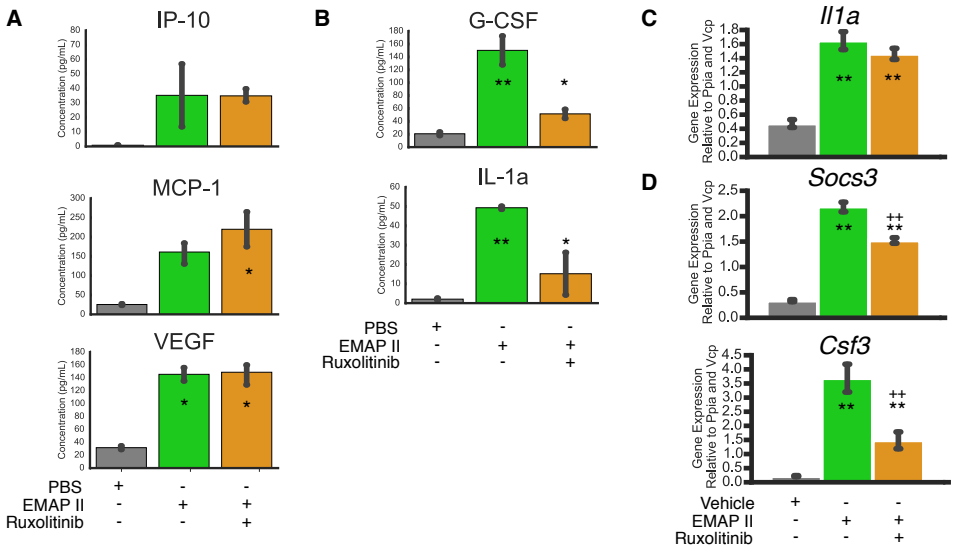

Figure 4.5. Cytokine profile induced by EMAP II in TEPMs. TEPMs were treated with EMAP II (2 µg/mL) overnight, and secreted cytokines quantified. (A) JAK-independent, EMAP II-mediated cytokines. Inhibition of elevated, secreted JAK-STAT3 target cytokines (B) JAK-dependent cytokine secretion. (Following one-way ANOVA, Tukey's HSD: PBS vs. EMAP II **p-value ≤ 0.01, EMAP II vs. Ruxolitinib + EMAP II, *p-value ≤ 0.05). Indicated is the arithmetic mean ± one standard error of mean (n = 3 independent TEPM preparations). Represented is one of 2 experiments. (C and D) Transcript levels following JAK-STAT inhibition. TEPMs were either pretreated with Ruxolitinib or vehicle (DMSO in PBS) for 2 hours, then EMAP II (2 µg/mL) was added for 2.5 hours. ** p-value ≤ 0.001 compared to vehicle; ++ p-value ≤ 0.001 compared to EMAP II. Indicated is the arithmetic mean ± one standard error of mean (n = 3-4 independent TEPM preparations).

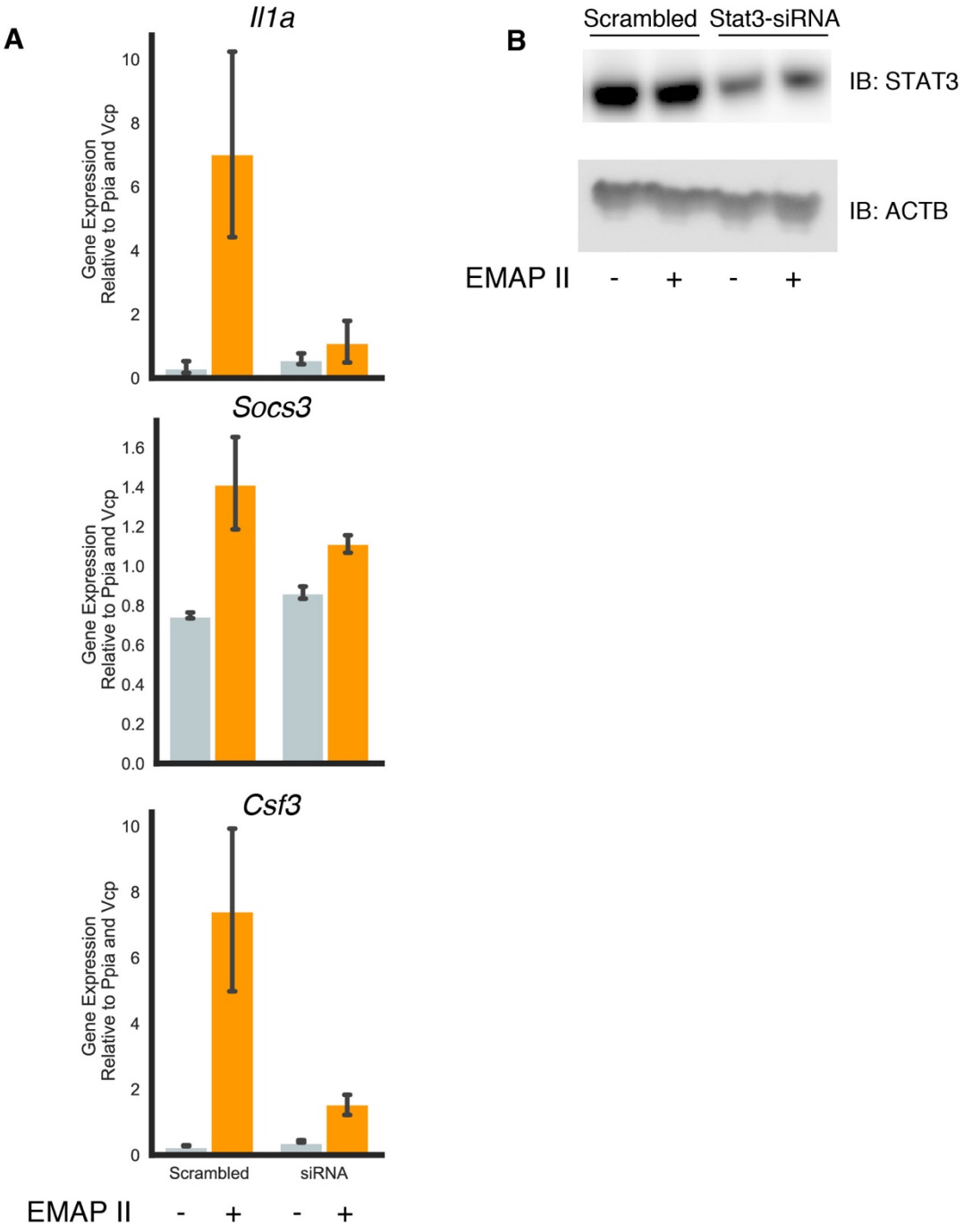

Figure 4.6. Transcripts induced by EMAP II in RAW264.7 cells. (A) Transcript levels of the same target genes as shown in Figure 4.5. Genes were measured in RAW264.7 cells transfected with either scrambled or siRNA against *Stat3* then exposed to EMAP II (2 µg/mL). (B) Immunoblot of total STAT3 amounts and loading control β-actin. Indicated is the arithmetic mean ± one standard error of mean (n = 3 replicates, 2 independent experiments.)

Chapter 5: The critical role of AIMP1 in lung development

5.1 Introduction

During mammalian lung development, precise coordination of signaling events occur. The five stages of the development, in mice, begin with the embryonic phase (~E9.5-E10.5) and transitions to the "pseudoglandular" phase (~E10.5-E16.5) when epithelial buds emerge and branch into its surrounding mesenchymal interface to produce the respiratory bronchial tree[8]. Following these two stages, during the "canalicular" (~16.5-E17.5) and "saccular" (~E17.5 until postnatal day 0.5) phases, the surrounding mesenchyme becomes less predominant while distal epithelial tubules remodel to form primary septae – they subdivide eventually into primitive alveolar sacs.

Beginning partially in the canalicular stage, alveolarization begins when epithelial progenitor cell populations within the outwardly growing tubules differentiate into Type I or II alveolar epithelial cells or pneumocytes in order to mediate gas-exchange and surfactant synthesis, respectively. The epithelial-mesenchymal interface is the site of continual exchange of signaling factors that spatiotemporally guide proper sacculation[3]. Numerous studies describe factors necessary for early lung budding and respiratory branching. However, the mechanisms of those factors that control the formation of interface are not well known.

Factors important for sacculogenesis are expressed at the epithelial-mesechymal interface, but so far, only a few have been identified[3,88]. The 34 kilodalton Aminoacyl tRNA Synthetase Interacting Multifunctional Protein 1 (AIMP1) is expressed at the interface of epithelial and mesenchymal cells throughout murine development. Its expression in the lung inversely correlates with the vascularization that begins in the canalicular stages. Structurally, AIMP1 has 3 domains: (1) an N-terminal leucine zipper, coiled coil; (2) intrinsically disordered region; (3) C-terminal Endothelial Monocyte Activating Polypeptide II (EMAP II). The N-terminal domain interacts with components of tRNA synthetases while the intrinsically disordered region (IDR) lacks a specific three-dimensional structure[89]. As a result, they were presumed to lack any physiological function including that found in AIMP1. However, recent studies have identified liquid-like properties of IDRs that allow them to transiently interact with molecules on either side of lipid membranes such as phosphoinositides, which are very crucial signaling

components of cellular motility and epithelial cellular polarity, or other intracellular components such F-actin[41,90,91]. Consistent with other proteins that contain IDRs, AIMP1 localizes to the cell surface membrane[92,93]. However, its function has not yet been characterized. Although functions of EMAP II have been characterized in various aspects of lung development and pathophysiology, the intracellular AIMP1 and its underlying molecular mechanism(s) has not.

With its localization at the epithelial-mesenchymal interface, AIMP1 may regulate sacculogenesis; disruption of the expression of AIMP1 may hinder proper lung development. The study presented here utilized an exon-deletion model that was generated on a C57BL/6 background to test the hypothesis that *Aimp1* regulates lung development. Ablation of *AIMP1* led to neonatal lethality and abnormal epithelial cell organization of both bronchiolar and alveolar regions. Having verified the localization of AIMP1 to the cell membrane, we found that AIMP1 interacted with various phosphoinositides. F-actin deposition was disrupted in fibroblasts from *Aimp1 -/-* mice , suggesting that AIMP1 plays a role in F-actin remodeling, a necessary feature for sacculogenesis and alveolarization. Together, these results suggest AIMP1 critically regulates lung development.

5.2 Methods

Mice Studies

All animal studies complied with the animal protocols approved by the Indiana University Institutional Animal Care and Use Committee. We generated and verified *AIMP1* -/- mutant mice as described in detail in the online supplement.

Generation of AIMP1 Knockout Mice

C57BL/6 mice were obtained from Jackson Laboratories. Studies using mice were performed according to the animal protocols approved by the Indiana University Institutional Animal Care and Use Committee. The UTSW Transgenic Mouse Core generated the *AIMP1 -/-* (AIMP1 KO) mice. Mouse embryonic stem (ES) cells were selected after transfection using electroporation with AIMP1 targeting vector, in which one loxP site and Frt sites contained neomycin resistance gene cassette were introduced

into intron 1 of AIMP1 gene, one loxP site was introduced into intron 2 of AIMP1 gene. ES stable clones were identified using Southern blotting and PCR sequencing analysis, and then were injected into blastocysts harvested from C57BL/6 mice. Chimeric founder mated with C57BL/6 female mice and created F1 offspring. F1 female mice mated with FLP transgenic male mice to create F2 mice carrying heterozygous floxed AIMP1 and FLP. Mating of female and male F2 created homozygous floxed AIMP1 F3 mice. Mating of female F2 with CAG-Cre transgenic mice generated heterozygous AIMP1 KO and CAG-Cre F3 mice. Mating these two types of F3 mice generate homozygous AIMP1 KO mice expressing Cre.

Cell lines and reagents

HEK293 and MDCK cell lines were obtained from ATCC and cultured in DMEM containing 10% fetal bovine serum (Seradigm), 1X Glutamax (Invitrogen), and 1X penicillin/streptavidin (Invitrogen). Cells were passaged below 80% confluency or harvested as indicated in the experiments.

Recombinant AIMP1 preparation

6x-His tagged EMAP II was prepared as previously described[33]. Endotoxin concentration in samples was <0.1 EU/mL as determined by LAL assay (88282, Pierce).

Transmission Electron Microscopy

The lung specimens were fixed in 3% Glutaraldehyde/0.1M phosphate buffer. After primary fixation the specimens were rinsed with phosphate buffered saline (PBS) followed by post fixation with 1% osmium tetroxide in phosphate buffer for one hour. After rinsing again with PBS the tissue specimens were dehydrated through a series of graded ethyl alcohols from 70 to 100%. After dehydration the specimens were infiltrated with 2 changes of 100% acetone and a 50:50 mixture of acetone and embedding resin (Embed 812, Electron Microscopy Sciences, Hatfield, PA) for over the weekend. Specimen vial lids were popped and acetone allowed to evaporate off for 3 hours. Then specimens were embedded in a fresh change of 100% embedding media. Following polymerization overnight at 60°C the blocks were then ready to section. Thin sections

were cut (80-90nm), stained with UA replacement stain, (Electron Microscopy Sciences, Hatfield, PA) then viewed on a Tecnai Spirit (ThermoFisher, Hillsboro, OR) with digital images taken with an AMT (Advanced Microscope Techniques, Danvers, MA) CCD camera.

Wet-to-dry lung weight ratios

Lungs were removed surgically from pups on day 0, weighed, recorded as the wet weight, and then dried at 65 degrees Celsius for 48 hours. The ratio was then calculated by dividing the wet with the dry weight.

Immunoblotting

Sections of the right lung were placed in tubes containing modified lysis buffer. The tubes were then placed and homogenized in Bullet Blender Storm (BBY24M, Next Advance Inc.). Protein concentrations were determined by Bradford reagent (Bio-Rad). Twenty micrograms of lung tissue homogenates were loaded into NuPage Novex 4-12% Bis-Tris Protein gels (Invitrogen), incubated in 20% ethanol for 5 minutes, and transferred onto nitrocellulose membranes using iBlot v2 (Invitrogen). The membranes were placed in 5% blocking buffer (BioRad) in tris-buffered saline with 0.05% Tween-20 for 1 hour at room temperature. Membranes were incubated overnight at 4 ^{o}C in primary antibodies listed in Supplementary Table.

Lung Tissue Immunofluorescence and Morphometry Analysis

Lung tissue sections were prepared as previously described with slight modifications [94]. Antigens on lung sections of five microns were retrieved and stained with antibodies according to Supplementary Table.

Biotinylation

After being grown to near confluency, HEK293 and MDCK cells were used for biotinylation assays (Pierce). The assays were done according to the manufacturer's instructions.

Lipid Overlay Assay

Putative interactions of recombinant AIMP1 and membrane lipids were performed according to manufacturer's instructions (Membrane Lipid Strips, Echelon Biosciences).

5.3 Results

***Aimp1* gene targeting, confirmation, and verification of null allele.** To determine the role of Aimp1 in development, we generated mice with a conditional floxed allele of the *Aimp1* gene to enable targeted deletion. The targeting vector was designed to allow for the loxP-mediated deletion of exon 2 of the *Aimp1* gene. The CMV-Cre genetic driver was used to generate a whole-body knockout of *Aimp1* in mice following the removal of the selection cassette. There was a global loss of *Aimp1* following homologous recombination (Figure 5.1A). Genomic PCR obtained from tail samples confirmed recombination of the floxed *Aimp1* allelle (Figure 5.1B,C). Immunoblotting established the loss of Aimp1 protein in lungs of knockout mice compared to littermate wildtype (AIMP1 WT) (Figure 5.1D). Heterozygous mice ($Aimp1^{+/-}$) were fertile and viable; they were further mated and their litters recorded. By the time neonatal progeny of the heterozygous mice were weaned, however, homozygous null *Aimp1*-deficient or knockout ($Aimp1^{-/-}$) mice were not recovered. This suggested that Aimp1 could impact murine development.

Homozygous null *Aimp1* mutation in mice causes neonatal lethality. Heterozygous mice were mated and sacrificed at various time points through development. Genotypes of progeny were recorded at embryonic days 14.5 (E14.5), 18.5 (E18.5), and day of birth (D0). Observed Mendelian ratios, 1:2.44:1.05, 1:3.1:1.89, 1:2.7:1.5, respectively, throughout mouse development were not significantly different from expected Mendelian ratios (Table 5.1). These observations suggest that *Aimp1* deficiency is not lethal during embryogenesis and follows Mendelian genetics.

AIMP1 deletion leads to a respiratory distress phenotype with impaired sacculogenesis. Preceding day of birth, mice were viable. However, D0 knockout mice appeared mildly cyanotic and died within 24 hours, suggesting that these mice suffered

from respiratory distress (Figure 5.2A). Analysis of Mendelian ratios of knockout to wildtype mice at the time of weaning supported neonatal lethality (Table 2). Gross morphology of the excised cardiothoracic lung blocks revealed mild distal alveolar dysplasia at the distal edges (Figure 5.2B). Although AIMP1 did not lethally affect embryogenesis, it could play a role in determining other aspects of lung development. Therefore, lungs at E14.5 and D0, during canalicular and saccular stages, were examined. Histologic analysis did not reveal any differences between genotypes in E14.5 (Figure 5.2C).

However, at both D0 and E18.5, an earlier time point in sacculogenesis, lung and body weights were significantly decreased (Table 5.3). In the knockout mice, lungs were dysplastic as determined by H & E staining (Figure 5.2C, right column). The bronchioles of the forming respiratory tubules in wildtype lungs were singly layered of columnar or cuboidal epithelial cells (Figure 5.2C, middle column). In contrast to the organized epithelium in WT mice, in D0 KO lungs, the epithelium was disorganized and its nuclei positioned at various levels, similar to that observed in the normal pseudostratified epithelium of the pseudoglandular stage (Figure 5.2C). Supporting the disorganization as observed in H & E, immunofluorescence of E18.5 lungs revealed that E-cadherin expression was no longer restricted to the lateral membrane between epithelial cells in knockout mice (Figure 5.2D). Rather it was observed in the apical membrane as well. Furthermore, CCSP expression was expressed in close proximity in distal epithelium of lungs of knockout but not in wildtype mice (Figure 5.2E). These results suggest that Aimp1 regulates the organization of epithelial cells during sacculogenesis.

Characterization of alveolar epithelial cells in knockout mice. It is possible that because of improper epithelial cell organization, lungs of knockout mice are leaky, incapable of clearing fluid upon birth, and as a result become cyanotic. To test this possibility, wet-to-dry ratios of lungs excised from wildtype and knockout mice were compared at D0. There was an insignificant difference between the ratios suggesting that there was a lack of difference in lung inflation upon the day of birth (Figure 5.3A). Similarly, lungs from both knockout and wildtype mice remained buoyant in lung

flotation tests at D0 (data not shown). Together, these results suggest that lungs in *Aimp1* -/- mice can properly inflate and do not suffer from pulmonary edema.

If lungs can properly inflate, then surfactant deficiencies or abnormalities are unlikely. To test this, by immunoblotting, there was no significant change in total surfactant protein C levels that were measured in D0 lung homogenates (Figure 5.3B). Similarly, immunofluorescence and transmission electron microscopy revealed no significant defects in differentiation or cells containing lamellar bodies, respectively (Figure 5.3C, D). These results suggest that Type II cell differentiation was not significantly altered.

Although Type II cellular differentiation was comparable between AIMP1 +/+ and -/- mice, Type I was not. Lungs of knockout mice had significantly decreased Type I cell marker Aquaporin 5 (AQP5) protein levels compared to D0 littermate controls as measured by immunoblotting (Figure 5.3E). The deficiency in Type I cells was traced back to E18.5 when immunofluorescence of another Type I marker, podoplanin (PDPN) also showed a significant decrease in expression in knockout mice (Figure 5.3F).

Adherens Junctions in knockout mice are disorganized. Establishment of the epithelial cell-cell contacts is crucial to development. With the observed disorganization and deficiency in Type I, we postulated that adherens junctions (AJ) in knockout mice might be disrupted. Immunoblotting for markers of AJ in addition to E-cadherin, beta-catenin and P120 in D0 mice showed no significant differences between genotype (Figure 5.4A, B). Despite insignificant differences in protein expression, there was aberrant localization in knockout lungs as evidenced in immunofluorescence of AJ (Figure 5.4C).

AIMP1 localizes to the actin cytoskeleton-plasma membrane interface. Whereas in some reports AIMP1 is described to remain cytoplasmic, we and others previously reported that AIMP1 localizes to the cellular membrane, coinciding with its expression in tissue at the epithelial-mesenchymal interface. Immunofluorescence using an antibody against AIMP1 shows a portion that co-localizes with phalloidin, a stain for F-actin (Figure 5.5A). Complementing the immunofluorescence, biotinylation of cell-surface

bound proteins followed by immunoblotting show a portion of AIMP1 localizes to the outer membrane (Figure 5.5B).

AIMP1 lacks a domain classically known to interact with the membrane. However, with advanced technological approaches, domain prediction analysis suggests that AIMP1 contains an intrinsically disordered region[95]. Therefore, it is plausible that AIMP1 can directly with the membrane by way of the region. We tested this by using recombinant AIMP1 on lipid overlay assays and found that it could bind to phosphoinositides, such as phosphatidylinositol 3,4-bisphosphate, phosphatidylinositol 3,5-bisphosphate, and phosphatidylinositol 4,5-bisphosphate (Figure 5.5C). The identified phosphoinositides have all been shown to play a role in cytoskeletal dynamics.

Mouse embryonic fibroblasts isolated from wildtype or knockout mice at E14.5 were cultured and analyzed for their F-actin structure. Immunofluorescence showed several impairments in F-actin deposition and adhesion points of contact in knockout MEF's (Figure 5.5D, E). These results suggest that at least a portion of AIMP1 localizes to the cellular surface where it can interact with phosphoinositidess and regulate F-actin deposition.

5.4 Discussion

This study was to examine the role of intracellular AIMP1 during murine lung development. Mechanisms of the transitions from canalicular to alveolar stages are poorly understood. Particularly in the lung, its morphology during development dictates the later function and phenotype. The data presented in this study suggests that AIMP1 plays a crucial role in lung development through its regulation of epithelial cellular organization and interaction with the lipid membrane.

The generated AIMP1 knockout mutation described in this study was lethal on the day of birth. A recent study identified components of the tRNA synthetase complex to be essential in the human genome, but AIMP1 was not[38]. Given that the gene *AIMP1* is highly conserved across organisms, its functionality as a scaffold of the multi-synthetase complex might be redundant, and alternative functions in mammals may have emerged, i.e., a moonlighting function[19,96-98]. Supporting this notion, disruption of AIMP1 does not seem to significantly alter bulk protein translation[37]; similar results were found when

utilizing SunSET (data not shown). Therefore an insufficiency in global protein translation seems unlikely to account for the lethal phenotype in this study.

Characterization of the lungs of AIMP1 knockout mice revealed an insufficiency of Type I but not Type II cells. During sacculogenesis, a bipotent progenitor cell population differentiates independently into $Aqp5^{+}$ Type I and $Sftpc^{+}$ Type II cells, which both mature into alveologenesis[6]. Early events such as lung bud formation or branching in the stages preceding the saccular stage were not more thoroughly investigated. Examination of lungs at the canalicular E14.5 stages revealed no gross abnormalities; only until E18.5 was epithelial cell disorganization significant. This makes it less likely that there were defects in branching morphogenesis. Rather these experiments suggest AIMP1 to mediate differentiation of the bipotent progenitor cell population into Type I cells beginning in sacculogenesis.

Notably, the phenotypes of the AIMP1 knockout mouse subtly resemble the Crumbs3 knockout mice, further supporting a role for AIMP1 in epithelial cell development[99]. These resembling phenotypes suggest AIMP1 could impact epithelial polarity. AIMP1 localizes to the epithelial-mesenchymal interface within lungs[27,29]. Within the cell, its expression was at the actin cytoskeleton membrane, consistent with other proteins that contain intrinsically disordered proteins and interact with phosphoinositides. Improper F-actin deposition was found in MEFs lacking AIMP1. Although it is currently unknown how F-actin might impact epithelial differentiation in the developing lung, it is essential in other contexts. AIMP1 may possibly regulate the F-actin dynamics, and in turn impact epithelial cell organization and Type I cell differentiation.

This study shows that although AIMP1 is not essential for embryogenesis, it is for proper lung development. AIMP1 regulates the epithelial cellular organization through F-actin dynamics, and in turn, reduces the Type I cell differentiation. Further studies of AIMP1 on the development of organ systems, as well as a deeper understanding of the mechanisms may uncover other alternative moonlighting functions.

5.5 Figures and Tables

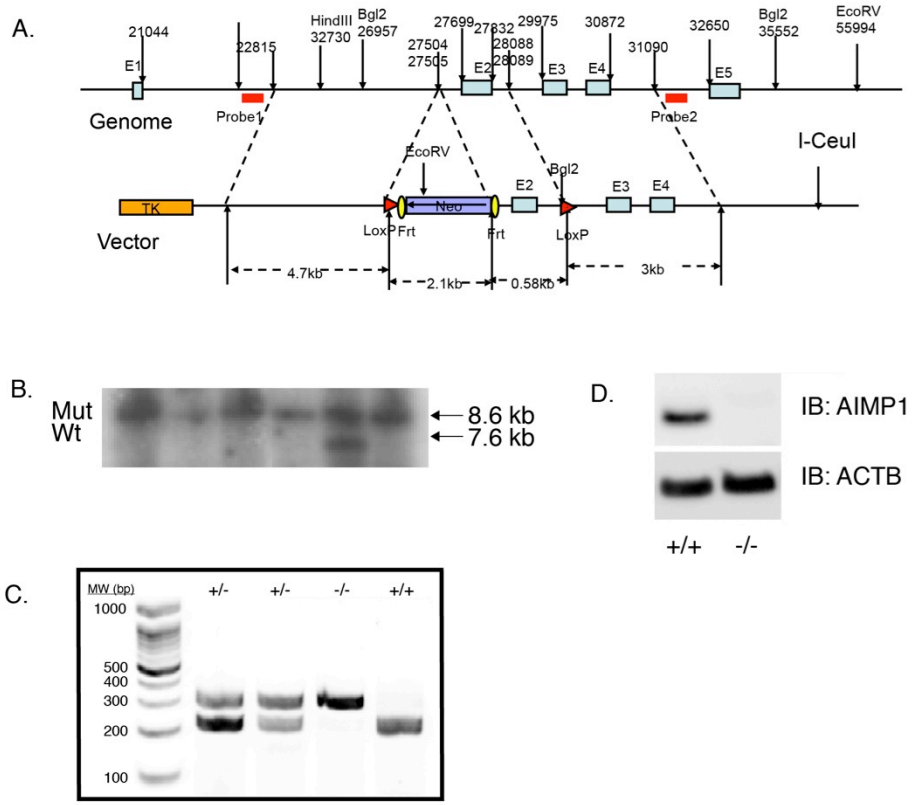

Figure 5.1. Generation of the *Aimp1* knockout mice. (A) Schematic of the *Aimp1* targeting construct used to generate knockout mice. Upper diagram illustrates the genomic structure of the *Aimp1* locus. Following homologous recombination as indicated by the dashed lines, the lower diagram indicates the NEO selection cassette. (B) Genomic DNA from wild-type and Aimp1 heterozygous mice were digested with the restriction enzyme Bgl2 and probed with a 32P-labeled 5' probe. The correctly sized bands on the Southern blot (i.e., 8.6 kb for the wild-type allele, 7.5 kb for the mutant allele) confirmed the homologous recombination event. Mut: mutant allele, Wt: wildtype allele. (C) Representative genotyping gel of genomic DNA obtained from tails of wildtype (+/+), heterozygous (+/-), knockout (-/-) mice. (D) Representative immunoblot probed for AIMP1 in the lysates of whole lung tissue obtained from +/+ and -/- mice.

		Genotype		
		+/+	+/-	-/-
E14	Observed	19	44	18
	Expected	20.25	40.5	20.5
E18.5	Observed	17	28	9
	Expected	13.5	27	13.5
D0	Observed	23	62	34
	Expected	29.75	59.5	29.75

Table 5.1. Observed counts of progeny obtained from heterozygous mice crossed over period of gestation. Chi-square test was used to evaluate if observed counts were not significantly different from expected at all ages.

		Genotype		
		+/+	+/-	-/-
D28	Observed	28	58	0
	Expected	21.25	43	21.25

Table 5.2. Observed counts of progeny obtained from heterozygous cross at the time of weaning. Chi-square test was used to evaluate if observed counts were not significantly different from expected at all ages.

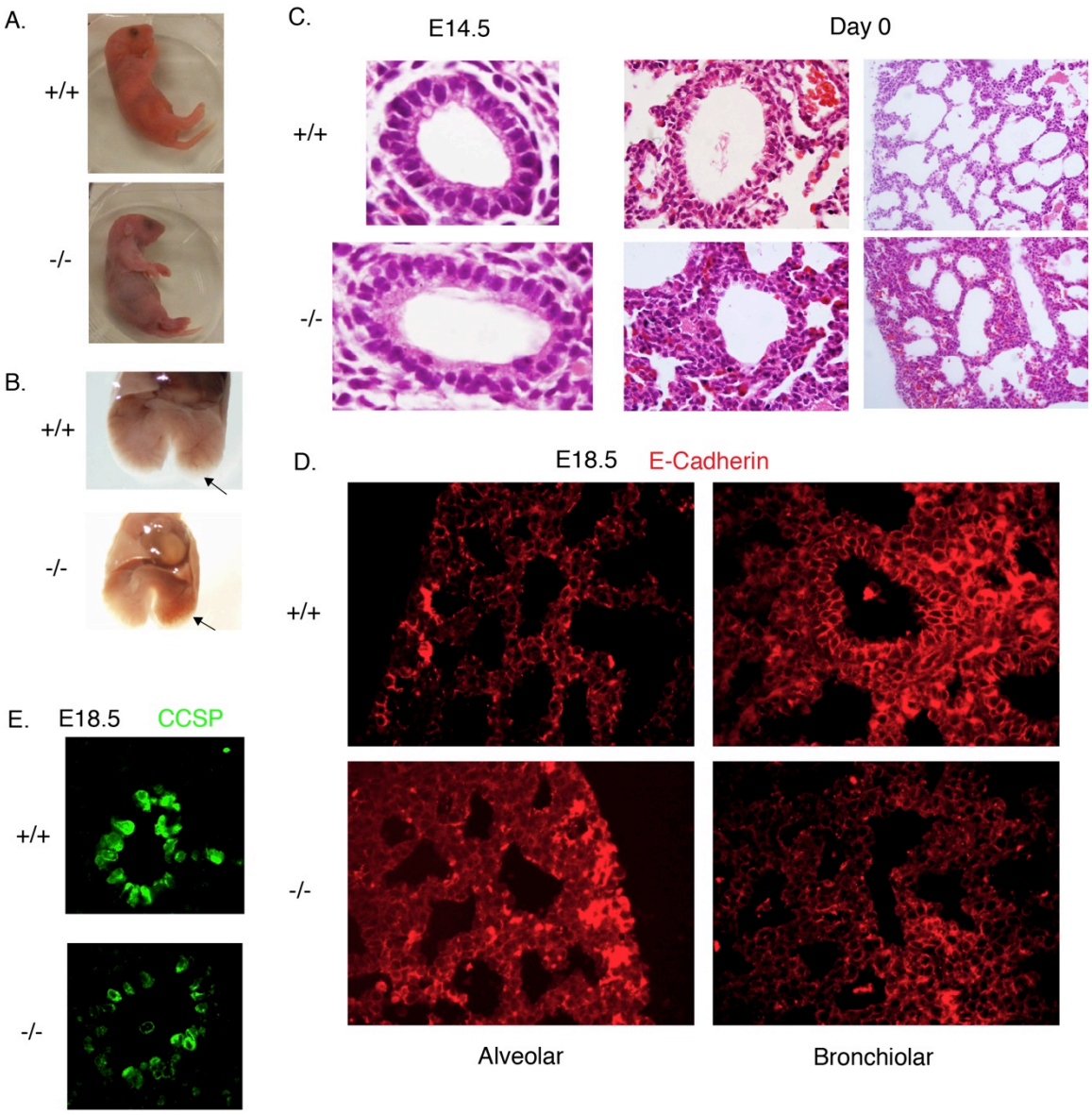

Figure 5.2. Respiratory distress phenotype of mice lacking Aimp1. (A) Representative picture of newborn pups from genotypes. Knockout mice present with cyanosis. (B) Representative picture of cardiothoracic block. Arrows point to distal edges where alveoli are dysplastic in -/-. (C) Hematoxylin and eosin (H & E) stains of lungs obtained from embryonic 14.5, and newborn, (D0) mice. (D) Representative immunofluorescent image of E-cadherin outlining the distal alveolar or bronchiolar epithelium of +/+ or -/- lungs. (E) Immunofluorescence of CCSP staining for bronchiolar epithelium.

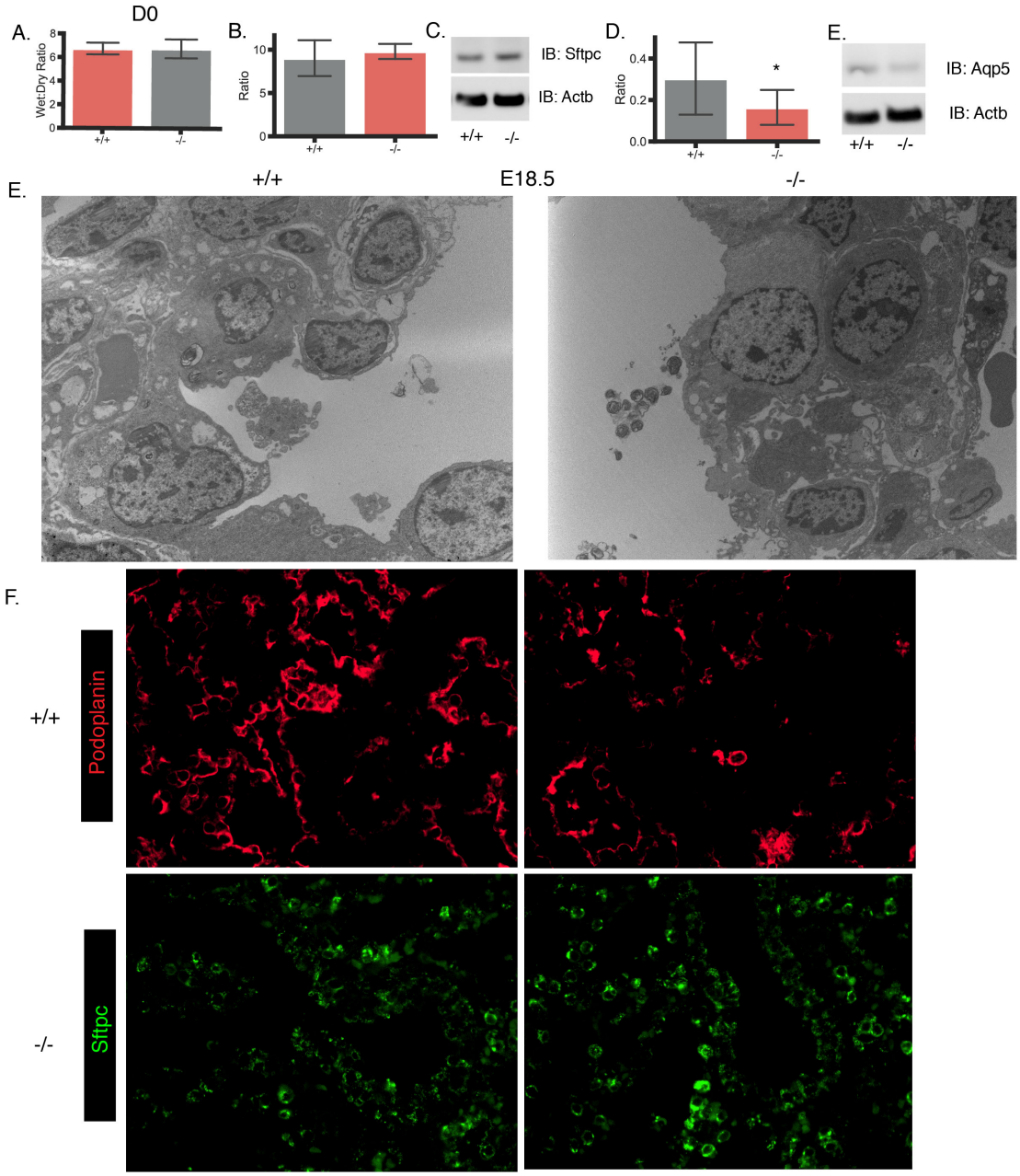

Figure 5.3. Characterization of the alveolar epithelial cells in knockout mice. (A) Wet:dry ratios of lungs at day of birth, n = 11, 8, respectively. (B) Non-significant difference in protein expression of Surfactant Protein C, SFTPC, type II cell marker. Representative immunoblot, ACTB (loading control). (C) Comparable expression and location of SFTPC positive cells in both genotypes. (D) Representative transmission electron microscopy showing comparable alveolar epithelium, including those containing lamellar bodies and glycogen. (E) Protein expression of Aquaporin 5, AQP5, Type I cell marker, in D0

whole lung homogenates. Representative immunoblot probed for AQP5. ** p-value ≤ 0.05, n = 3 per genotype. (F) Representative immunofluorescent image of podoplanin, Type I cell marker at E18.5.

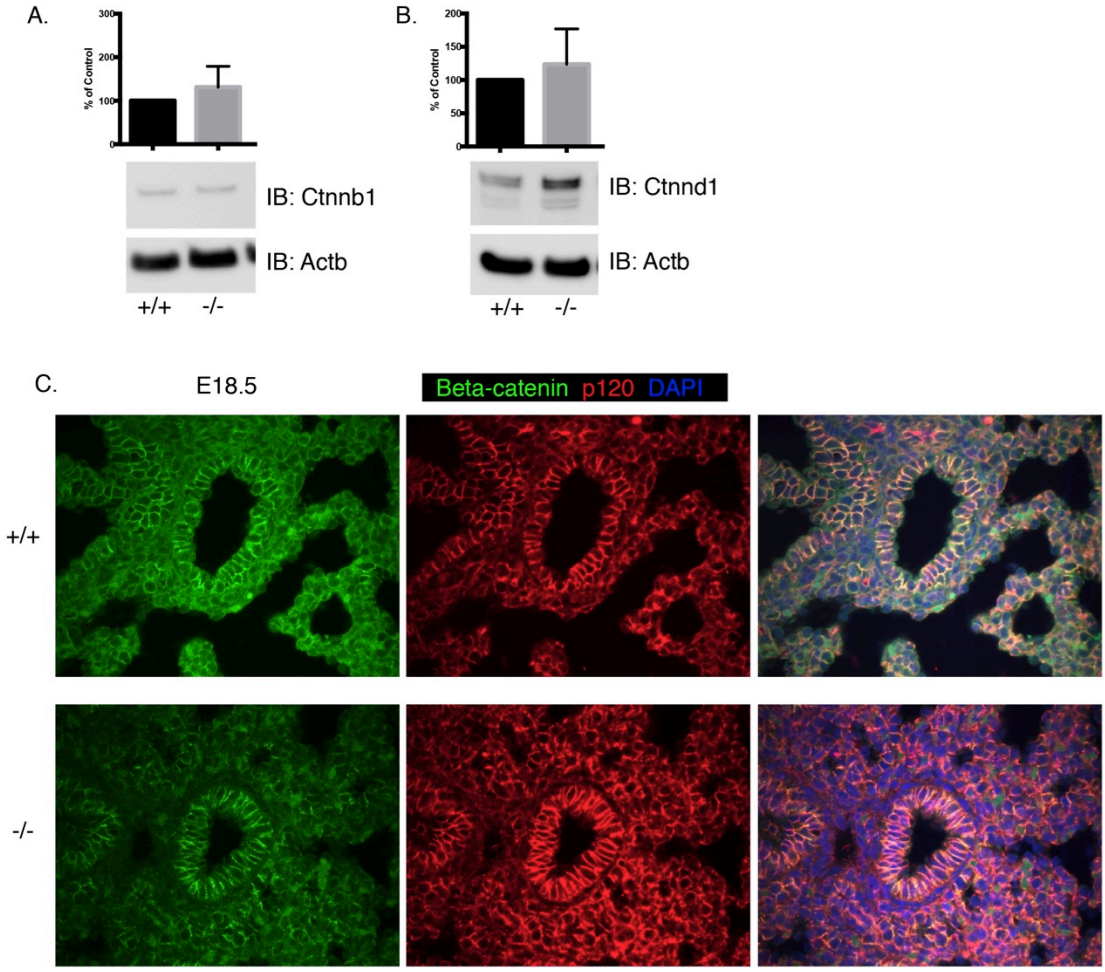

Figure 5.4. Assessing the integrity of adherens junction in knockout mice. (A) Non-significant difference in protein expression of β-catenin, Ctnnb1, compared to Actb (loading control). (B) Non-significant difference in protein expression of p120, Ctnnd1, compared to Actb (loading control). (C) Representative immunofluorescence staining of β-catenin and p120 at E18.5.

	Genotype	+/-	-/-	+/+
E18.5				
	Body Weight (mg) ± SEM	1048.6 ± 32	928.7 ± 49**	1106.9 ± 47
	Lung Weight (mg) ± SEM	34.3 ± 1.2	28.1 ± 2**	38.8 ± 3.8
	Lung (mg)/Body (g) ± SEM	32.9 ± 0.5	32.1 ± 1.4	35.6 ± 0.09
D0				
	Body Weight (mg) ± SEM	1354.8 ± 27.1	1133.8 ± 26.6**	1364.9 ± 48.7
	Lung Weight (mg) ± SEM	35.6 ± 1.1	34.4 ± 1.6	35.8 ± 2.4
	Lung (mg)/Body (g) ± SEM	26.4 ± 0.6	29.8 ± 1.1**	25.9 ± 1.3

Table 5.3. Body weights and lung weights of progeny from cross between heterozygous Aimp1 +/- mice. For E18.5, n = 23, 14, 8; for D0, n = 50, 27, 19, respectively. **p-value ≤ 0.01, Tukey's post-hoc test following significant 1-way ANOVA.

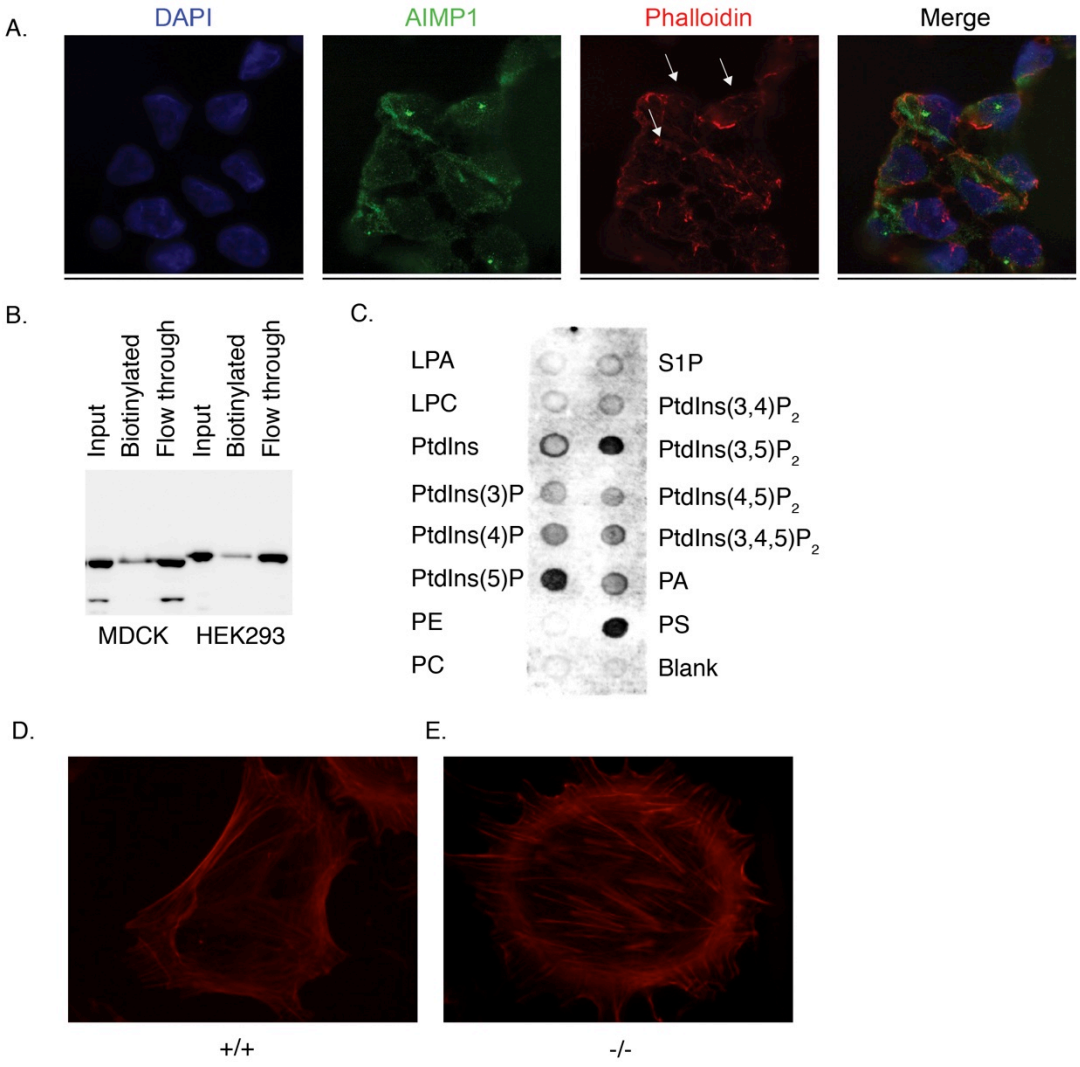

Figure 5.5. A fraction of AIMP1 resides at the actin cytoskeletal membrane interface. (A) Immunofluorescence of AIMP1, Phalloidin in HEK293 cells grown to confluency. AIMP1 is expressed at the membrane, and arrows point to co-localization of AIMP1 and Phalloidin. (B) Representative immunoblot of biotinylated proteins obtained from cell surface-bound proteins in MDCK and HEK293 cells. (C) Lipid overlay assay to indcate which membrane lipids interact with recombinant AIMP1. (D, E) Representative phalloidin stains of indicated genotypes.

Chapter 6: Concluding Remarks and Future Direction

The work presented in this thesis details the mechanisms of a moonlighting protein in lung development and BPD. While the murine model of BPD was established, a quantitative PCR robust workflow is adapted to reconcile several conflicting reports regarding a key signaling angiogenic factor *Vegf-a* (Chapter 2) and used in subsequent studies to measure transcription levels.

The studies on the effects of EMAP II in the BPD model are integrative as they measured not only traditional outcomes such as morphometric analysis and inflammation but also pulmonary function testing (Chapter 3). It is noteworthy to discuss the following from Chapter 3: (1) EMAP II recruits galectin-3^{+} macrophages during BPD pathogenesis; and (2) utilizing male mice. At the time of completing Chapter 3, the origin, regenerative potential, and heterogeneity of macrophage populations within a specific organ including the lung was unclear. A recent surge of studies regarding the populations has identified three main sub-populations in the lung under homeostatic conditions[100,101]. Two of the three are the alveolar macrophage (AM) and "primitive" interstitial macrophage (pIM) derive from the fetal liver and yolk sac, respectively; the third is the "definitive" interstitial macrophage (dIM) that derive from circulating bone-marrow derived monocytes and replace the pIM over time. Under normal developmental conditions in mice, the three populations appear in waves over time. In neonates, galectin-3 is predominantly expressed on interstitial macrophages at birth but predominantly in AM at postnatal day 6[101]. Macrophages in the lung can maintain their populations independently of circulating precursors in homeostasis, but others are recruited from the bone marrow in pathologic conditions. In the pathogenesis of BPD, it is not known what subpopulations exist.

In light of the results from Chapter 3, these recent studies argue for investigation into the identity and regenerative potential of macrophage subpopulations recruited by EMAP II. Its expression at the epithelial-mesenchymal interface may allow for the moonlighting properties of EMAP II to be a signal for monocyte/macrophage recruitment between the alveoli and lumen. This work will be useful not only to understand the role of EMAP II in context of macrophage biology during normal lung development, but also a population to target BPD pathogenesis.

The pulmonary functional testing in Chapter 3 is performed on gender-matched male to avoid the effects of estrogen as a confounding variable. Males among preterm infants diagnosed with BPD have higher morbidities and associated risks than do their female counterparts[102,103]. This is possibly due to differences in estrogen levels between males and females[104]. Estrogen found in females is needed for alveolar formation and their proper size in rodent models. This suggests that estrogen replacement therapy may lower BPD incidence. The only known-to-date randomized controlled clinical trial utilizing the replacement therapy did not demonstrate significant difference in either incidence of BPD or morbidity[105]. The clinical trial did contain many limitations including, but not limited to, low sample sizes. It remains unclear whether the replacement therapy is viable against BPD incidence, particularly in very low birth weight infants. Estrogen effects also confound studies on the association of pulmonary hypertension with BPD. Large discrepancies exist in the results of studies regarding the effect of estrogen; confounding discrepancies occur partly due to conflicting results in animal models compared to that found in human models[106].

The neutralization of EMAP II rescues mice from BPD outcomes including secondary pulmonary hypertension. This raises new questions. One of which was the signaling mechanism(s) that occurred in those macrophages recruited by EMAP II.

The transcription profile activated by EMAP II was unique and unexpected considering several pieces of evidence that suggest it to primarily serve a pro-inflammatory role (Chapter 4). Yet activation of JAK/STAT signaling in the context of macrophage polarization is generally anti-inflammatory. The dynamic bimodal phase of transcription activation further reinforce the spatiotemporal regulation performed by EMAP II that can be seen in several contexts. Further studies remain to explore the time-dependent and context-specific transcriptional complex formations that may occur upon exposure to EMAP II in macrophages and other subsets of the lung.

While many experiments demonstrate the physiological effects of EMAP II, they also highlight how little was known about the intracellular AIMP1. The discovery of the moonlighting function and its impact on epithelial cell organization through the regulation of F-actin dynamics is not expected (Chapter 5). Other phenotypes were

present in the knockout mice in line with a disruption to epithelial cell organization. The knockout mice born were cyanotic and succumbed to respiratory distress.

The impact of AIMP1 on F-actin deposition found *in vitro* argue for future studies that delineate the *in vivo* contribution of AIMP1 to lung development and BPD. It remains to be explored the impact of the various protein domains of AIMP1. This may be possible using models of cell-specific deletions to circumvent the neonatal lethal phenotype remain to be explored. In particular, as F-actin dynamics are crucial to the ability of macrophages to serve their physiological role in phagocytosis, a key future study would be to determine if there is a role for intracellular AIMP1 in innate immunity.

6.1 Clinical Implications

Despite recent clinical trials and therapeutic attempts against its pathogenesis, BPD remains the leading sequelae among prematurely born infants. Yet few therapies such as caffeine or vitamin A have been shown to lower the incidence of BPD. Their protective effects have been primarily attributed to lowering pulmonary inflammation at the onset of mechanical ventilation or oxygen therapy. This has spurned several studies to target inflammation in BPD pathogenesis and its link with disrupting pulmonary function. However, targeting inflammatory mediators such as TNF-alpha has been unsuccessful, leaving a factor that initiates inflammatory mediators to be discovered.

Several pathologies, including BPD, are linked with elevated EMAP II levels. The experiments in this thesis provide evidence that EMAP II is not only elevated at the time of BPD but also initiated early in its pathogenesis (Chapter 3). This presents a translational need to test whether elevated EMAP II levels can be an early diagnostic marker of BPD. A future study would be needed to correlate EMAP II levels with human BPD outcomes including secondary pulmonary hypertension at the onset of ventilation in human tracheal aspirates, distinguishing it from other potential biomarkers at onset of BPD; translated from the mouse model, it is possible that increased EMAP II levels in patients diagnosed with BPD may also have worsened pulmonary function outcomes later in life. This may be due to downstream inflammation caused by unknown subsets of macrophages. Those macrophages recruited by EMAP II were hypothesized to have a pro-inflammatory, activated state. However, evidence suggests that it is not simply

inflammatory (Chapter 4). Contrary to the hypothesis, the study reveals a transcriptional subset unique from traditionally classified M1 or M2 macrophages and is driven in part by STAT3, a transcription factor whose physiological function is highly context driven. Future studies are warranted, which would distinguish EMAP II-recruited macrophages and compared to those subsets activated by traditionally identified mediators such as TNF-alpha, although some overlap is to be expected. Recent studies do indicate that the galectin-3 expressing macrophages recruited by EMAP II also are the same macrophage subset recruited in other lung pathophysiological processes such as pulmonary fibrosis [107]. This may represent a potential macrophage subset to target against the pathogenesis of BPD.

6.2 Concluding remarks

EMAP II/AIMP1 has been associated with lung pathologies such as bronchopulmonary dysplasia (BPD) with unclear moonlighting mechanisms. This thesis delineates the mechanisms, which will allow for better, effective targeting of the protein to limit BPD. The work highlights the physiological roles of the protein serving through newly found moonlighting mechanisms, particularly in macrophages, in the context of lung development and pathogenesis in BPD. The workflow, employed in this thesis and future studies too, makes it possible for robust quantification of gene expression analysis in studies of lung development. Increases in macrophages accompany the BPD phenotype due to sustained and elevated EMAP II, which suggest *in vivo* future studies of the macrophage subsets. The unusual, mixed transcriptional profile of recruited macrophages exposed to EMAP II reinforces the basis for future studies of macrophage subsets. Clearly EMAP II plays an important role on macrophage biology. The full-length precursor AIMP1 impacts the proper development of the epithelium of a lung in relation to its composition and functional structure. Understanding the mechanisms may aid in guiding future therapeutic studies against pulmonary pathogenesis. Collectively, these findings demonstrate a critical role of the moonlighting protein AIMP1 in both lung development and BPD pathogenesis.

References

1. Baraldi E and Filippone M. Chronic lung disease after premature birth. *N Engl J Med*. 2007;357:1946-55.

2. Marino S, Cilfone NA, Mattila JT, Linderman JJ, Flynn JL and Kirschner DE. Macrophage polarization drives granuloma outcome during Mycobacterium tuberculosis infection. *Infect Immun*. 2015;83:324-38.

3. Schittny JC. Development of the lung. *Cell Tissue Res*. 2017;367:427-444.

4. Herriges M and Morrisey EE. Lung development: orchestrating the generation and regeneration of a complex organ. *Development*. 2014;141:502-13.

5. Laresgoiti U, Nikolic MZ, Rao C, Brady JL, Richardson RV, Batchen EJ, Chapman KE and Rawlins EL. Lung epithelial tip progenitors integrate glucocorticoid- and STAT3-mediated signals to control progeny fate. *Development*. 2016;143:3686-3699.

6. Desai TJ, Brownfield DG and Krasnow MA. Alveolar progenitor and stem cells in lung development, renewal and cancer. *Nature*. 2014;507:190-4.

7. Beers MF and Moodley Y. When Is an Alveolar Type 2 Cell an Alveolar Type 2 Cell? A Conundrum for Lung Stem Cell Biology and Regenerative Medicine. *Am J Respir Cell Mol Biol*. 2017;57:18-27.

8. Ornitz DM and Yin Y. Signaling networks regulating development of the lower respiratory tract. *Cold Spring Harb Perspect Biol*. 2012;4.

9. Hillman NH, Kallapur SG and Jobe AH. Physiology of transition from intrauterine to extrauterine life. *Clin Perinatol*. 2012;39:769-83.

10. Shaffer TH, Alapati D, Greenspan JS and Wolfson MR. Neonatal non-invasive respiratory support: physiological implications. *Pediatr Pulmonol*. 2012;47:837-47.

11. Gerhardt T, Hehre D, Feller R, Reifenberg L and Bancalari E. Pulmonary mechanics in normal infants and young children during first 5 years of life. *Pediatr Pulmonol*. 1987;3:309-16.

12. Liu L, Oza S, Hogan D, Perin J, Rudan I, Lawn JE, Cousens S, Mathers C and Black RE. Global, regional, and national causes of child mortality in 2000-13, with projections to inform post-2015 priorities: an updated systematic analysis. *Lancet*. 2015;385:430-40.

13. Patel RM, Kandefer S, Walsh MC, Bell EF, Carlo WA, Laptook AR, Sanchez PJ, Shankaran S, Van Meurs KP, Ball MB, Hale EC, Newman NS, Das A, Higgins RD, Stoll BJ, Eunice Kennedy Shriver National Institute of Child H and Human Development Neonatal Research N. Causes and timing of death in extremely premature infants from 2000 through 2011. *N Engl J Med*. 2015;372:331-40.

14. Collaborators GBDRF. Global, regional, and national comparative risk assessment of 84 behavioural, environmental and occupational, and metabolic risks or clusters of risks, 1990-2016: a systematic analysis for the Global Burden of Disease Study 2016. *Lancet*. 2017;390:1345-1422.

15. McEvoy CT, Jain L, Schmidt B, Abman S, Bancalari E and Aschner JL. Bronchopulmonary dysplasia: NHLBI Workshop on the Primary Prevention of Chronic Lung Diseases. *Ann Am Thorac Soc*. 2014;11 Suppl 3:S146-53.

16. Stoll BJ, Hansen NI, Bell EF, Walsh MC, Carlo WA, Shankaran S, Laptook AR, Sanchez PJ, Van Meurs KP, Wyckoff M, Das A, Hale EC, Ball MB, Newman NS, Schibler K, Poindexter BB, Kennedy KA, Cotten CM, Watterberg KL, D'Angio CT, DeMauro SB, Truog WE, Devaskar U, Higgins RD, Eunice Kennedy Shriver National Institute of Child H and Human Development Neonatal Research N. Trends in Care Practices, Morbidity, and Mortality of Extremely Preterm Neonates, 1993-2012. *JAMA*. 2015;314:1039-51.

17. Murray PJ. Macrophage Polarization. *Annu Rev Physiol*. 2017;79:541-566.

18. Michael Z, Spyropoulos F, Ghanta S and Christou H. Bronchopulmonary Dysplasia: An Update of Current Pharmacologic Therapies and New Approaches. *Clin Med Insights Pediatr*. 2018;12:1179556518817322.

19. Jeffery CJ. Moonlighting proteins - nature's Swiss army knives. *Sci Prog*. 2017;100:363-373.

20. Chen C, Zabad S, Liu H, Wang W and Jeffery C. MoonProt 2.0: an expansion and update of the moonlighting proteins database. *Nucleic Acids Res*. 2018;46:D640-D644.

21. Tsai BM, Wang M, Clauss M, Sun P and Meldrum DR. Endothelial monocyte-activating polypeptide II causes NOS-dependent pulmonary artery vasodilation: a novel effect for a proinflammatory cytokine. *Am J Physiol Regul Integr Comp Physiol*. 2004;287:R767-71.

22. Nuhrenberg TG, Voisard R, Fahlisch F, Rudelius M, Braun J, Gschwend J, Kountides M, Herter T, Baur R, Hombach V, Baeuerle PA and Zohlnhofer D. Rapamycin attenuates vascular wall inflammation and progenitor cell promoters after angioplasty. *FASEB J*. 2005;19:246-8.

23. Awasthi N, Schwarz MA, Verma V, Cappiello C and Schwarz RE. Endothelial monocyte activating polypeptide II interferes with VEGF-induced proangiogenic signaling. *Lab Invest*. 2009;89:38-46.

24. Clauss M, Voswinckel R, Rajashekhar G, Sigua NL, Fehrenbach H, Rush NI, Schweitzer KS, Yildirim AO, Kamocki K, Fisher AJ, Gu Y, Safadi B, Nikam S, Hubbard WC, Tuder RM, Twigg HL, 3rd, Presson RG, Sethi S and Petrache I. Lung endothelial monocyte-activating protein 2 is a mediator of cigarette smoke-induced emphysema in mice. *J Clin Invest*. 2011;121:2470-9.

25. Yuan C, Yan L, Solanki P, Vatner SF, Vatner DE and Schwarz MA. Blockade of EMAP II protects cardiac function after chronic myocardial infarction by inducing angiogenesis. *J Mol Cell Cardiol*. 2015;79:224-31.

26. Schluesener HJ, Seid K, Zhao Y and Meyermann R. Localization of endothelial-monocyte-activating polypeptide II (EMAP II), a novel proinflammatory cytokine, to lesions of experimental autoimmune encephalomyelitis, neuritis and uveitis: expression by monocytes and activated microglial cells. *Glia*. 1997;20:365-72.

27. Schwarz M, Lee M, Zhang F, Zhao J, Jin Y, Smith S, Bhuva J, Stern D, Warburton D and Starnes V. EMAP II: a modulator of neovascularization in the developing lung. *Am J Physiol*. 1999;276:L365-75.

28. Schwarz MA, Kandel J, Brett J, Li J, Hayward J, Schwarz RE, Chappey O, Wautier JL, Chabot J, Lo Gerfo P and Stern D. Endothelial-monocyte activating polypeptide II, a novel antitumor cytokine that suppresses primary and metastatic tumor growth and induces apoptosis in growing endothelial cells. *J Exp Med*. 1999;190:341-54.

29. Zhang F and Schwarz MA. Temporo-spatial distribution of endothelial-monocyte activating polypeptide II, an anti-angiogenic protein, in the mouse embryo. *Dev Dyn*. 2000;218:490-8.

30. Schikorski D, Cuvillier-Hot V, Boidin-Wichlacz C, Slomianny C, Salzet M and Tasiemski A. Deciphering the immune function and regulation by a TLR of the cytokine

EMAPII in the lesioned central nervous system using a leech model. *J Immunol*. 2009;183:7119-28.

31. Tandle AT, Calvani M, Uranchimeg B, Zahavi D, Melillo G and Libutti SK. Endothelial monocyte activating polypeptide-II modulates endothelial cell responses by degrading hypoxia-inducible factor-1alpha through interaction with PSMA7, a component of the proteasome. *Exp Cell Res*. 2009;315:1850-9.

32. Kao J, Houck K, Fan Y, Haehnel I, Libutti SK, Kayton ML, Grikscheit T, Chabot J, Nowygrod R, Greenberg S and et al. Characterization of a novel tumor-derived cytokine. Endothelial-monocyte activating polypeptide II. *J Biol Chem*. 1994;269:25106-19.

33. Schwarz MA, Zhang F, Gebb S, Starnes V and Warburton D. Endothelial monocyte activating polypeptide II inhibits lung neovascularization and airway epithelial morphogenesis. *Mech Dev*. 2000;95:123-32.

34. Quintos-Alagheband ML, White CW and Schwarz MA. Potential role for antiangiogenic proteins in the evolution of bronchopulmonary dysplasia. *Antioxid Redox Signal*. 2004;6:137-45.

35. Uhlen M, Fagerberg L, Hallstrom BM, Lindskog C, Oksvold P, Mardinoglu A, Sivertsson A, Kampf C, Sjostedt E, Asplund A, Olsson I, Edlund K, Lundberg E, Navani S, Szigyarto CA, Odeberg J, Djureinovic D, Takanen JO, Hober S, Alm T, Edqvist PH, Berling H, Tegel H, Mulder J, Rockberg J, Nilsson P, Schwenk JM, Hamsten M, von Feilitzen K, Forsberg M, Persson L, Johansson F, Zwahlen M, von Heijne G, Nielsen J and Ponten F. Proteomics. Tissue-based map of the human proteome. *Science*. 2015;347:1260419.

36. Hyeon DY, Kim JH, Ahn TJ, Cho Y, Hwang D and Kim S. Evolution of the multi-tRNA synthetase complex and its role in cancer. *J Biol Chem*. 2019;294:5340-5351.

37. Han JM, Lee MJ, Park SG, Lee SH, Razin E, Choi EC and Kim S. Hierarchical network between the components of the multi-tRNA synthetase complex: implications for complex formation. *J Biol Chem*. 2006;281:38663-7.

38. Wang T, Birsoy K, Hughes NW, Krupczak KM, Post Y, Wei JJ, Lander ES and Sabatini DM. Identification and characterization of essential genes in the human genome. *Science*. 2015;350:1096-101.
39. De Craene JO, Bertazzi DL, Bar S and Friant S. Phosphoinositides, Major Actors in Membrane Trafficking and Lipid Signaling Pathways. *Int J Mol Sci*. 2017;18.
40. Wu CY, Lin MW, Wu DC, Huang YB, Huang HT and Chen CL. The role of phosphoinositide-regulated actin reorganization in chemotaxis and cell migration. *Br J Pharmacol*. 2014;171:5541-54.
41. Deryusheva E, Nemashkalova E, Galloux M, Richard CA, Eleouet JF, Kovacs D, Van Belle K, Tompa P, Uversky V and Permyakov S. Does Intrinsic Disorder in Proteins Favor Their Interaction with Lipids? *Proteomics*. 2019;19:e1800098.
42. Balla T. Phosphoinositides: tiny lipids with giant impact on cell regulation. *Physiol Rev*. 2013;93:1019-137.
43. Liu Y and Bankaitis VA. Phosphoinositide phosphatases in cell biology and disease. *Prog Lipid Res*. 2010;49:201-17.
44. Treutlein B, Brownfield DG, Wu AR, Neff NF, Mantalas GL, Espinoza FH, Desai TJ, Krasnow MA and Quake SR. Reconstructing lineage hierarchies of the distal lung epithelium using single-cell RNA-seq. *Nature*. 2014;509:371-5.
45. Bartis D, Mise N, Mahida RY, Eickelberg O and Thickett DR. Epithelial-mesenchymal transition in lung development and disease: does it exist and is it important? *Thorax*. 2014;69:760-5.
46. Borthwick LA, McIlroy EI, Gorowiec MR, Brodlie M, Johnson GE, Ward C, Lordan JL, Corris PA, Kirby JA and Fisher AJ. Inflammation and epithelial to mesenchymal transition in lung transplant recipients: role in dysregulated epithelial wound repair. *American journal of transplantation : official journal of the American Society of Transplantation and the American Society of Transplant Surgeons*. 2010;10:498-509.
47. Chen Y, Legan SK, Mahan A, Thornton J, Xu H and Schwarz MA. Endothelial-monocyte activating polypeptide II disrupts alveolar epithelial type II to type I cell transdifferentiation. *Respiratory research*. 2012;13:1.

48. Kim KK, Kugler MC, Wolters PJ, Robillard L, Galvez MG, Brumwell AN, Sheppard D and Chapman HA. Alveolar epithelial cell mesenchymal transition develops in vivo during pulmonary fibrosis and is regulated by the extracellular matrix. *Proc Natl Acad Sci U S A*. 2006;103:13180-5.

49. Vyas-Read S, Wang W, Kato S, Colvocoresses-Dodds J, Fifadara NH, Gauthier TW, Helms MN, Carlton DP and Brown LA. Hyperoxia induces alveolar epithelial-to-mesenchymal cell transition. *Am J Physiol Lung Cell Mol Physiol*. 2014;306:L326-40.

50. Wang AM, Doyle MV and Mark DF. Quantitation of mRNA by the polymerase chain reaction. *Proc Natl Acad Sci U S A*. 1989;86:9717-21.

51. Defoiche J, Zhang Y, Lagneaux L, Pettengell R, Hegedus A, Willems L and Macallan DC. Measurement of ribosomal RNA turnover in vivo by use of deuterium-labeled glucose. *Clinical chemistry*. 2009;55:1824-33.

52. Topp H and Schoch G. Whole-body degradation rates of transfer-, ribosomal-, and messenger ribonucleic acids and resting metabolic rate in 3- to 18-year-old humans. *Pediatr Res*. 2000;47:163-8.

53. Imbeaud S, Graudens E, Boulanger V, Barlet X, Zaborski P, Eveno E, Mueller O, Schroeder A and Auffray C. Towards standardization of RNA quality assessment using user-independent classifiers of microcapillary electrophoresis traces. *Nucleic Acids Res*. 2005;33:e56.

54. Schroeder A, Mueller O, Stocker S, Salowsky R, Leiber M, Gassmann M, Lightfoot S, Menzel W, Granzow M and Ragg T. The RIN: an RNA integrity number for assigning integrity values to RNA measurements. *BMC molecular biology*. 2006;7:3.

55. Eikmans M, Rekers NV, Anholts JD, Heidt S and Claas FH. Blood cell mRNAs and microRNAs: optimized protocols for extraction and preservation. *Blood*. 2013;121:e81-9.

56. Ross DT, Scherf U, Eisen MB, Perou CM, Rees C, Spellman P, Iyer V, Jeffrey SS, Van de Rijn M, Waltham M, Pergamenschikov A, Lee JC, Lashkari D, Shalon D, Myers TG, Weinstein JN, Botstein D and Brown PO. Systematic variation in gene expression patterns in human cancer cell lines. *Nature genetics*. 2000;24:227-35.

57. Vandesompele J, De Preter K, Pattyn F, Poppe B, Van Roy N, De Paepe A and Speleman F. Accurate normalization of real-time quantitative RT-PCR data by geometric averaging of multiple internal control genes. *Genome biology*. 2002;3:RESEARCH0034.
58. Carmeliet P, Ferreira V, Breier G, Pollefeyt S, Kieckens L, Gertsenstein M, Fahrig M, Vandenhoeck A, Harpal K, Eberhardt C, Declercq C, Pawling J, Moons L, Collen D, Risau W and Nagy A. Abnormal blood vessel development and lethality in embryos lacking a single VEGF allele. *Nature*. 1996;380:435-9.
59. Asikainen TM, Ahmad A, Schneider BK and White CW. Effect of preterm birth on hypoxia-inducible factors and vascular endothelial growth factor in primate lungs. *Pediatr Pulmonol*. 2005;40:538-46.
60. Hosford GE and Olson DM. Effects of hyperoxia on VEGF, its receptors, and HIF-2alpha in the newborn rat lung. *Am J Physiol Lung Cell Mol Physiol*. 2003;285:L161-8.
61. Lin YJ, Markham NE, Balasubramaniam V, Tang JR, Maxey A, Kinsella JP and Abman SH. Inhaled nitric oxide enhances distal lung growth after exposure to hyperoxia in neonatal rats. *Pediatr Res*. 2005;58:22-9.
62. Maniscalco WM, Watkins RH, D'Angio CT and Ryan RM. Hyperoxic injury decreases alveolar epithelial cell expression of vascular endothelial growth factor (VEGF) in neonatal rabbit lung. *Am J Respir Cell Mol Biol*. 1997;16:557-67.
63. Maniscalco WM, Watkins RH, Roper JM, Staversky R and O'Reilly MA. Hyperoxic ventilated premature baboons have increased p53, oxidant DNA damage and decreased VEGF expression. *Pediatr Res*. 2005;58:549-56.
64. Jimenez FR, Lewis JB, Belgique ST, Wood TT and Reynolds PR. Developmental lung expression and transcriptional regulation of claudin-6 by TTF-1, Gata-6, and FoxA2. *Respiratory research*. 2014;15:70.
65. Lingappan K, Srinivasan C, Jiang W, Wang L, Couroucli XI and Moorthy B. Analysis of the transcriptome in hyperoxic lung injury and sex-specific alterations in gene expression. *PLoS One*. 2014;9:e101581.
66. Bustin SA, Beaulieu JF, Huggett J, Jaggi R, Kibenge FS, Olsvik PA, Penning LC and Toegel S. MIQE precis: Practical implementation of minimum standard guidelines

for fluorescence-based quantitative real-time PCR experiments. *BMC molecular biology*. 2010;11:74.

67. Hellemans J, Mortier G, De Paepe A, Speleman F and Vandesompele J. qBase relative quantification framework and software for management and automated analysis of real-time quantitative PCR data. *Genome biology*. 2007;8:R19.

68. Bengtsson M, Stahlberg A, Rorsman P and Kubista M. Gene expression profiling in single cells from the pancreatic islets of Langerhans reveals lognormal distribution of mRNA levels. *Genome research*. 2005;15:1388-92.

69. Nonis A, De Nardi B and Nonis A. Choosing between RT-qPCR and RNA-seq: a back-of-the-envelope estimate towards the definition of the break-even-point. *Anal Bioanal Chem*. 2014;406:3533-6.

70. Wang C, Gong B, Bushel PR, Thierry-Mieg J, Thierry-Mieg D, Xu J, Fang H, Hong H, Shen J, Su Z, Meehan J, Li X, Yang L, Li H, Labaj PP, Kreil DP, Megherbi D, Gaj S, Caiment F, van Delft J, Kleinjans J, Scherer A, Devanarayan V, Wang J, Yang Y, Qian HR, Lancashire LJ, Bessarabova M, Nikolsky Y, Furlanello C, Chierici M, Albanese D, Jurman G, Riccadonna S, Filosi M, Visintainer R, Zhang KK, Li J, Hsieh JH, Svoboda DL, Fuscoe JC, Deng Y, Shi L, Paules RS, Auerbach SS and Tong W. The concordance between RNA-seq and microarray data depends on chemical treatment and transcript abundance. *Nat Biotechnol*. 2014;32:926-32.

71. Fleige S and Pfaffl MW. RNA integrity and the effect on the real-time qRT-PCR performance. *Molecular aspects of medicine*. 2006;27:126-39.

72. Perez-Novo CA, Claeys C, Speleman F, Van Cauwenberge P, Bachert C and Vandesompele J. Impact of RNA quality on reference gene expression stability. *BioTechniques*. 2005;39:52, 54, 56.

73. Stahlberg A, Kubista M and Pfaffl M. Comparison of reverse transcriptases in gene expression analysis. *Clinical chemistry*. 2004;50:1678-80.

74. Stahlberg A, Hakansson J, Xian X, Semb H and Kubista M. Properties of the reverse transcription reaction in mRNA quantification. *Clinical chemistry*. 2004;50:509-15.

75. Hruz T, Wyss M, Docquier M, Pfaffl MW, Masanetz S, Borghi L, Verbrugghe P, Kalaydjieva L, Bleuler S, Laule O, Descombes P, Gruissem W and Zimmermann P.

RefGenes: identification of reliable and condition specific reference genes for RT-qPCR data normalization. *BMC genomics*. 2011;12:156.

76. Graven KK, Bellur D, Klahn BD, Lowrey SL and Amberger E. HIF-2alpha regulates glyceraldehyde-3-phosphate dehydrogenase expression in endothelial cells. *Biochim Biophys Acta*. 2003;1626:10-8.

77. Ho YS, Dey MS and Crapo JD. Antioxidant enzyme expression in rat lungs during hyperoxia. *Am J Physiol*. 1996;270:L810-8.

78. Krick S, Eul BG, Hanze J, Savai R, Grimminger F, Seeger W and Rose F. Role of hypoxia-inducible factor-1alpha in hypoxia-induced apoptosis of primary alveolar epithelial type II cells. *Am J Respir Cell Mol Biol*. 2005;32:395-403.

79. Willenborg S, Lucas T, van Loo G, Knipper JA, Krieg T, Haase I, Brachvogel B, Hammerschmidt M, Nagy A, Ferrara N, Pasparakis M and Eming SA. CCR2 recruits an inflammatory macrophage subpopulation critical for angiogenesis in tissue repair. *Blood*. 2012;120:613-25.

80. Owen JL and Mohamadzadeh M. Macrophages and chemokines as mediators of angiogenesis. *Front Physiol*. 2013;4:159.

81. Bernhagen J, Krohn R, Lue H, Gregory JL, Zernecke A, Koenen RR, Dewor M, Georgiev I, Schober A, Leng L, Kooistra T, Fingerle-Rowson G, Ghezzi P, Kleemann R, McColl SR, Bucala R, Hickey MJ and Weber C. MIF is a noncognate ligand of CXC chemokine receptors in inflammatory and atherogenic cell recruitment. *Nat Med*. 2007;13:587-96.

82. Tandle AT, Mazzanti C, Alexander HR, Roberts DD and Libutti SK. Endothelial monocyte activating polypeptide-II induced gene expression changes in endothelial cells. *Cytokine*. 2005;30:347-58.

83. Lee DD, Lal CV, Persad EA, Lowe CW, Schwarz AM, Awasthi N, Schwarz RE and Schwarz MA. Endothelial Monocyte-Activating Polypeptide II Mediates Macrophage Migration in the Development of Hyperoxia-Induced Lung Disease of Prematurity. *Am J Respir Cell Mol Biol*. 2016;55:602-612.

84. Koch S and Claesson-Welsh L. Signal transduction by vascular endothelial growth factor receptors. *Cold Spring Harb Perspect Med*. 2012;2:a006502.

85. Shay T and Kang J. Immunological Genome Project and systems immunology. *Trends Immunol*. 2013;34:602-9.
86. Consortium EP. An integrated encyclopedia of DNA elements in the human genome. *Nature*. 2012;489:57-74.
87. Guo H, Jin D and Chen X. Lipocalin 2 is a regulator of macrophage polarization and NF-kappaB/STAT3 pathway activation. *Mol Endocrinol*. 2014;28:1616-28.
88. Whitsett JA, Kalin TV, Xu Y and Kalinichenko VV. Building and Regenerating the Lung Cell by Cell. *Physiol Rev*. 2019;99:513-554.
89. Kulkarni P and Uversky VN. Intrinsically Disordered Proteins: The Dark Horse of the Dark Proteome. *Proteomics*. 2018;18:e1800061.
90. Wright PE and Dyson HJ. Intrinsically disordered proteins in cellular signalling and regulation. *Nat Rev Mol Cell Biol*. 2015;16:18-29.
91. Babu MM. The contribution of intrinsically disordered regions to protein function, cellular complexity, and human disease. *Biochem Soc Trans*. 2016;44:1185-1200.
92. Liu J and Schwarz MA. Identification of protease-sensitive sites in Human Endothelial-Monocyte Activating Polypeptide II protein. *Exp Cell Res*. 2006;312:2231-7.
93. Lu H, Chelvanambi S, Poirier C, Saliba J, March KL, Clauss M and Bogatcheva NV. EMAPII Monoclonal Antibody Ameliorates Influenza A Virus-Induced Lung Injury. *Mol Ther*. 2018;26:2060-2069.
94. Bennett KM, Afanador MD, Lal CV, Xu H, Persad E, Legan SK, Chenaux G, Dellinger M, Savani RC, Dravis C, Henkemeyer M and Schwarz MA. Ephrin-B2 reverse signaling increases alpha5beta1 integrin-mediated fibronectin deposition and reduces distal lung compliance. *Am J Respir Cell Mol Biol*. 2013;49:680-7.
95. Zeno WF, Baul U, Snead WT, DeGroot ACM, Wang L, Lafer EM, Thirumalai D and Stachowiak JC. Synergy between intrinsically disordered domains and structured proteins amplifies membrane curvature sensing. *Nat Commun*. 2018;9:4152.
96. Guo M and Schimmel P. Essential nontranslational functions of tRNA synthetases. *Nat Chem Biol*. 2013;9:145-53.
97. Jeffery CJ. Why study moonlighting proteins? *Front Genet*. 2015;6:211.

98. Mirande M. The Aminoacyl-tRNA Synthetase Complex. *Subcell Biochem*. 2017;83:505-522.
99. Whiteman EL, Fan S, Harder JL, Walton KD, Liu CJ, Soofi A, Fogg VC, Hershenson MB, Dressler GR, Deutsch GH, Gumucio DL and Margolis B. Crumbs3 is essential for proper epithelial development and viability. *Mol Cell Biol*. 2014;34:43-56.
100. Ginhoux F and Guilliams M. Tissue-Resident Macrophage Ontogeny and Homeostasis. *Immunity*. 2016;44:439-449.
101. Tan SY and Krasnow MA. Developmental origin of lung macrophage diversity. *Development*. 2016;143:1318-27.
102. Stevenson DK, Verter J, Fanaroff AA, Oh W, Ehrenkranz RA, Shankaran S, Donovan EF, Wright LL, Lemons JA, Tyson JE, Korones SB, Bauer CR, Stoll BJ and Papile LA. Sex differences in outcomes of very low birthweight infants: the newborn male disadvantage. *Arch Dis Child Fetal Neonatal Ed*. 2000;83:F182-5.
103. Elsmen E, Hansen Pupp I and Hellstrom-Westas L. Preterm male infants need more initial respiratory and circulatory support than female infants. *Acta Paediatr*. 2004;93:529-33.
104. Anadkat JS, Kuzniewicz MW, Chaudhari BP, Cole FS and Hamvas A. Increased risk for respiratory distress among white, male, late preterm and term infants. *J Perinatol*. 2012;32:780-5.
105. Trotter A, Maier L, Kron M and Pohlandt F. Effect of oestradiol and progesterone replacement on bronchopulmonary dysplasia in extremely preterm infants. *Arch Dis Child Fetal Neonatal Ed*. 2007;92:F94-8.
106. Lahm T, Tuder RM and Petrache I. Progress in solving the sex hormone paradox in pulmonary hypertension. *Am J Physiol Lung Cell Mol Physiol*. 2014;307:L7-26.
107. Byrne AJ, Maher TM and Lloyd CM. Pulmonary Macrophages: A New Therapeutic Pathway in Fibrosing Lung Disease? *Trends Mol Med*. 2016;22:303-316.

Curriculum Vitae

Dong Il Lee

EDUCATION

Ph.D., Indiana University | Cellular & Integrative Physiology — May 2017 – Aug. 2019

Dissertation Title: "Understanding the Integrated Pathophysiological Role of a Moonlighting Protein in Lung Development"

University of Notre Dame — Aug. 2016 – Dec. 2016
Graduate course: Molecular Biology

Indiana University – South Bend — May 2015 – June 2015
Post-baccalaureate course: Social Statistics

Baylor College of Medicine — July 2012 – April 2013
Entered Ph.D. Cardiovascular Sciences

B.S., University of Georgia | Biochemistry & Molecular Biology, Biology (Double Major); Minor: Religion — Aug. 2007 – May 2012

PUBLICATIONS

Peer-reviewed:

- **Lee DD**, Hochstetler A, Murphy C, Lowe CW, and Schwarz, MA. "A Distinct Transcriptional Profile in Response to Endothelial Monocyte Activating Polypeptide II is Partially Mediated by JAK-STAT3 in Murine Macrophages" *American Journal of Physiology – Cellular Physiology*, June 19, 2019. — 2019

- Kuc N*, Doermann A*, Shirey C, **Lee DD**, Lowe CW, Awasthi N, Schwarz RE, Stahelin RV, and Schwarz MA. "Pancreatic Ductal Adenocarcinoma Cell Secreted Extracellular Vesicles Containing Ceramide-1-Phosphate Promote Pancreatic Cancer Stem Cell Motility" *Biochemical Pharmacology*, Sept. 15, 2018. 2018

- Schwarz MA, **Lee DD**, Bartlett S. "Aminoacyl tRNA synthetase complex interacting multifunctional protein 1 simultaneously binds Glutamyl-Prolyl-tRNA synthetase and scaffold protein aminoacyl tRNA synthetase complex interacting multifunctional protein 3 of the multi-tRNA synthetase complex" *The International Journal of Biochemistry & Cell Biology*, April 19, 2018.

- Legan SK, **Lee DD**, Margaret A. Schwarz. "α5β1 integrin mediates pulmonary epithelial cyst formation" *Developmental Dynamics*, April 29, 2017. 2017

- **Lee DD**, Lal CV, Persad EA, Lowe CW, Schwarz AM, Awasthi N, Schwarz RE, and Schwarz MA. "EMAP II Mediates Macrophage Migration in Development of Hyperoxia-Induced Lung Disease of Prematurity" *American Journal of Respiratory Cellular and Molecular Biology*, June 02, 2016. 2016

- **Lee DD** and Schwarz MA. "Adapted Approach to Profile Genes While Reconciling *Vegf-a* mRNA Expression in the Developing and Injured lung" *American Journal of Physiology – Lung Cellular and Molecular Physiology*, 308(12):L1202-11, June 15, 2015. 2015

Peer-reviewed, manuscripts in preparation:

- **Lee DD**, Hochstetler A, Sah E, Lowe CW, Xu H, Santiguel S, Pajakowski A, Schwarz MA, "*AIMP1 is critical for lung organogenesis and disrupts F-actin assembly through phosphoinositide interactions*" 2019

- **Lee DD**, Zacharias L, Zborek K, Park SJ, Sah E, Pajakowski A, Schwarz MA. "*Systems Analysis of Metabolites During Lung Development and Bronchopulmonary Dysplasia"*

- **Lee DD**, Hochstetler A, Zborek K, Park SJ, Lowe CW, Pajakowski A, Kaplan MH, Schwarz MA. "*AIMP1 fine-tunes macrophage polarization through SHP-1"*

GRANTS AND FUNDING

- NIH Fellowship, 5T32HL091816-10. IU Training Program in Molecular Physiology and Clinical Mechanisms of Lung Disease. Project title: "Molecular and Metabolic Mechanisms of Bronchopulmonary Dypslasia" — Oct. 2018 – Aug. 2019

CONFERENCE PRESENTATIONS

- **Daniel D. Lee**, Lauren Zacharias, Sang Jun Park, Kirsten Zborek, Eric Sah, Adam Pajakowski, Ralph DeBerardinis, Margaret A. Schwarz, "Metabolic Perturbations Include Homocysteine Degradation and Polyamine Synthesis in Pathogenesis of Bronchopulmonary Dysplasia" (Selected for Poster Presentation, Experimental Biology, ASBMB/Biochemistry and Molecular Biology) — Apr. 2019
- **Daniel D. Lee**, Margaret A. Schwarz, "Distinct Transcriptional Profile Activated by SCYE1 Through JAK-mediated STAT3 in Partially Activated Macrophages" (Selected for Poster Presentation, Experimental Biology, ASBMB/Biochemistry and Molecular Biology), April 2018. — Apr. 2018
- **Daniel D. Lee**, Charitharth V. Lal, Niranjan Awasthi, Roderich E. Schwarz, Margaret A. Schwarz, "Limiting Macrophage Recruitment through Vascular Mediator EMAP II in the Developing Lung" (Selected for Oral Presentation, North American Vascular Biology Organization). — Oct. 2015

- **Daniel D. Lee**, Charitharth V. Lal, Niranjan Awasthi, Roderich E. Schwarz, Rashmin C. Savani, Margaret A. Schwarz. "A Therapeutic Strategy to Improve Lung Function in Bronchopulmonary Dysplasia" (Poster Presentation, Harper Cancer Research Institute, University of Notre Dame) Apr. 2015

PATENT

- **Daniel D. Lee** and Margaret A. Schwarz. Antibody against Endothelial Monocyte Polypeptide II. (Patent US2019/0175502 A1) June 2019

RESEARCH EXPERIENCES

Ph.D., Indiana Univ. School of Medicine May 2017 – Aug. 2019

A. Research projects: Designing, interpreting, analyzing the following projects and subsequent experiments & writing manuscripts:
   - Define a role for intracellular protein-protein interaction of intracellular precursor EMAP II (AIMP1) in macrophages
   - Describe the mechanism of EMAP II on recruited macrophages
   - Characterize the metabolomics of lung development and in BPD
   - Model the role of lipid mediators in lung development
   - Investigate a role for AIMP1 in cardiovascular development

B. Grant submissions: Writing pre-doctoral fellowships (e.g., NIH F31, AHA pre-doctoral) and assisting Dr. Margaret Schwarz in developing and writing grants to following organizations:
   NIH (R01 and R21), American Heart Association, March of Dimes

Research Associate, Indiana Univ. School of Medicine, South Bend, Indiana — Oct. 2013 – April 2017

A. Research projects: Designing, interpreting, analyzing the following projects and subsequent experiments & writing manuscripts:

- Define the physiological mechanism of Endothelial Monocyte Activating Polypeptide (EMAP II) in premature lung disease – leading to publication
- Study impact of high oxygen supplementation on lung development modeling premature lung disease – leading to publication
- Study function of EMAP II in cardiac and lung development using mice models
- Investigate mechanism by which protein-protein interactions of intracellular precursor of EMAP II in lung development
- Investigate function of EMAP II in protection from acute myocardial infarction studied
- Delineate signaling mechanisms regulating cell migration induced by EMAP II
- In vitro modeling how lungs develop and interaction of lung epithelium with its environment studied using pulmonary bodies

B. Grant submissions: Assisting Dr. Margaret Schwarz in developing and writing grants to following organizations: NIH (R01 and R21), American Heart Association, March of Dimes

Student Researcher, Baylor College of Medicine, Houston, Texas — July 2012 – Apr. 2013

Designing, interpreting, and analyzing experiments for research projects:

- Characterize TGF-ß signaling in mesenchymal stem cells originating from young and aged bone marrow, heart, and skeletal muscle in different conditions
- Inquire *Ajuba* as possible inhibitor of microRNAs that act on Hippo signaling pathway components and identify target genes of Pitx2 and Yap-TEAD in Hippo knockout mice
- Describe role of microRNAs involved in formation of arrhythmogenic right ventricular cardiomyopathy
- Determine which blood vessels involved in thermoregulation and expression of TRP channels in mice tail artery

Student Researcher, University of Georgia, Athens, Georgia — Aug. 2010 – May 2012

Being introduced to research projects, doing experiments, and analyzing experimental data:

- Identify and distinguish glycosyltransferases from normal and ovarian cancer tissue
- Interrogate the compositional change of cell walls in Switchgrass suspension cells grown in maltose or sucrose carbon source in regard to sugars and polysaccharides
- Investigate how Populus suspension-cultured cells would be changed by different amounts of chitinase
- Study impact of sterility in *dcaf-1* mutant *C. elegans*

COMMUNITY SERVICES

- Ministry to help people in need: Non-profit organization to not only raise money but also seek out children in need, acquire necessities and gifts then deliver them – all done through benefit music concerts — Dec. 2002 – Present
  Most recent to benefit Hannah's House, a local maternity home (www.cLifej.net, Dec. 2018) — 2004 – Present
- Invited musician: Performing benefit concerts and banquets to help those in need and special music for various organizations playing piano, trumpet, organ, guitar, and drums (including e.g. Performing & Visual Arts of Coweta County and Annual Banquet of United Methodist Women at Berry College in Georgia; Farmington United Methodist Church in Farmington, Illinois; Evangel Heights United Methodist Church in South Bend, Indiana) — 2011
- Recruiter and Organizer: Bulldawg Outreach to Nursing Homes and Elderly, motivating others and helping organize events for elderly members around Athens, Georgia. — 2010
- Student Recruiter: Asian American Student Association at University of Georgia. Recruited members to join Association and took part in leading cultural awareness events

TEACHING and LEADERSHIP EXPERIENCES

- Lecturer, Indiana University School of Medicine – South Bend, Indiana: — Jan. 2014 – Present
- Foundations of Health and Disease I: Principles of cardiovascular Physiology (2019, 1st year medical students)
- Developing and overseeing research projects of undergraduate students, leading to presentation awards (1st place), publication

- English Teacher at Elite Academy, South Korea: Teaching PSAT Writing, SAT Subject, Math, and Verbal classes for college preparatory students — Summer 2011
- Teacher at ChildU Academy, South Korea: Teaching all subjects as native English speaker to elementary and middle school children — Summer 2011
- Leader and Organizer, University of Georgia: Leading and organizing tutors to teach Calculus II, Physics, Biology — Spring 2010; Fall 2011
- Conference Host, University of Georgia: Personal advising, planning & facilitating children's activities at ages 6-18, and administrative tasks of several camps — Summer 2010

CLINICAL EXPERIENCES

- Visiting, sharing, and caring for the sick, the elderly, and those in need — 1998 – Present
- Shadowing in Emergency Medicine, Hospitalist, and Family Medicine (total about 60 hours as of April 2016): Including the task of taking and presenting patient histories in the emergency room — 2013, 2016

HOBBIES & INTERESTS

- Music Production and Performance: Songwriting, composing new songs and instrumentals (10+ songs copy-written), remixing
- Sprinter: Unattached in 800m event (during time at University of Georgia)
- Weightlifting
- Making pottery
- Computer Programming, Graphics and Computer-Related Tasks